Backreaction and Time Dependence in a Holographic Kondo Model

---

Dissertation by Max-Niklas Newrzella

Backreaction and Time Dependence in a Holographic Kondo Model

Dissertation
an der Fakultät für Physik
der Ludwig–Maximilians–Universität
München

vorgelegt von
Max-Niklas Newrzella
aus Würzburg

München, den 31. August 2017

Dissertation

submitted to the faculty of physics of the
Ludwig–Maximilians–Universität München

by Max-Niklas Newrzella

supervised by Prof. Dr. Johanna Karen Erdmenger

1st Referee: Prof. Dr. Johanna Karen Erdmenger
2nd Referee: Prof. Dr. Dieter Lüst

Date of submission: 31 August 2017
Date of oral examination: 19 October 2017

Dedicated to Alena and Mathis.

Zusammenfassung

Diese Dissertation befasst sich mit der Anwendung der holographischen Dualität zwischen Eich- und Gravitationstheorien für die Untersuchung von magnetischen Störstellen in Modellen der Festkörperphysik. Wir verallgemeinern ein holographisches Kondo-Modell um zeitabhängige Phänomene und die Rückwirkung des Defektes auf die Geometrie in der dualen Gravitationstheorie zu erforschen.

Wir entwickeln einen allgemeinen Ansatz, um diese Rückwirkung in holographischen Modellen zu berücksichtigen, in denen Störstellen oder Ränder der Geometrie durch Hyperflächen der Kodimension eins im Inneren des dualen Gravitationsmodells dargestellt werden. Dies erlaubt es uns die Verschränkungsentropie der Störstelle mit der Umgebung auf verschiedenen Längenskalen zu berechnen. Wir bestimmen hierfür die Volumen bestimmter Minimalflächen in der dualen Gravitationstheorie, die proportional zu den Verschränkungsentropien sind. Es wird gezeigt, dass die Defektentropie im holographischen Kondo-Modell das sogenannte g-Theorem erfüllt, welches besagt, dass die Freiheitsgrade unter einem Renormierungsgruppenfluss von hohen zu niedrigen Temperaturen abnehmen.

Weiterhin untersuchen wir die zeitliche Evolution des holographischen Kondo-Modells nachdem wir die Kopplung der Störstelle mit ihrer Umgebung quenchen, d.h. ihren Wert im Verlaufe der Zeit sprunghaft ändern. Wir beschränken uns in diesem Teil der Arbeit auf vernachlässigbare Rückwirkung der Geometrie. Die komplexen Eigenfrequenzen, also die sogenannten Quasinormalmoden, der Freiheitsgrade auf dem Defekt werden durch die numerischen Lösungen der Evolutionsgleichungen bestimmt. Der Vorteil unserer numerischen Methode liegt darin, dass keine holographische Renormierung notwendig ist und das Modell auch fernab des thermischen Gleichgewichtes untersucht werden kann. Ein Resultat ist, dass die zeitliche Entwicklung bereits kurz nach dem Quench allein durch die Quasinormalmoden sehr gut approximiert werden kann. Wir untersuchen das dynamische Verhalten am Phasenübergang und bestimmen den dynamischen kritischen Exponenten numerisch zu $z = 2$.

Am Ende der Arbeit geben wir einen Ausblick darüber, wie beide Ansätze kombiniert werden können um die Rückwirkung auf die Geometrie nach Quenchen zu berechnen. Hierfür verwenden wir eine Linearisierung der Gravitationsgleichungen, da in diesem Falle die linearisierte Rückwirkung aus den obigen Ergebnissen integriert werden kann.

Diese Dissertation basiert auf Ergebnissen die, in Kollaboration mit anderen, vom Autor unter der Betreuung von Prof. Dr. Johanna Erdmenger zwischen Juni 2014 und August 2017 am Max Planck Institut für Physik in München erhalten wurden. Eine chronologische Auflistung der relevanten Publikationen ist

[1] J. Erdmenger, M. Flory, and M.-N. Newrzella. Bending branes for DCFT in two dimensions. *JHEP*, 01:058, 2015.

[2] J. Erdmenger, M. Flory, C. Hoyos, M.-N. Newrzella, and J. M. S. Wu. Entanglement Entropy in a Holographic Kondo Model. *Fortsch. Phys.*, 64:109–130, 2016.

[3] J. Erdmenger, M. Flory, C. Hoyos, M.-N. Newrzella, A. O'Bannon, and J. Wu. Holographic impurities and Kondo effect. *Fortsch. Phys.*, 64:322–329, 2016.

[4] J. Erdmenger, M. Flory, M.-N. Newrzella, M. Strydom, and J. M. S. Wu. Quantum Quenches in a Holographic Kondo Model. *JHEP*, 04:045, 2017.

[5] J. Erdmenger, M. Flory, M.-N. Newrzella, M. Rozali, and J. M. S. Wu. Spatio-temporal evolution of the Kondo cloud in a holographic Kondo model. *In Arbeit.*

Abstract

This thesis is about applications of gauge/gravity duality to the study of impurities in strongly coupled condensed matter theories. In particular, we are interested in generalisations of a holographic Kondo model involving time dependence and backreaction to the geometry. The Kondo model adds an interaction term between a magnetic impurity and its environment to a free electron gas. In contrast to that, the holographic model considers strongly interacting degrees of freedom apart from the impurity and takes a large-N limit for the $SU(N)$-representation of the impurity. Similar to the large-N Kondo model in condensed matter theory, a phase transition at a critical temperature T_c replaces the cross-over transition which is present at finite N.

We elaborate a generic approach to backreaction in holographic models in which impurities are represented by codimension one hypersurfaces in the bulk of the gravity dual. By applying this approach to the holographic Kondo model, we compute the impurity entropy numerically by using the Ryu-Takayanagi prescription, which states that entanglement entropy is represented by the volume of specific minimal surfaces in the gravity dual . It is shown that the impurity entropy satisfies the g-theorem, which states that the impurity degrees of freedom are screened as we follow the renormalisation group flow from high to low energies. The framework is readily applicable to different models in conformal field theories with defects, impurities or boundaries.

Furthermore, we apply numerical methods to investigate the temporal evolution of the impurity degrees of freedom after quenching the Kondo coupling in the probe limit. We extract quasinormal modes, i.e. the complex eigenfrequencies of the degrees of freedom, in both phases by solving the partial differential equations governing the system. Moreover, by quenching the coupling parameter right onto its critical value, criticality in the dynamics of the system is revealed. We quantify the dynamic critical exponent $z = 2$ of the system, which matches our expectations from dynamical mean-field theory.

Last, but not least, we give an outlook on a way to combine both approaches to evaluate the backreaction due to such quenches. The goal of this study is the extraction of the spatio-temporal evolution of the Kondo cloud via our holography model. By restricting ourselves to a linearisation of the gravity equations, we can directly use the data gained in the previous part, i.e. the evolution of the field content on the hypersurface, to integrate the linearised backreaction.

This thesis is based on original work by the author and collaborators, which has been obtained under the supervision of Prof. Dr. Johanna Erdmenger between June 2014 and August 2017 at the Max Planck Institute for Physics in Munich, Germany. A list of relevant publications, chronologically order, given by

[1] J. Erdmenger, M. Flory, and M.-N. Newrzella. Bending branes for DCFT in two dimensions. *JHEP*, 01:058, 2015.

[2] J. Erdmenger, M. Flory, C. Hoyos, M.-N. Newrzella, and J. M. S. Wu. Entanglement Entropy in a Holographic Kondo Model. *Fortsch. Phys.*, 64:109–130, 2016.

[3] J. Erdmenger, M. Flory, C. Hoyos, M.-N. Newrzella, A. O'Bannon, and J. Wu. Holographic impurities and Kondo effect. *Fortsch. Phys.*, 64:322–329, 2016.

[4] J. Erdmenger, M. Flory, M.-N. Newrzella, M. Strydom, and J. M. S. Wu. Quantum Quenches in a Holographic Kondo Model. *JHEP*, 04:045, 2017.

[5] J. Erdmenger, M. Flory, M.-N. Newrzella, M. Rozali, and J. M. S. Wu. Spatio-temporal evolution of the Kondo cloud in a holographic Kondo model. *To be published.*

Contents

Chapter 1

Introduction

> *"The ancient Japanese considered the Go board to be a microcosm of the universe. Although, when it is empty, it appears to be simple and ordered, the possibilities of gameplay are endless. They say no two Go games have ever been alike – just like snowflakes. So, the Go board actually represents an extremely complex and chaotic universe. And that's the truth of our world, Max! It can't be easily summed up with math, there is no simple pattern."*
>
> Sol – π [6]

At first, gravity seems to be the most natural thing to a human being. However, if we investigate it more closely, its role in our understanding of nature remains obscure. According the Einstein's general relativity, the gravitational force does not depend on space or time in the sense that it *is* just space and time. It sets the stage for a play of quanta along with a variety of unexpected behaviour. So far, we seem to understand a fair part of the physics of the quanta. The yet unsolved challenge is, actually, to understand the stage.

Black holes and entropy

To begin with, general relativity allows for black hole solutions which are beyond common imagination. Usual matter configurations like dust clouds can eventually collapse under their own gravitational potential to form event horizons, which can be considered as the defining boundary of a black hole. Once you are inside an event horizon, you can never get back outside, no matter how hard you try. However, the strangest part is that, according to

classical general relativity, you probably would not even notice when crossing the horizon. As you are reading this sentence, you could perfectly well be swallowed up by a black hole. Their event horizon is a non-local object in the sense that for finding its exact location, you'd need to know everything about the future evolution in all of spacetime, which is clearly unfeasible to measure, let alone to predict.

At first, black holes were considered to be unrealistic mathematical artefacts of Einstein's equations. Then, throughout the last decades, it became apparent that (supermassive) black holes most likely exist at least at the centers of galaxies. In 2002, the authors of [7] reported the observation of stars bound in orbit around the center of mass of the milky way. The star with smallest orbit, called S2, has an orbital radius which does not allow for a collisionless passage next to any known massive objects inside – apart from a black hole.

Most recently, experiments have probably confirmed their existence once and for all. In [8], the LIGO and VIRGO collaborations reported an observation of gravitational waves on September 14, 2015 at approximately 09:50 UTC. Their observation matches precisely the theoretical expectations for a signal after two black holes merge into a larger one, thereby unleashing an equivalent of around three solar masses in the form of gravitational waves into the environment. Following this, another black hole merger was observed on December 26, 2015 [9]. Both measurements had a significance of more than 5σ, which is the threshold to claim the detection of a signal.

Apart from black holes, general relativity is infamous for not being renormalisable as a quantum theory. This is already apparent from power-counting arguments: The Einstein-Hilbert action is given by

$$S = \frac{c^4}{16\pi\, G_N} \int \mathrm{d}^4x\, \sqrt{g}\, R\,, \tag{1.1}$$

where g is the metric, G_N is Newton's gravitational constant and R is the scalar curvature. The action is supposed to have units *energy*$\times$*time*. With the ingredients of (1.1), this means the mass dimension of the gravitational coupling is given by $[G_N] = 2-d$ in d spacetime dimensions, which is *negative* in the 3+1 dimensions we live in. This means that perturbation theory needs more and more terms appearing in each additional loop order in order to renormalise the theory up to that order, i.e. to render the results finite. Each of those *counter terms* comes along with an additional parameter to be fixed by experiments. Unlike for renormalisable theories, this procedure does not break down at some point in canonically quantised general relativity and due to the fact, that we cannot measure infinitely many parameters, the theory is non-renormalisable.

Is canonically quantised general relativity hence useless? Not quite. If you consider it as an effective field theory, valid up to some energy scale E, you are fine. Effective field theories know their place and seen as such, general relativity predicts its own breakdown at high energies, essentially set by the Planck scale

$$E_P = \sqrt{\hbar\, c^5 / G_N}\,, \tag{1.2}$$

where $\hbar$ is the reduced Planck constant and c the speed of light. The higher order terms we must add to the Einstein-Hilbert action (1.1) come along with factors E/E_P of increasing order, so they are suppressed at low energies compared to the Planck scale. Thus, we can quantise gravity and work with it as long as we do not spoil its validity by going to higher energies than E_P. The point is rather that canonically quantised general relativity is not *UV complete*, i.e. not valid at arbitrary high energy scales. A UV completion of general relativity would be known as a true candidate for *quantum gravity*.

In a seminal paper, Hawking [10] considered the quantisation of general relativity around the background geometry of a matter configuration collapsing under its own potential and eventually turning into a black hole. The striking result of this paper is that black holes emit particles of any available kind with a thermal spectrum. Due to this, we can assign thermodynamic properties like a temperature and entropy to black hole event horizons. That black holes carry entropy was first suggested by Bekenstein [11], who also conjectured the dependency of the entropy on the black hole parameters. Hawking's computation confirmed this conjecture up to constant factors, such that the entropy of a black hole is nowadays known as the Bekenstein-Hawking entropy. It reads

$$S_{BH} = \frac{k_B\, c^3\, A}{4\, G_N\, \hbar}\,, \tag{1.3}$$

where A is the area of the black hole event horizon and k_B is Boltzmann's constant.

This formula is striking for a quite some reasons. First of all, it connects thermodynamics, gravity, quantum theory and areas of minimal surfaces all in one simple equation. Then, it naturally leaves the question of the microscopic origin of the entropy. Lastly, we know that event horizons are natural boundaries for our knowledge as no information may ever approach an observer outside of it.

A black hole must decay over time if it emits energy in the form of particles in a thermal spectrum. Then, what is its ultimate faith? Does it emit thermalised radiation until the end or is the spectrum changing? Does this process stop at some point, is there a remnant?

All of these questions remain unsolved but provoked a very different discussion about the apparent incompatibility of general relativity and quantum theory, the so-called *black hole information loss paradox*. In a nutshell, this paradox is given by the following: Consider a quantum field theory which is in a pure state such that at least part of the configuration collapses into a black hole. A basic principle of quantum theory is unitary time evolution, given by the operator $e^{i\hat{H}t}$, where $\hat{H}$ denotes the Hamilton operator. Unitary evolution means that no information about the system is ever lost. However, if the spectrum of a black hole is truly thermal, it does *not* contain any useful information about its microstates anymore. What happens to the information that falls into the black hole, is it stored in some way inside or right at the event horizon, or does it get lost in the process of black hole formation?

Holographic principle and gauge/gravity duality

Another implication of the Bekenstein-Hawking entropy (1.3) lies in the yet unknown microscopic description, although progress in the framework of string theory was made e.g. by Strominger and Vafa [12]. In the microcanonical ensemble, the entropy is a measure for the number of degrees of freedom of the theory. In a classical theory, you would expect that the number of degrees of freedom scales with the spatial volume, however (1.3) explicitly shows an area law: The entropy of a black hole scales with its surface area. This led 't Hooft [13] and Susskind [14] to the formulation of the *holographic principle*. It provides guidance for the formulation of quantum gravity, telling that its degrees of freedom should scale with the surface of the worldvolume on which the theory is defined.

In 1997, Juan Maldacena published a seminal paper [15], in which he provided a very concrete example of the holographic principle, known as the *AdS/CFT correspondence*. Starting from type IIB string theory, he demonstrated that at low energies (in comparison with the Planck energy), two completely different theories must be regarded as physically equivalent: One of them is a conformal field theory (CFT) which is $\mathcal{N} = 4$ $SU(N)$ Super Yang-Mills theory in 3+1 dimensions. The other one is type IIB superstring theory, a possible candidate for a theory of quantum gravity, placed in $\mathrm{AdS}_5 \times S^5$, which has 4+1 uncompactified dimension. Hence, the conjecture really states a duality between a quantum field theory without the notion of gravity and a theory of quantum gravity in one additional dimension. Or, to turn it around, the degrees of freedom of quantum gravity can equally well be defined by a theory on its surface, which precisely matches the expectations from the holographic principle.

Since its origins, the AdS/CFT conjecture has been elaborated and more

entries have been added to what is called the holographic dictionary. This entire framework of mapping quantum field theories to theories, which include dynamic gravity, is referred to as *gauge/gravity duality*. The duality is supposed to work as long as the asymptotics are those of Anti de-Sitter space. So, one can add relevant operators that leave the UV of the quantum theory the same, but perturb its behaviour at low energies, which corresponds to the geometry away from the asymptotic boundary in the gravity dual. Hence, the gravity dual must not necessarily be Anti de-Sitter throughout the bulk, but only asymptotically.

Black holes, once more, play a prominent role in gauge/gravity duality. If we consider a conformal field theory at finite temperature, its gravity dual is supposed to contain a black hole, where the temperature of the field theory is identified with the Hawking temperature of the black hole [16]. Moreover, globally conserved currents are dualised into gauge field in the gravity theory. The currents can be sourced by chemical potentials and the interplay between temperature and chemical potential gives rise to the possibility of phase transitions. Depending on the dimensionality and the ingredients, complex phase diagrams can emerge.

Another popular element of the dictionary is given by entanglement entropy. It is a measure for the loss of information we suffer if we restrict our attention to a subsystem of a quantum theory. Recall that the entropy of a black hole, given in (1.3), scales with the area of the event horizon, which is actually a minimal surface for a fixed time slice of the geometry. The same formula remarkably also holds true for cosmological event horizons, as shown in [17] by Gibbons and Hawking. Both kinds of event horizons provide fundamental boundaries to our knowledge about the world we live in.

Inspired by this, Ryu and Takayanagi proposed in [18, 19] that minimal surfaces in the bulk of the gravity dual are linked to the entanglement entropy of subspaces in the field theory. The minimal subspaces are chosen such that they asymptotically approach the boundaries of the subregions in the field theory, whose entanglement entropy is to be computed. The holographic formula for the entanglement entropy of a subregion A in the field theory w.r.t. to its environment is then suggested to be given by

$$S(A) = \frac{\min_S \text{area}(S)}{4\, G_N}\,, \qquad S|_{\partial\mathcal{M}} \to \partial A\,. \tag{1.4}$$

This is just the Bekenstein-Hawking formula (1.3) with the following adaptions: On the left-hand side we now have the entanglement entropy of a subregion A, rather than a thermal entropy, and the area of the event horizon on the right-hand side is exchanged for the area of a minimal surface A in bulk of the gravity dual, which approaches the boundary ∂A of the subregion

A asymptotically. This proposal was generalised to a covariant description in [20] and was reinforced by the results of [21, 22].

Emergence of spacetime

It is thrilling to find such a deep connection between quantum information theoretic quantities, like entanglement entropy, and simple minimal surfaces in a theory of gravity. This, along with further hints, led quite a couple of researchers to the conclusion that there must exist a deep general relationship between (quantum) information theory and gravity. Many believe, roughly stated, that gravitation and spacetime actually emerges from the entanglement structure of an underlying pure quantum theory. In such a theory, gravity might not be a fundamental force. Even more drastically, it might not have any notion of space and time at all. This concept goes by the name *emergence of spacetime*.

Nowadays, string theory appears to be a good, if not the best, candidate for quantum gravity in the sense that it is a quantised theory and generically gives rise to the gravitational force. The quanta of the metric find their origin in the quadrupole momenta of closed strings. A drawback is that it suffers from background dependence. That is, you first need to assume some background geometry to find its quanta as excitations of the strings. Gauge/gravity duality yields a possible way to define string theory in a truly background independent manner.

There are even more radical proposals, though. One motivated by pure mathematics finds its foundations in the search for a non-commutative version of differential geometry and is called is the spectral action principle developed by Connes et al. [23–25]. In their work, they start from a pure quantum description containing so-called spectral triples and eventually find that Riemannian geometry emerges from this, if the square root of the line element $\mathrm{d}s^2$ is given by the Dirac operator $\not{D}$.

In gauge/gravity duality, lots of publications showed that one can in principle reconstruct the dual gravity geometry by considering the renormalisation group flow of the quantum theory, for an overview see e.g. [26–29].

Other authors, such as Verlinde, Padmanabhan and Jacobson [30–32], describe general relativity as an *entropic force* whose origin can be explained by the area law of entanglement entropy of an underlying quantum field theory. That the entanglement entropy of quantum field theories naturally satisfies an area law is well established nowadays, see e.g. [33, 34].

Emergence of spacetime also plays a role in condensed matter theory, in which the application of tensor networks is common, see [35] for an overview. Especially, the multi-scale entanglement renormalisation ansatz

(MERA) yields a tensor network appropriate for the description of ground states of conformal field theories [36]. Upon defining the unitary gates as some sort of volume elements, the emerging geometry resembles that of Anti de-Sitter space, thus essentially providing some kind of discrete gauge/gravity duality [37].

The structure of MERA tensor networks was the starting point for still another discussion, in which holography is applied to investigate quantum error correction codes [38–41]. Those are algorithms for quantum computers, which are supposed to make sure that the logical qubits used in quantum computations are protected from the environment, as interaction typically results in a collapse of the wave function. Generically, the ansatz to solve this problem is by distribution the logical qubits, which are used in the computation, across multiple physical qubits, which are the hardware of the quantum computer.

A completely different topic, in which the emergence of spacetime potentially could play a role, is about self-learning algorithms, which are fundamental in the quest of creating artificial intelligence. Today, *deep learning* [42] is one the most prominent approaches to teach classical computers how to identify patterns in data, needed e.g. for image recognition, text translation, or self-driving cars. It provides state-of-the art results in many of these tasks. Learning algorithms typically define a way in which information is processed along some computational graph. As the name suggests, deep learning usually abstracts information by processing it in a very deep graph. It consists of input layers, a variety of hidden layers and output layers, where the information flow goes from input to hidden (to hidden to ...) to output layers, which models the neural network in human brains.

It is not completely understood, why deep learning works so well, which is sometimes summarised as "the unreasonable effectiveness of deep learning". Especially, the design of the networks usually follows trial and error. There were some papers recently [43–45], which provided hints that some deep learning algorithms naturally implement something like a renormalisation group flow. The idea is that those layers farer away from the input layers carry more and more abstract versions of the data provided. For example, in image recognition, concepts like 'line', 'ellipse', 'eye', 'face', 'human', 'crowd' would represent a natural flow from hidden to output layers. Typically, convolutional neural networks are used in image recognition, which display a hyperbolic network geometry, similar to Anti de-Sitter space or MERA tensor networks, respectively.

We must obviously keep in mind that the topics of emergent spacetime and many of the examples here still involve quite a lot of speculations. Some of them might turn out to bare deep relationships between quantum entan-

glement and gravity. Others might reveal themselves as beautiful ideas that are plain wrong.

Applications of gauge/gravity duality

Gauge/gravity duality involves emergent spacetime in the holographic direction and finds various applications in the landscape of modern theoretical physics. One of the probably most famous results is a universal bound of the ratio of shear viscosity η of entropy density s in strongly coupled quantum field theories [46]. The bound reads

$$\frac{\eta}{s} \leq \frac{\hbar}{4\pi\, k_B}\,, \tag{1.5}$$

and seems so far to be satisfied by heavy-ion collisions [47]. There has been progress both in understanding the spectra of mesons in large-N QCD [48, 49] and why the quark-gluon plasma thermalises so rapidly after heavy-ion collisions [50–52]. As for applications to condensed matter theory we find, among many others, holographic models for the (fractional) quantum Hall effect [53–55], superconductivity [56, 57], and impurities in host metals [58–60].

A holographic Kondo model

This thesis will focus on the last application and, more precisely, on the holographic Kondo model presented in [60]. Jun Kondo introduced his famous model about magnetic impurities in some host metal in [61], governed by the Hamiltonian

$$H = H_0 + J\,\vec{S}\cdot\vec{s}(\vec{r})\,, \tag{1.6}$$

where H_0 denotes the free Hamiltonian governing the degrees of freedom of the host metal, J denotes the Kondo coupling constant and the operator parametrised by J is a spin-spin interaction between the host metal and the magnetic impurity, $\vec{S}$, localised at some point $\vec{r}$. If J is antiferromagnetic, the localised Kondo interaction imprints itself in a logarithmic contribution to the resistivity of the host metal, in dependence of the temperature T of the system. At some T_*, this leads to a minimum in the resistivity, which is experimentally confirmed [62] and hence called the *Kondo effect* in this context.

The coupling J turns out to be running in the temperature T, i.e. at low temperatures the coupling is becoming stronger until perturbation theory breaks down. It diverges at one-loop order at some finite temperature T_K, the *Kondo temperature*. What happens beyond that, and especially why

the experimentally observed resistivities do not diverge logarithmically as suggested by the Kondo model in the perturbative regime, is referred to as the *Kondo problem*. In a way, the Kondo problem captures the same phenomenological ingredients as QCD: The coupling features asymptotical freedom at very high energies and the system becomes strongly coupled at low energies, leading to non-applicability of the high energy theory.

It is a fruitful playground for the development of various techniques in quantum field theory. Wilson's numerical renormalisation group method [63] was the first successful approach to the Kondo problem. It solved the RG flow entirely, which involves a cross-over approximately around the Kondo temperature.

In 2013, Erdmenger et al. [60] published yet another approach to the Kondo problem. They suggested a holographic model motivated in a D-brane construction in type IIB string theory. Upon taking the Maldacena limits and reducing the degrees of freedom to the relevant ones to find a gravity dual of the Kondo model, they found a tractable bottom-up model. Here, the impurity is mapped to a codimension one hypersurface which carries localised degrees of freedom, a scalar field and a gauge field. At low temperatures, the model features a phase transition similar to the what is found in holographic superconductors, and the scalar field condenses. This phenomenology is very similar to a large-N conformal field theory ansatz used to solve the original Kondo model.

Results presented in this thesis

In this thesis, we will present two main extensions to the bottom-up model of [60], which are given by backreaction to the geometry and time dependence of the Kondo coupling. Backreaction is found to imprint itself in a non-trivial embedding of the hypersurface dual to the impurity. We apply the Israel junction conditions, which are matching conditions for the metric in general relativity, in order to find the equations of motion of the hypersurface embedding. We solve those equations numerically and analyse the impurity entropy which can be computed from the embeddings. As for time dependence of the Kondo coupling, we quench the system between both phases of the holographic model. From the evolution of the fields, we extract quasinormal modes and investigate the critical dynamics at the phase transition. The original results achieved by the author of this thesis are given by the following:

1. The construction of a generic framework to incorporate backreaction of impurities to the bulk geometry of the gravity dual via the Israel

junction conditions. This partly overlaps with the results of [64, 65], in which boundaries in conformal field theories have been handled in a similar way. The framework has already been presented by Mario Flory in [66], with whom the author closely collaborated. The results have been published in [1].

2. The numerical computation of entanglement entropies and impurity entropies in the given framework applied to a holographic Kondo model presented in [60]. The author developed the numerics used for the computations in this project and most of the numerical analysis. The results have been published in [2].

3. The construction of a numerical evolution scheme to compute the temporal behaviour of the fields constrained to the defect hypersurface in [60]. Most of the implementation has been worked out and published by Migael Strydom in [67]. There are two essential differences to this theses: Firstly, the gauge fixing has been changed in order to be able to compare the numerical results with [68], which shows excellent agreement. Secondly, the algorithm presented in [67] has been further optimised by introducing analytic Jacobian matrices at each step in the time evolution algorithm, which increases the performance by more than an order of magnitude.

4. The numerical analysis of the results after quenching the Kondo coupling has been performed by the author. We argue that the behaviour of the normal mode hint towards the formation of the Kondo resonance below the critical temperature. Furthermore, the critical dynamics at the phase transition is shown and fits to the expectations from dynamical mean-field theory, in accordance with the large-N ansatz for the Kondo model. Results have been published in [4].

5. The computational approach to linearised backreaction and computation of the impurity entropy after quenching the system has been worked out in large parts by the author in collaboration with Moshe Rozali. Results are to be published in [5].

Structure of this thesis

This thesis is structured as follows: In the following chapter 2, we introduce the reader to the relevant concepts of superstring theory and sketch the derivation of the original AdS/CFT correspondence by Juan Maldacena [15] and its generalisations to systems at finite temperature and finite chemical

potential. We will have a focus on how we can calculate the entanglement entropy between subregions on the field theory side by computing the area of minimal surfaces on the gravity side, which was suggested by Ryu and Takayanagi [19]. This will play an important role in chapter 4, where we compute the impurity entropy by utilising this element of the holographic dictionary.

In the next chapter 3, we introduce the framework in which the rest of this thesis is settled. Starting with an overview on the original Kondo model by Jun Kondo [61] and solution techniques in condensed matter theory, we move on to discuss the proposed holographic model of Erdmenger et. al. [60] who suggested a top-down model in type IIB string theory and developed a tractable bottom-up model from it. We discuss the main results of this paper and possible generalisation, some of which will be elaborated in the rest of the thesis.

In chapter 4, we explain a framework to compute backreaction in generic holographic models, in which boundaries or defects are represented by codimension one hypersurfaces in the gravity bulk. We use this framework to compute the impurity entropies in the holographic Kondo model of [60] via numerical methods. The results are compared to known results from the field theory side.

Chapter 5 is devoted to quenches in the holographic Kondo model of [60]. We explain the numerical approach to compute the evolution of the system after the Kondo coupling κ_T is changed in time by different quench protocols. Afterward, the evolution of the system is used to extract the quasinormal modes of the scalar operator. The numerical results are compared to closely related results published in [68], in which different numerical methods have been deployed. We outline how to combine backreaction and time dependence in 5.8 to investigate the spatio-temporal evolution of the Kondo screening cloud after quenching the coupling. The actual computations are left for future research.

Finally, we conclude the thesis in chapter 6 and suggest possible other directions for future research.

Chapter 2

Gauge/gravity duality

> *"But as the Go game progresses, the possibilities become smaller and smaller. The board does take on order. Soon, all the moves are predictable. [...] So maybe, even though we're not sophisticated enough to be aware of it, there is a pattern. An order – underlying every Go game."*
>
> Max – π [6]

In 1997, Juan Maldacena published the first realisation of the holographic principle [13, 14], the AdS/CFT correspondence [15]. It describes a duality between two distinct theories in the sense that gauge-invariant quantities like expectation values, partition function or correlation functions are identical, although the mathematical formalism to obtain them is completely different. In particular, the AdS/CFT correspondence maps $\mathcal{N} = 4$ Super Yang-Mills theory in 3+1 dimensions to type IIB superstring theory on $\mathrm{AdS}_5 \times S^5$. The first theory is a supersymmetric gauge theory, whereas the other one yields a good candidate for quantum gravity. Ever since, this duality has been supplemented by additional ingredients like temperature, finite density or entanglement entropy. There have been applications in various fields like heavy-ion collisions, condensed matter theory and quantum information theory. This nowadays established framework of mapping quantum field theories to dual theories of gravity is called gauge/gravity duality or holography.

Its origins lie in superstring theory, from which it emerges in specific models in the low-energy limit. In this chapter, we want to introduce the most essential topics needed in order to understand Maldacena's derivation. We will give a very concise overview on superstring theory, with a focus on its low-energy behaviour, which is given by supergravity. Equipped with these

tools, we go on to explain the original duality between $\mathcal{N} = 4$ Super Yang-Mills and type IIB superstring theory on $\mathrm{AdS}_5 \times S^5$. At the end, we show how to incorporate temperature and finite density into the correspondence, and have a focus on the definition of entanglement entropy and its holographically dual description.

Due to the focus of this thesis on applications of gauge/gravity duality, this chapter cannot provide a self-contained introduction to all of superstring theory, the AdS/CFT correspondence, and its generalisations and applications. For further reading, we therefore refer the reader to [69–74], which provide exhaustive overviews on the various topics.

2.1 Superstring theory in a nutshell

Quantum field theory as we know it from elementary particle physics deals with the quantisation of fields which are to mimic point particles in spacetime. We can start with the action of a massive point particle, which is the integral over its worldline, viewed as an embedding $\gamma : I \hookrightarrow \mathcal{M}$ of some interval I into the ambient spacetime $\mathcal{M}$ with metric G, and given by[1]

$$S_{pp} = -M \int_\gamma \mathrm{d}s = -M \int_I \mathrm{d}\tau \sqrt{\gamma_* G}\,, \tag{2.1}$$

where M denotes the particles rest mass and $\mathrm{d}s$ is the square root of the line element on the particles path. It can be rewritten in terms of the pullback $\gamma_* G$ of the metric to the particles one-dimensional worldline. The interval I denotes the range of the auxiliary time-like coordinate τ, which parametrises the path γ.

Bosonic string theory

In contrast, string theory starts with extending the dimensions of the underlying objects to be quantised. Instead of point particles with a one-dimensional worldline, it deals with strings which span a 1+1-dimensional worldsheet. Thus, its action is the natural extension of (2.1) to a 1+1-dimensional worldsheet Σ, which is given by the Nambu-Goto action

$$S_{NG} = -T_F \int_\Sigma \mathrm{d}^2 x \, \sqrt{X_* G}\,, \tag{2.2}$$

where x denote the coordinates on the worldsheet and T_F is the string tension, which naturally replaces the mass of the point particle in (2.1). The

[1] In this thesis, we will often write $\sqrt{\gamma}$ if we refer to $\sqrt{|\det(\gamma)|}$.

independent variable of this action is given by the embedding $X : \Sigma \hookrightarrow \mathcal{T}$ of the worldsheet into a D-dimensional *target space* $\mathcal{T}$ with metric G, which is left arbitrary at this point. Moreover, the dimensionality of the target space $\mathcal{T}$ will be derived later on due to consistency conditions on the quantised theory.

Although (2.2) is the natural extension to the point particle action, it is unclear how to quantise it as there is no way to normalise the degrees of freedom, given by the embedding's components, in a canonical way. Therefore, one uses a mathematical trick and introduces the induced metric $\gamma = X^*G$ as an auxiliary degree of freedom. We can subsequently rewrite the action as

$$S_P = \frac{-1}{4\pi\,\alpha'} \int_\Sigma \mathrm{d}^2x\,\sqrt{\gamma}\,G_{MN}\,\gamma^{ij}\,\partial_i X^M\,\partial_j X^N\,, \tag{2.3}$$

where the auxiliary variable denotes the induced metric on the worldsheet. In addition, we replaced the string tension by $T_F = (2\pi\,\alpha')^{-1}$, where $l_s = \sqrt{\alpha'}$ denotes the string length. This is called the Polyakov action, in which it becomes apparent that the coordinates X^M of the string's embedding are the dynamical variables of the theory. It essentially is an action of several scalar fields on the worldsheet Σ, which is therefore called a *non-linear sigma-model*. Upon computing the variation of S_P w.r.t. the auxiliary variable γ in order to find its equation of motion, we do not find an evolution equation for γ but rather a constraint equation for the X^M. This is not surprising as γ appears with no derivatives in the action. The constraint is given by $T^i_{\ i} = 0$, where T denotes the energy-stress tensor of the field content on the worldsheet. This is a first hint, that string theory really is a two dimensional conformal field theory on the worldsheet Σ.

Moreover, the theory is invariant with respect to Weyl transformations, $\gamma \to e^{2\sigma}\gamma$, where σ is an arbitrary function of the coordinates. There are two more symmetries, given by diffeomorphism invariance and D-dimensional Poincaré invariance if G is the D-dimensional Minkowski metric.

Having said that, how many degrees of freedom are we actually dealing with? As the number of embedding coordinates correspond to the dimension D of the target space, this is the question at hand. There are several ways to obtain the target space dimension, for which we will refer to the literature, see e.g. [71–73]. The most common constraint is that the theory is supposed to have a local Weyl invariance also after quantisation, that is there should not be a Weyl anomaly. For bosonic string theory, as represented by the action (2.3), the number of dimensions of the target space turns out to be $D = 26$.

Superstring theory

Bosonic string theory, however, cannot be the final answer. It has a severe issue, which is that after quantising the X^M on the worldsheet, its ground state has negative energy and is, hence, tachyonic. This yields that bosonic string theory is inherently unstable. A solution to fix this issue is to introducing fermionic superpartners Ψ^M for all bosonic coordinates X^M on the worldsheet. In 1+1-dimensions, it is possible to have Majorana fermions, whose spinor components are given by

$$\Psi^M = \begin{pmatrix} \psi_-^M \\ \psi_+^M \end{pmatrix} , \tag{2.4}$$

and which satisfy a reality condition

$$\Psi^C = \Psi \, , \tag{2.5}$$

where C denotes charge conjugation. Choosing this constraint makes sense in the light of the Ψ^M being superpartners of coordinates which are supposed to be real.

Supersymmetry on the worldsheet is then introduced by adding an action for the Ψ^M to the Polyakov action and imposing a supersymmetry generator Q to act on both fields as

$$X^m \mapsto X^M + \bar{\epsilon}\Psi^M \, , \qquad \Psi^M \mapsto \Psi^M - i\,\gamma^N \partial_N X^M \,\epsilon \, , \tag{2.6}$$

where we omitted spinor indices and ϵ is a Majorana spinor parametrising the supersymmetry transformation. Indeed, if we add

$$-\frac{i}{4\pi\,\alpha'} \int_\Sigma *(\bar{\Psi}^M \not{D}\, \Psi^N) g_{MN} \tag{2.7}$$

to the bosonic action (2.3), we find that the total action is invariant under (2.6).

The equations of motion are in terms of light-cone coordinates $\sigma^\pm = \tau \pm \sigma$ given by

$$\partial_+ \psi_-^M = 0 \, , \qquad \partial_- \psi_+^M = 0 \, , \tag{2.8}$$

which is why the ψ_+ (ψ_-) component is naturally identified with *left-* (*right-*) moving degrees of freedom. As for the boundary conditions, the best approach is to divide the discussion into the open and closed string sectors.

For open strings, theirs are localised on D-branes, just as for the bosonic string. At $\sigma = 0$, we can always redefine the fermionic coordinates such

that $\psi_+^M(\tau, \sigma = 0) = \psi_-^M(\tau, \sigma = 0)$. However, at $\sigma = \pi$, we have to choose between two boundary conditions,

$$\psi_+^M(\tau, \sigma = \pi) = \psi_-^M(\tau, \sigma = \pi) \qquad \text{Ramond (R)}\,, \tag{2.9}$$

$$\psi_+^M(\tau, \sigma = \pi) = -\psi_-^M(\tau, \sigma = \pi) \qquad \text{Neveu-Schwarz (NS)}\,, \tag{2.10}$$

which introduces two different sectors in the open string spectrum. The ground state of the NS sector is tachyonic like the ground state in bosonic string theory. In the case of superstring theory, however, we can project the spectrum to physical states by the *GSO projection* [75]. After applying it, no more tachyonic states are present in the spectrum.

For closed strings, we use periodic boundary conditions. Then, we can either choose (2.9) or (2.10) for both left- and right-movers, which decouple. This yields four sectors, labelled by the NS/NS, R/R, NS/R and R/NS boundary conditions. All of those are included in the spectrum. The homogeneous boundary conditions (R/R and NS/NS) give rise to states which transform as bosons under target space transformations, while the mixed boundary conditions (NS/R and R/NS) give rise to fermionic states. Again, we find a tachyonic mode in the NS/NS-sector, which can be projected out consistently by the GSO projection.

There are four consistent choices of the GSO projection for the closed string, either of which defines a valid superstring theory in the end. Two of those are called type IIA and type IIB superstring theory. For the subject of gauge/gravity duality, these are the interesting ones so we restrict our attention to them in the following.

Before we turn our attention to D-branes, which are additional dynamical objects in string theory, we state that type IIA and type IIB superstring theory are defined in $D = 10$ dimensions. Once more, like for the bosonic string, this can be derived by requiring the Weyl anomaly to cancel.

D-branes

At the massless level, the R/R-sector of type IIA includes a 1-form field $C_{(1)}$ and a three-form field $C_{(3)}$. Type IIB, on the other hand, supports a scalar field $C_{(0)}$, a two-form field $C_{(2)}$, and a four-form field $C_{(4)}$. In general, $(p+1)$-form fields can couple to $p+1$-dimensional hypersurfaces, so especially to Dp-branes, just by adding their integral

$$\int_{Dp} C_{(p+1)}\,, \tag{2.11}$$

where the integration is over the worldvolume of the Dp-brane. We can also turn it around and state that Dp-branes carry charges of the respective

$p+1$-form fields defined in the theory. These charges are conserved, so the charged Dp-branes cannot decay. Thus, the stable D-branes in type IIA have odd dimensions (D0, D2, D4, etc.), whereas the ones in type IIB have even dimensions (i.e. D1, D3, D5, and D7-branes). D-branes of different dimensions are possible in either theory, but they eventually decay into the ones which can be stabilised by the R/R-charges [76]. This renders D-branes to be dynamical intrinsic objects of superstring theory.

On the other hand, the NS/NS-sector includes the dilaton field ϕ, a symmetric tensor g_{mn} and an antisymmetric Kalb-Ramond field B_{mn} at the massless level. The tensor g_{mn} provides a candidate for the spacetime metric and D-branes couple naturally to the coherent background of massless fields in the NS/NS-sector by the *DBI action*, which reads

$$S_{\mathrm{DBI}} = -\tau_p \int_{Dp} \mathrm{d}^{p+1}x\, e^{-\phi} \sqrt{|\det\left(X_* g + X_* B + 2\pi\alpha' F\right)|}\,, \tag{2.12}$$

where $\tau_p = \left[(2\pi)^p \left(\alpha'\right)^{(p+1)/2}\right]^{-1}$ is the tension, and $X_* g$ and $X_* B$ are the pullbacks of the metric g and Kalb-Ramond field B due to the embedding $X : Dp \hookrightarrow \mathcal{M}$ of the $p+1$-dimensional Dp-brane into the 10-dimensional ambient spacetime $\mathcal{M}$. The additional object in the DBI action, F, finds its origin in the fact that D-branes provide Dirichlet boundary conditions for the open string. At the massless level, the open string has a gauge field A, whose field strength F couples to D-branes.

In perturbative string theory, the string coupling is given by $g_s = \langle e^{\phi} \rangle$, so the DBI action scales inversely with the string coupling. This shows that Dp-branes are inherently non-perturbative objects in string theory.

A web of dualities

Up to this point, we considered string theory as a framework to derive several consistent versions for the quantisation of strings. It turns out that there are five of these theories, which are labelled type I, type IIA, type IIB, heterotic $SO(32)$, and heterotic $E_8 \times E_8$. Here, we will introduce an essential point of superstring theory, which is the fact that all of these distinct string theories can be identified.

This idea, first suggested by Edward Witten in 1995, ignited the so-called second superstring revolution. The different versions of string theory are nodes in a *web of dualities*, in which they are related by T- and S-duality. This is sketched in figure 2.1. Each of these nodes are conjectured to be limiting cases of *M-theory*, which is supposed to be the UV completion of the unique eleven dimensional theory of supergravity. Although a complete

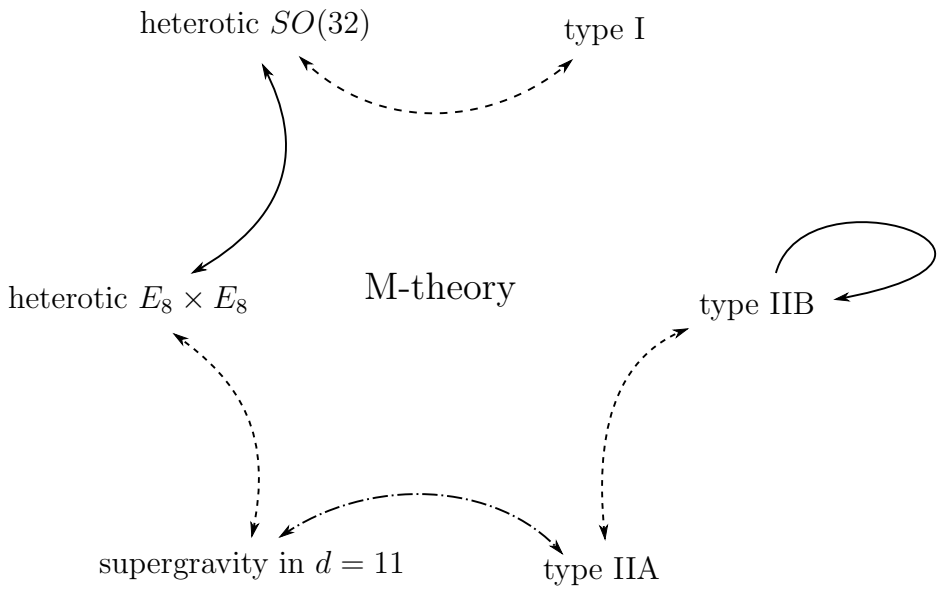

Figure 2.1: The web of dualities between different versions of string theory. Continuous lines denote T-duality, dashed lines denote S-duality, and the dash-dotted line denotes dimensional reduction. All of these theories are conjectured to emerge as limiting cases of M-theory.

understanding of M-theory is lacking so far, it presumably contains an analogue to D-branes. Those are called *M-branes*, coming in two versions, M2- and M5-branes, which are magnetically dual. We will not go into more detail about M-theory, but only state that M2-branes are the starting point for a holographic duality between ABJM theory and M-theory on $\mathrm{AdS}_4 \times S^7$ [77].

T-duality

The best way to introduce T-duality is to investigate what happens if one of the 10 dimensions of the theory, say the X^9-direction, is compactified on a circle. Looking at the embedding coordinate X^9 for a single closed string, we need to identify

$$X^9(\tau, \sigma + 2\pi) = X^9(\tau, \sigma) + 2\pi\, m\, R\,, \tag{2.13}$$

where R denotes the radius of the circle and $m \in \mathbb{N}_+$ denotes the winding number of the string, that is, how often it winds around the compactified dimension. We can still quantise this string, although it will be subject to several constraints arising from the compactification. For example, its total

momentum in the X^9-direction is quantised to $p^9 = n/R$, where $n \in \mathbb{Z}$. In the end, the formula for its mass will read

$$M^2 = \left(\frac{m\,R}{\alpha'}\right)^2 + \left(\frac{n}{R}\right)^2 + \frac{2}{\alpha'}(N + N' - 2)\,, \tag{2.14}$$

where N and N' denote the number of excitations. Looking at this equation, we see that the spectrum is invariant under the transformation

$$R \to \alpha'/R\,, \qquad n \to m \quad \text{and} \quad m \to n\,. \tag{2.15}$$

This is remarkable, as it means we interchange a string of total momentum n/R wrapping a circle of radius R m-times with one of momentum mR/α' that wraps a circle of radius α'/R n-times. This symmetry holds exactly for the whole theory and very "stringy", in the sense that point particles cannot wrap a compactified dimension and, hence, cannot obey a symmetry of this kind.

For open strings, it seems impossible that a similar symmetry holds true. However, we recall that open strings' endpoints can be constrained to D-branes. Say, we compactify the X^9 direction as above on a circle of radius R. If we have a D8-brane, that does not wrap the compactified dimension, open strings can start on it, wrap m times around the compactified dimension, and end on it. In this way, they can also wind around the X^9-direction without being able to unwind, as their ends are fixed to an object, the D-brane. These winding states contribute to the mass by m^2/R^2. There is no contribution from the momentum in the X^9-direction, as the string is attached to the D8-brane.

On the other side, if we compactify the X^9-direction on a circle of radius α'/R and have no D-brane as considered before, the open string *can* have a momentum along the compactified direction. However, just like for the closed string above, it needs to be quantised and its the contribution to the mass formula is similarly given by $n^2\,\tilde{R}^2/\alpha'^2$. Once more, contribution is exactly the contribution of the string ending on an D8-brane under the T-duality transformation (2.15).

To obtain the same mass spectrum, we saw that we need D-branes of different dimensions in the theories we consider as dual. This holds in general. That is, D-branes of even dimension are replaced by such of odd dimension, and vice versa. However, this is just what is happening in type IIA and IIB string theory: One supports only even dimensional D-branes, the one one just odd dimensional D-branes.

Hence, we see a hint that type IIA and type IIB superstring theory are related by T-duality. In fact, it turns out that T-duality is an exact duality

transformation mapping type IIA to type IIB and vice versa, see figure 2.1. For open strings, Dirichlet conditions and Neumann conditions interchange on the compactified dimension subject to the T-duality transformation. If they had quantised momenta of $p^9 = n/R$ in the compactified direction, after the transformation they will have no momenta in this direction as there appears an additional D-brane setting Dirichlet conditions in this direction. However, they are winding n-times around the circle with new radius $R = \alpha'/R$.

S-duality

Another symmetry relating different superstring theories is S-duality, which is a duality between strongly-coupled and weakly-coupled theories. In superstring theory, the coupling constant g_s is related to the vacuum expectation value of the dilaton by

$$g_s = \langle e^{\phi} \rangle \,, \tag{2.16}$$

which also appears in the type IIB supergravity action (2.18). In type IIB string theory, we have two massless scalars, the dilaton ϕ and a 0-form field $C_{(0)}$. Combining them into a complex scalar field $\tau = C_{(0)} + ie^{-\phi}$, there is an $SL(2,\mathbb{R})$-symmetry in the equations of motion, which maps

$$\tau \mapsto \frac{a\,\tau + b}{c\,\tau + d}\,, \qquad \begin{pmatrix} a & b \\ c & d \end{pmatrix} \in SL(2,\mathbb{R})\,, \tag{2.17}$$

where $ad - bc = 1$. The group reduces to $SL(2,\mathbb{Z})$ when the theory is quantised, as the fluxes become quantised. If $C_{(0)} = 0$, the above symmetry can be used to transform $\langle e^{\phi} \rangle = g_s \mapsto 1/g_s$, which exchanges strongly coupled type IIB with weakly coupled type IIB string theory and vice versa. In this sense, type IIB string theory is self-dual under S-duality, which is also shown in figure 2.1.

Low-energy limit of Type IIB string theory

In the low-energy limit, the spectra of type IIA and type IIB superstring theory reduce to their massless states. They always contain a symmetric rank two tensor field, which can be identified with the graviton, hinting that the low-energy limits are given by type IIA and IIB supergravity. In the context of this thesis, especially the action of type IIB supergravity is

interesting. Its bosonic part is given by

$$S_{IIB} = \frac{1}{2\,\kappa_{10}^2}\left(\int \mathrm{d}^{10}X\,\sqrt{G}\,\left(e^{-2\phi}\,\left(R + 4\,\partial_M\phi\,\partial^M\phi - \frac{1}{2}\left|H_{(3)}\right|^2\right)\right.\right. \\ \left. -\frac{1}{2}\left|F_{(1)}\right|^2 - \frac{1}{2}\left|\tilde{F}_{(3)}\right|^2 - \frac{1}{4}\left|\tilde{F}_{(5)}\right|^2\right) \\ \left. -\int C_{(4)}\wedge H_{(3)}\wedge F_{(3)}\right), \tag{2.18}$$

where $\kappa_{10}^2 = (2\pi)^7\,\alpha'^4$ is the gravitational coupling in 10 dimensions. The fields correspond to the coherent background of the massless excitations in the NS/NS- and R/R-sector of type IIB string theory. Moreover, $F_{(p+1)}$ and $H_{(3)}$ are the field strength tensors of the $C_{(p)}$ and $B_{(2)}$ form fields, and the tilded version of $F_{(3)}$ and $F_{(5)}$ are defined by

$$\tilde{F}_{(3)} = F_{(3)} - C_{(0)}\wedge H_{(3)}\,, \tag{2.19}$$

$$\tilde{F}_{(5)} = F_{(5)} - \frac{1}{2}\,C_{(2)}\wedge H_{(3)} + \frac{1}{2}B_{(2)}\wedge F_{(3)}\,. \tag{2.20}$$

A particular minimiser of this action is given by stacking N Dp-branes on top of each other. The ansatz for this solitonic solution reads

$$\mathrm{d}s^2 = \frac{1}{\sqrt{H(y)}}\,\eta_{MN}\,\mathrm{d}X^M\,\mathrm{d}X^N + \sqrt{H(y)}\,\delta_{ij}\,\mathrm{d}Y^i\,\mathrm{d}Y^j\,, \tag{2.21}$$

$$e^{\phi} = g_s\,H(y)^{(3-p)/4}\,, \tag{2.22}$$

$$C_{(p+1)} = \left(H(y)^{-1} - 1\right)\,\mathrm{d}X^0\wedge\cdots\wedge\mathrm{d}X^p\,, \tag{2.23}$$

$$B_{(2)} = 0\,, \tag{2.24}$$

where η is the Minkowski metric, $M, N \in \{0\ldots p\}$ denote dimensions which span the D-brane worldvolume, $i, j \in \{p+1\ldots 9\}$ those of the ambient spacetime and $y = \sqrt{y_i\,y^i}$ with summations over i is the ambient distance to the stack of D-branes. The function H is defined by

$$H(y) = \left(1 - \left(\frac{L}{y}\right)^{7-p}\right)\,, \tag{2.25}$$

which is similar to the blackening factor in black hole spacetimes. The length scale L defines the radius in both components in (2.21) and can be derived in terms of the Reggae slope to be

$$L^{7-p} = (4\pi)^{\frac{5-p}{2}}\,g_s\,N\,\Gamma[(7-p)/2]\,(\alpha')^{\frac{7-p}{2}}\,, \tag{2.26}$$

where N denotes the number of Dp-branes. It is encoded in the total flux of the $C_{(p+1)}$ gauge field through the branes, which is given by

$$\mathcal{C} = \frac{1}{2\,\kappa^2} \int_{S^{8-p}} *(\mathrm{d}C_{(p+1)} + C_{(p+1)} \wedge C_{(p+1)})\,, \tag{2.27}$$

where the terms in the brackets yield the field strength of $C_{(p+1)}$ and the integral is over any S^{8-p} sphere which includes the Dp-branes in its interior.

2.2 AdS/CFT correspondence

2.2.1 Maldacena limit in type IIB string theory

In 1997, Juan Maldacena published a seminal paper on "The Large N limit of superconformal field theories and supergravity" [15], in which he conjectured a duality between a superstring theory and a quantum field theory without gravitational degrees of freedom, in the sense that the background geometry is fixed. The physical content of both theories turns out to be the same. This is very remarkable, as the superstring theory is defined in a higher dimensions than the quantum field theory, to which it is conjectured to be dual. Moreover, it was the first realisation of the *holographic principle* which was coined by Susskind [14] and 't Hooft [13], who were proposing it as a guiding principles for the formulation of quantum gravity.

As was mentioned in the previous section, type IIB string theory supports D-branes of even dimensionality. Maldacena investigated the large-N limit of type IIB superstring theory with a stack of N coincident D3-branes whose embedding into the ten dimensional spacetime of type IIB string theory is given in table 2.1. The dots denote the dimensions in which the branes are extended, whereas the dashes denote those in which they are fixed. They span four dimensions, including the temporal one.

coordinates	0	1	2	3	4	5	6	7	8	9
N D3-branes	•	•	•	•	–	–	–	–	–	–

Table 2.1: Embedding of D3-branes as used by Maldacena to derive the original AdS/CFT correspondence [15]

In superstring theory, there are two points of view when it comes to D-branes: On the one hand, they supply Dirichlet boundary conditions for open strings picture and on the other hand, they act as sources to supergravity, so they generically couple to closed strings. In the following, we will describe

superstring theory with a fixed stack of N D3-branes from both perspectives and see, how two different theories emerge in the low energy limit. Then, by applying a combined strong coupling and large-N limit, the theories further reduce to classical supergravity (replacing the superstring theory) and a strongly coupled $\mathcal{N} = 4$ super-Yang-Mills (SYM) theory.

Open string picture

From the point of view of open strings, D-branes can be regarded as objects on which strings can end. That is, they set Dirichlet boundary conditions on the world area theory of the strings, which after all is also where the D-branes got their name from. In this case, the strings are defined in terms of perturbation theory and we need a small string coupling $g_s \ll 1$ in order for this to be reliable.

At low energies, the theory is described by the worldvolume theory on the branes, which is given by a supersymmetric gauge theory with gauge group $U(N)$ and effective coupling $N\, g_s$ for N D-branes. For D3-branes, the decomposition of the perturbative open string excitations yields six scalar fields ϕ^i (encoding the position of the D3-brane in the six dimensions transversal to it) and a $U(N)$ gauge field A_μ (for the four parallel dimensions to the D3-branes) in the bosonic sector of the worldvolume theory.

At leading order in α', we can decompose the bosonic full action into

$$S = S_{\text{open}} + S_{\text{closed}} + S_{\text{int}}\,, \tag{2.28}$$

where the closed string action reads

$$S_{\text{closed}} = \frac{1}{2\,\kappa} \int \mathrm{d}^{10}x\, \sqrt{g} e^{-2\phi} \left(R + 4\,\partial_M \phi\, \partial^M \phi\right) + \dots\,, \tag{2.29}$$

where $2\,\kappa'^2 = (2\pi)^7\, \alpha'^4\, g_s^2$, ϕ is the dilaton and R the curvature scalar of the metric g. The open string part finds its origins in the DBI action (2.12) for D3-branes,

$$S_{\text{DBI}} = \frac{-1}{(2\pi)^3\, \alpha'^2\, g_s} \int \mathrm{d}^4x\, e^{-\phi} \sqrt{-\det\left(X_* g + 2\pi\alpha' F\right)}\,, \tag{2.30}$$

where $X_* g$ denotes the pullback of the metric w.r.t. the embedding $X : Dp \hookrightarrow \mathcal{M}$. Here, we take $\mathcal{M}$ to be 10 dimensional Minkowski space. Expanding this action for small fluctuations around the background embedding yields

$$S_{\text{open}} = \frac{-1}{2\pi\, g_s} \int \mathrm{d}^4x\, \left(\mathrm{Tr}\left(\frac{1}{4} F_{\mu\nu} F^{\mu\nu}\right) + \frac{1}{2} \eta^{\mu\nu}\, \partial_\mu x^i\, \partial_\nu x^i\right) + \dots \tag{2.31}$$

where we defined six scalars $x^i = X^{i+3}/2\pi\,\alpha'$ on the worldvolume which describe the fluctuations of the embedding in the directions transverse to the D3-branes. The leading order interaction term between the dilaton and the gauge field is given by

$$S_{\text{int}} = \frac{-1}{8\pi\, g_s} \int \mathrm{d}^4x\, \mathrm{Tr}\,(\phi\, F_{\mu\nu} F^{\mu\nu}) + \dots \tag{2.32}$$

In the limit $\alpha' \to 0$, the action (2.31) turns out to be identical to the bosonic part of the action of $\mathcal{N} = 4$ Super-Yang-Mills theory in $3+1$ dimensions at a coupling $g_{YM}^2 = 2\pi\, g_s$. In the same limit, the action (2.29) yields free type IIB supergravity since the gravitational coupling $\kappa^2 \sim \alpha'^4 \to 0$ vanishes. The interaction term (2.32) vanishes, too, which is due to the action (2.32) not being canonically normalised. Upon rescaling the dilaton, we find that $S_{\text{int}} \sim \kappa$, which vanishes in the same limit.

Hence, we can summarise that D3-branes from the point of view of open strings yield two decoupled theories as we take the limit $\alpha' \to 0$: On the one hand, the open string action yields $\mathcal{N} = 4$ $SU(N)$ Super-Yang-Mills theory on the worldvolume of the stack of N D3-branes i.e. in 3+1 dimensions. On the other hand, we find free type IIB supergravity in ten dimensions.

Closed string picture

The starting point for the closed string point of view is that D3-branes are also massive extended objects in type IIB supergravity, which is the point-like limit of type IIB superstring theory. As already mentioned around (2.18), D-branes can be regarded as solitonic solutions of that theory, sourcing the gravitational field. Such solutions feature a curvature radius L which needs to be large in order for perturbation theory to be reliable in supergravity. In the described case, due to (2.26), this means that $N\, g_s \gg 1$, which is the exact opposite of what is required for perturbation theory on the worldvolume theory, as $N\, g_s = g_{YM}^2$ describes the coupling of the Super-Yang Mills theory.

If we evaluate the discussion in section 2.1 for D3-branes, a solution ansatz for the type IIB supergravity action is given by

$$\mathrm{d}s^2 = H(r)^{-1/2}\, \eta_{\mu\nu}\, \mathrm{d}x^\mu \mathrm{d}x^\nu + H(r)^{1/2} \delta_{ij} \mathrm{d}x^i \mathrm{d}x^j\,, \tag{2.33}$$

$$e^{2\,\phi} = g_s^2\,, \tag{2.34}$$

$$C_{(4)} = \left(1 - H(r)^{-1}\right) \mathrm{d}x^0 \wedge \mathrm{d}x^1 \wedge \mathrm{d}x^2 \wedge \mathrm{d}x^3 + \mathrm{d}x^4\,, \tag{2.35}$$

where $\mu, \nu \in \{0,1,2,3\}$, $i, j \in \{4, \dots, 9\}$, and H is given by $H(r) = 1 + L^4/r^4$ with the curvature radius $L^4 = 4\pi\, g_s\, N\, \alpha'^2$. There are two important limits for H, given by its two summands. If $r \ll L$, which is called the *near-horizon*

limit, it is given by $H \approx L^4/r^4$, while for $r \gg L$ it approximately 1. If we consider the metric in the near-horizon limit, we find

$$\begin{aligned} \mathrm{d}s^2 &= \frac{r^2}{L^2}\,\eta_{\mu\nu}\,\mathrm{d}x^\mu \mathrm{d}x^\nu + \frac{L^2}{r^2}\,\delta_{ij}\,\mathrm{d}x^i \mathrm{d}x^j \\ &= \frac{L^2}{z^2}\left(\eta_{\mu\nu}\,\mathrm{d}x^\mu \mathrm{d}x^\nu + \mathrm{d}z^2\right) + L^2\,(\mathrm{d}s^2)_{S^5}\,, \end{aligned} \tag{2.36}$$

where in the second equality, we mapped $z = L^2/r$ and $(\mathrm{d}s^2)_{S^5}$ is the metric on the S^5-sphere. The approximation in the near-horizon limit is the metric for $\mathrm{AdS}_5 \times S^5$. If we take the second limit $r \gg L$, the metric reduces to ten-dimensional Minkowski space

$$\mathrm{d}s^2 = \eta_{MN}\,\mathrm{d}X^M\,\mathrm{d}X^N\,, \tag{2.37}$$

where $M, N \in \{0, \ldots, 9\}$.

Combining those two limits, we find closed strings of two kinds: Those close to the stack of N D3-branes ($r \ll L$) and those far away ($r \gg L$). Of course, there is also an intermediate regime where $r \approx L$. However, if we assume r/α' to be fixed while we send $\alpha' \to 0$, we find that the closed strings near the D3-branes and those far away decouple. This particular limit is called the *Maldacena limit*, due to its origin in [15].

To summarise, the closed strings far away from the branes yield free type IIB supergravity and those close to the branes are perturbations of the $\mathrm{AdS}_5 \times S^5$ solution to type IIB supergravity. A valid UV-completion to the latter is known to be type IIB superstring theory, so we regard it as type IIB superstring theory in the perturbative regime.

The whole picture

Combining both points of view we have for the stack of N D3-branes, we saw two different theories emerge in the decoupling limit, both of which contained two decoupled theories on their own. In the open string perspective, we find $\mathcal{N} = 4$ $SU(N)$ Super-Yang-Mills theory in $3+1$ dimensions plus an additional free type IIB supergravity theory in ten dimension. The closed string perspective gave us type IIB string theory on $\mathrm{AdS}_5 \times S^5$ close to the branes and, once more, free type IIB supergravity theory in ten dimensions.

Both theories contain free type IIB supergravity in ten dimensions as a factor, which obviously is equivalent. The non-trivial part is to conjecture that the other factors, given by $\mathcal{N} = 4$ $SU(N)$ Super-Yang-Mills theory in $3+1$ dimensions on one hand and type IIB string theory on $\mathrm{AdS}_5 \times S^5$ on the other, are *also* equivalent.

This is the *AdS/CFT conjecture*, first suggested in [15]. In order for the conjecture to work, we find that the parameters of both theories need to be related to each other by

$$g_{YM} = \sqrt{2\pi\, g_s} \qquad \text{and} \qquad L^4 = 2\, g_{YM}^2\, N\, \alpha'^2\,, \tag{2.38}$$

where the first identity comes from identifying the action (2.31) with the bosonic part of $\mathcal{N} = 4$ Super Yang-Mills and the second one is given by (2.26) for a stack of N D3-branes.

There are several versions of the conjecture on the market. What we stated above is known as the *strong* form of the conjecture, which is highly non-trivial. However, probably the best understood version of the statement is the *weak* form of the conjecture. It takes two more limits into account.

Firstly, we can take the *large-N* limit, $N \to \infty$. On the field theory side, this is physically sensible only if we additionally require $\lambda := g_{YM}^2\, N$ to stay finite, which is called the *'t Hooft-limit* with λ the 't Hooft-coupling [78]. Looking at the parameter relations (2.38), this yields finite L^2/α' but $g_s \ll 1$. So the string coupling and, hence, loop amplitudes are suppressed and we end up with string theory at tree level, which is classical string theory on $\mathrm{AdS}_5 \times S^5$ on the gravity side of the duality. The field theory side will be a $SU(\infty)$ gauge theory, however with $N\, g_{YM}^2$ finite, which is called the *planar limit.*. This reflects the fact that only Feynman diagrams with planar topology are non-vanishing.

Secondly, we can send the 't Hooft coupling to infinity, $\lambda = g_{YM}^2\, N \to \infty$. So on the field theory side, we not only have an $SU(\infty)$ gauge theory, but it is moreover strongly coupled. Looking at the relations (2.38) again, we see that the gravity side reduces to a much more tractable one: $\lambda \to \infty$ corresponds to $\alpha'/L^2 \to 0$, i.e. the string length $l_s = \sqrt{\alpha'}$ is vanishing compared to the curvature radius of $\mathrm{AdS}_5 \times S^5$. This is great if we want to compute anything, as the classical type IIB string theory can be well approximated by type IIB supergravity in this pointlike limit.

It is this last version, the *weak* form of the duality, which is mostly used in the literature. We have a weakly coupled classical gravity theory dynamically dual to a strongly coupled quantum gauge theory. Usually, faced with the latter, we cannot compute any correlators analytically anymore and need to resort to numerical techniques such as lattice theory, which are restricted in their usage, especially in this case. The AdS/CFT conjecture, however, equipped us with a mighty tool to elaborate such theories even in the worst case scenario of infinite coupling.

2.2.2 Field-operator map

Apart from its conceptual beauty, the whole point of AdS/CFT duality is to be able to compute physically sensible results. In physics, this means we need to compute correlators. A part of the prescription for doing this by applying the AdS/CFT duality is known as the field-operator map. It maps fields on the gravity side of the duality to corresponding gauge-invariant operators on the field theory side, and vice versa. This can be done for various sorts of operators like scalars, conserved currents, fermions, etc. The scope of this thesis will be about scalar operators, so we will restrict this section to an overview on how to deal with them. At the end, we will see the duality at its computational level, i.e. as an equivalence of the generating functionals of both theories.

Considering all gauge-invariant scalar operators in $\mathcal{N} = 4$ $SU(N)$ Super-Yang-Mills theory, an involved decomposition of the type IIB supergravity action yields that there are scalar fields for every one of them on the gravity side of the correspondence. They contribute to the action in a similar fashion as

$$S = -n \int \mathrm{d}^d \, \mathrm{d}z \, \sqrt{g} \, \left(g^{\mu\nu} \, \partial_\mu \phi \, \partial_\nu \phi + V(\phi) \right) \,, \tag{2.39}$$

where $n \sim N^2$ is a normalisation factor, $V = m^2 \, \phi^2 + O(\phi^4)$ is the scalar potential. To get here, we already performed a Kaluza-Klein decomposition of the form

$$\Phi(z, x, y) = \sum_i^\infty \phi^i(z, x) \, \mathcal{Y}^i(y) \,, \tag{2.40}$$

where the $\mathcal{Y}^i$ are spherical harmonics on S^5, z is the radial coordinates introduced in (2.36), and x and y denote the rest of the coordinates in the AdS- and S^5-factor of the same metric, respectively. We then suppressed the index i for the scalar fields to keep the notation simple.

By varying (2.39) w.r.t. ϕ, we obtain the equation of motion for the scalar field which is of course just the Klein-Gordon equation in AdS_5,

$$g^{\mu\nu} \, \nabla_\mu \nabla_\nu \, \phi = \partial_\phi V(\phi) \,. \tag{2.41}$$

A great deal of computations in gauge/gravity duality involves boundary analysis of the fields at asymptotic infinity, i.e. around $z \to 0$. This can easily be done here by inserting a power-law ansatz $\phi \sim c(x) \, z^\Delta$ into its equation of motion, which after Fourier transforming the x-coordinates to their corresponding momenta k^μ yields

$$\left(\Delta^2 - d \, \Delta + L^2 m^2 \right) z^\Delta - k^2 z^{\Delta+2} = 0 \,. \tag{2.42}$$

At asymptotic infinity, $z \to 0$, this equation is satisfied if and only if Δ is equivalent to one of the $\Delta_\pm$ given by

$$\Delta_\pm \equiv \frac{1}{2}\left(d \pm \sqrt{d^2 + 4\,L^2\,m^2}\right)\,, \tag{2.43}$$

which gives us two independent modes for a second order differential equation in z as expected. Note, that one of these modes, Δ_+, is *normalisable*, while the other one, Δ_-, is *non-normalisable* in the sense that the action (2.39) is finite or diverging, respectively, if we substitute the asymptotic modes for the scalar field.

Once the two independent asymptotic modes are found, we can expand (2.42) order by order in the radial coordinate z. The coefficients of higher-order terms can generically be solved in terms of the two coefficients of the asymptotic modes.

Some fanciness of AdS-space enters the game at this point. Due to its negative scalar curvature, it supplies a positive contribution $d^2\,\phi^2/4$ to the scalar potential. Hence, even a negative mass square $m^2 < 0$ can result in a stable scalar theory in AdS-space, if it satisfies

$$m^2 \geq -d^2/4\,L^2\,, \tag{2.44}$$

which is called the Breitenlohner-Freedman bound [79]. As we can see in equation (2.43), this simply corresponds to the point at which the square root vanishes. Lower masses would imprint themselves in imaginary asymptotic boundary expansions, which do not make sense anymore. If the Breitenlohner-Freedman bound is saturated, it seems like there is only one valid asymptotic solution to the scalar equation of motion available. This, however, cannot be true for a second order differential equation. The solution to this puzzle is that there is another mode of the same power in z, but with a logarithmic factor $\log(z)$ entering the expansion at leading order, i.e. $\phi(z,x) \sim z^{\Delta_*}(a + b\log(z))$, where $\Delta_* = d/2$. At higher order in the asymptotic expansions, the order of logarithmic terms will increase with each order in z, which makes computing the expansions considerably harder. This is the case we will encounter in the main part of this thesis, due to fixing the conformal dimension of the scalar operator to $d/2$ which saturates the Breitenlohner-Freedman bound.

It turns out, that the (non-)normalisable modes have a precise physical meaning in the context of AdS/CFT correspondence. In [16, 80], it was suggested that they encode the vacuum expectation value and the source of the dual scalar operator on the field theory side of the duality. Moreover, the leading powers in the expansion (2.43) encode the conformal dimension of this

operator. By applying dimensional analysis, we find that the normalisable mode yields the vacuum expectation value $\langle \mathcal{O} \rangle$, while the scalar operator's source J is equivalent to the non-normalisable mode. The expansion of the scalar field around $z \to 0$ thus begins with

$$\phi(z, x) \sim J(x)\, z^{\Delta_-} + \langle \mathcal{O}(x) \rangle\, z^{\Delta_+} + \dots \,. \tag{2.45}$$

Usually, we add classical sources to a quantum field theory by adding a source term to the partition function, which then is called the generating functional, and depends on the source field by

$$\mathcal{Z}[J(x)] = \frac{1}{\mathcal{Z}_0} \int D[\Phi]\, e^{-S_E - \int \mathrm{d}^d x\, J(x)\mathcal{O}(x)} \,, \tag{2.46}$$

where S_E is the Euclidean action of the quantum theory and $\mathcal{Z}_0$ is the partition function without the source term. By taking variational derivatives w.r.t. the source $J(x)$, and require it to vanish afterwards, we can compute arbitrary correlation function of the system. Unfortunately, correlators computed in this fashion contain unconnected diagrams. We can factor them out by defining the generating functional for connected Green's functions as

$$\mathcal{W}[J(x)] = -\log\left(\mathcal{Z}[J(x)]\right) \equiv \left\langle e^{\int \mathrm{d}^4 x\, \mathcal{O} \cdot J} \right\rangle_{\text{conn}} \,, \tag{2.47}$$

which is closely related to the free energy, the thermodynamic potential in the canonical ensemble.

In [16, 80], the foundations were set to identify this generating functional with the on-shell action S_{SG} of the dual supergravity theory in order to compute correlation functions in the respective dual theory. In order to do this, we need to require the sources J_i to match the leading order coefficients in their corresponding fields on the gravity side, where the indices i now denote the whole set of operators and sources appearing in the theory. The identification of generating functionals is then given by

$$\mathcal{W}[J(x)] \stackrel{!}{=} S_{SG}|_{\lim_{z\to 0} \phi_i(z,x) z^{-\Delta_{i,-}} = J_i(x)} \,, \tag{2.48}$$

where the ϕ_i now denote all fields appearing in the dual gravity theory with leading order expansion powers $\Delta_{i,-}$. Why does the Euclidean action S_{SG} appear instead of the whole generating functional of the supergravity action? This is due to the fact, that we work with the weak form the the correspondence, in which we have classical supergravity instead of quantum type IIB superstring theory on the gravity side of the duality. The Euclidean action is simply the leading order saddle point approximation to the string theory

partition function for connected diagrams, which is why it is the object of interest in this context.

In order to obtain physically meaningful, i.e. finite, results, we will need to renormalise both sides of the duality as both sides of the duality. One way to see why, is that we already coined the *non-normalisable mode* to correspond to the source term in the gravity dual, and mentioning that non-normalisable means that the on-shell action, which appears also in (2.48), diverges in the presence of such a mode. The prescription to do this on the gravity side of the duality is called *holographic renormalisation* [26, 27]. Essentially, it is done by taking an IR cutoff in the gravity theory by imposing a lower bound to the radial coordinate $z = z_0 > 0$, and only integrating up to z_0 for defining the on-shell action.[2] Having introduced an additional boundary, we need to include boundary terms. The field content in these boundary terms is then chosen such that in the limit $z_0 \to 0$ the on-shell action is rendered finite and leaves a maximal symmetry group unbroken. We will not go into more details regarding the prescription of holographic renormalisation, because it will not be needed in the context of this thesis.

2.2.3 Summary

In this section, we described the derivation of the original AdS/CFT duality by Maldacena [15]. In its weak form, it describes a highly non-trivial duality between a strongly coupled quantum field theory on the on hand and a higher dimensional classical theory of supergravity at low curvatures on the other.

The sources and vacuum expectation values of the strongly coupled field theory are mapped to expansion coefficients in the dual gravity theory. To compute correlators of the strongly coupled field theory, we need to evaluate the on-shell action of the supergravity theory and take variational derivatives with respect to the sources.

We will now go on and consider generalisations to the original AdS/CFT correspondence, like the incorporation of temperature, final chemical density and entanglement entropy. Before we do this, however, we summarise the strongest form of the duality in the following box, which it deserves:

[2] Remember that $z = L^2/r \to 0$ at asymptotic infinity, so imposing a cutoff near $z = 0$ really is a IR cutoff in the gravity theory. It is interesting to note at this point that the IR divergencies of the gravity side correspond to UV divergencies of the field theory side. This is one of the reasons why the radial coordinate r can be identified with the energy scale μ of the renormalisation group flow on the field theory side. So, the AdS/CFT correspondence is often thought of as geometrising the renormalisation group flow of the field theory.

The AdS/CFT conjecture - strongest form

$\mathcal{N} = 4$ $SU(N)$ Super Yang-Mills theory with coupling constant g_{YM}

is dynamically equivalent to

type IIB superstring theory with string length $l_s = \sqrt{\alpha'}$ and string coupling g_s on $\mathrm{AdS}_5 \times \mathrm{S}^5$ with radius L and N units of $F_{(5)}$-flux through S^5

where

$$g_{YM}^2 = 2\pi g_s\,, \qquad 2\, g_{YM}^2\, N = L^4/\alpha'^2\,.$$

2.3 Generalisations of AdS/CFT

The original AdS/CFT correspondence provides a powerful method to understand $\mathcal{N} = 4$ $SU(N)$ Super-Yang-Mills theory in the large-N and strongly coupled limit from a new point of view. However, so far it is defined at zero temperature and without classical sources like chemical potentials. The correspondence is promising to shed light on universal features e.g. in condensed matter theory or heavy-ion collisions. In such setups, however, we need to incorporate different circumstances, which include the coupling of the system to a reservoir at finite temperature and finite chemical potential. A generalised version of AdS/CFT including such features is often referred to as *gauge/gravity duality*.

Apart from that, a promising "observable" which gained more and more attention among the quantum gravity community recently is entanglement entropy. This is a measure for the entanglement between two subspaces of the Hilbert space, where typically one chooses spatial subregions. There are suggestions how to compute entanglement entropy using holography. In this section we will first explain how to model environments at finite temperature and finite density holographically. Finally, the holographic dual to entanglement entropy on the gravity side of the duality is introduced.

2.3.1 Digression: Statistical ensembles and potentials

We want to model strongly coupled quantum systems at finite temperature and density. Thereby, we automatically enter the regime of thermodynamics.

This section is devoted to remind us of the fundamental concepts of statistical mechanics, so that we are able to generalise these to holographic dualities. To begin with, we recapitulate the most important thermodynamic potentials which follow from the microcanonical, the canonical, and the grand canonical ensemble on a classical level. Then we proceed by explaining how to deal with quantum systems in the same manner. This will be useful to explain the notion of entanglement entropy and the related topic of why event horizons are always associated with a temperature.

In the *microcanonical ensemble* we consider the total energy of the system fixed. The microcanonical partition function is then defined as the number of all microstates of total energy E by

$$\mathcal{Z}_{\text{micro}} = \text{Tr}(1)\,, \tag{2.49}$$

where Tr defines the sum over all accessible states. The crucial assumption in the microcanonical ensemble is that we assign the same probability $p = 1/\mathcal{Z}_{\text{micro}}$ to all states accessible at the fixed energy E. Now, we are able to define the *entropy* of the system as

$$S = \langle \log(\mathcal{Z}_{\text{micro}}) \rangle = \langle \log(1/p) \rangle = -\langle \log(p) \rangle = -\text{Tr}\left(p \, \log(p)\right)\,. \tag{2.50}$$

Consider the configuration of the classical system to be a random variable over the probability distribution set by the uniform probability $p = 1/\mathcal{Z}_{\text{micro}}$. The entropy then defines the average *surprise* per sampling[3], if we draw a random state from the set of possible states of total energy E, and is indeed maximised if we use the uniform probability. The entropy of the system is the thermodynamic potential of the microcanonical ensemble, meaning that we can use it to derive macroscopic information about the system. For example, the statistical definition of the inverse temperature β of the system is given by deriving the entropy with respect to the energy,

$$\beta \equiv \frac{\partial S}{\partial E}\,. \tag{2.51}$$

Likewise, the pressure p is defined by deriving w.r.t. the volume V, and chemical potentials μ_k are defined by deriving w.r.t. fixed particle numbers N_k where k labels different sorts of particles. To summarise, the entropy $S(E, V, N_k)$ is the thermodynamic potential of the microcanonical ensemble, in which the independent variables are the energy E, the volume V and the

[3] To obtain the connection between expected surprise and entropy, we can think about a system in which one of the states has probability $p_0 = 1$ and, due to normalisation, all other states obey $p_i = 0$. Then, the entropy is zero due to (2.50), which is intuitive, since we know the outcome of making observations in advance.

particle numbers N_k. Other ensembles are defined by performing Legendre transformations on one or more of the conjugated variables (E, β), (V, p) and (N_k, μ_k).

The *canonical ensemble* follows from the microcanonical ensemble by a Legendre transformation of (E, β), i.e. instead of the energy E, we use the temperature T or, equivalently, its inverse β as independent variable. The new thermodynamic potential is the (Helmholtz) free energy F which is defined by

$$\beta\, F(\beta, V, N_k) = \beta E(\beta) - S(E(\beta), V, N_k)\,. \tag{2.52}$$

Physically, this requires us to couple the system of interest to an infinite heat bath. Under the assumption that changes in our system are negligible for the temperature in the heat bath, one can derive that the partition function of the system becomes

$$\mathcal{Z}_{\text{can}} = \operatorname{Tr} \exp\left(-\beta E\right)\,. \tag{2.53}$$

Hence, the contribution of states to the partition function is weighted by $\exp(-\beta E)$. Unlike fixing the energy, fixing the temperature in an experimental environment is much more convenient, which is why the canonical ensemble is more useful for applications.

For the same reason and especially in condensed matter applications, it is unfeasible to keep the particle number fixed. The intrinsic quantity associated to the particle number is the chemical potential. The *grand canonical ensemble* follows from the Legendre transformation of (N_k, μ_k), which exchanges the particle numbers and chemical potentials as independent variables. Once again, this need us to couple our system to an infinite particle reservoir for each particle sort labelled by k. The thermodynamic potential is given by the Landau free energy Ω, which is defined as

$$\Omega(\beta, V, \mu_k) = F(\beta, V, N_k(\mu_k)) - \mu_k\, N_k(\mu_k)\,. \tag{2.54}$$

In order to fix the associated chemical potentials μ_k instead of the particle numbers, we change to the grand canonical ensemble by defining its partition function $\mathcal{Z}_{\text{grand}}$ as

$$\mathcal{Z}_{\text{grand}} = \operatorname{Tr} \exp\left(-\beta\left(E - \sum_k \mu_k N_k\right)\right)\,. \tag{2.55}$$

If we want to proceed to quantum systems, we need to initialise some notation. First of all, quantum mechanics deals with states $|\Psi\rangle \in \mathcal{H}$ which are vectors in some Hilbert space $\mathcal{H}$. A state is said to be *pure* if it is a vector

in $\mathcal{H}$. We can compute expectation values of observables $\mathcal{O}$ in the state $|\Psi\rangle$ by

$$\langle\mathcal{O}\rangle_\Psi = \langle\Psi|\mathcal{O}|\Psi\rangle \ , \tag{2.56}$$

where $\langle\Psi|$ is the co-vector to $|\Psi\rangle$ w.r.t. the scalar product defined over $\mathcal{H}$.

Given a state $|\Psi\rangle$, we can define a projection operator $\rho_\Psi \equiv |\Psi\rangle\langle\Psi|$, which is also called the *state/density matrix/operator*, where all four possible notations appear equivalently in the literature. Any expectation values can now be rewritten in the form

$$\langle\mathcal{O}\rangle_\Psi = \mathrm{Tr}\,(\rho_\Psi\mathcal{O}) \ , \tag{2.57}$$

where the trace Tr sums over an arbitrary normalised orthogonal set of basis vectors of the Hilbert space, e.g. eigenstates of the Hamilton operator. We can define a *mixed state* by

$$\rho = \sum_i p_i \ |\phi_i\rangle\langle\phi_i| \ , \tag{2.58}$$

where $|\phi_i\rangle \in \mathcal{H}$ and the probabilities of each state p_i are normalised, $\sum_i p_i = 1$. A mixed state is a genuine statistical mixture of pure states and, in general, there is no way to define a pure state $|\Psi\rangle$ whose state operator matches the one of the mixed state. The state operator always satisfies $\mathrm{Tr}\rho = 1$. If and only if the density matrix is the projection operator of a pure state, it also satisfies $\rho^2 = \rho$ or, equivalently, $\mathrm{Tr}(\rho^2) = 1$.

In the context of thermodynamics, the state matrix ρ replaces any occurrences of the probability distribution p in the discussion about classical statistical mechanics. We always have a Hamilton operator $\hat{H}$ defining the dynamics of the quantum theory. In equilibrium, any operators and states are supposed to be stationary. This means that, in particular, the state operator ρ commutes with the Hamilton operator,

$$\partial_t\rho \equiv [\rho, \hat{H}] = 0 \, , \tag{2.59}$$

which means that both operators can be diagonalised simultaneously in terms of energy eigenstates $\hat{H}\,|i\rangle = E_i\,|i\rangle$.

The microcanonical ensemble is then given by defining the partition function as in (2.49), but the trace being over all energy eigenstates $|i\rangle$ with eigenvalues $E_i = E$. The microcanonical partition function $\mathcal{Z}_{\mathrm{micro}}$ then just turns out to be the multiplicity of the energy level E.[4] The von Neumann

[4] Obviously, there are problems in this definition, because the energy levels of a quantum system are typically discrete and hence the derivatives w.r.t. the energy are probably not well-defined. The technical solution to this is to define an energy width ΔE in which the states may be, which also explains the terminology for the *density* operator.

entropy associated with a given the state operator reads

$$S(\rho) = -\mathrm{Tr}\left(\rho \log \rho\right) , \tag{2.60}$$

where $\log \rho$ is well-defined due to the state matrix being diagonalisable.

In the canonical ensemble, similar to the probability of a configuration of energy E in the classical context, the state matrix is now given by

$$\rho = \frac{1}{\mathcal{Z}_{\mathrm{can}}} e^{-\beta \hat{H}} , \tag{2.61}$$

where $\mathcal{Z}_{\mathrm{can}}$ is the canonical partition function

$$\mathcal{Z}_{\mathrm{can}} = \mathrm{Tr}\left(e^{-\beta \hat{H}}\right) , \tag{2.62}$$

which normalises the state operator such that $\mathrm{Tr}\rho = 1$.

Finally, in the same fashion, the grand canonical ensemble is defined by its partition function

$$\mathcal{Z}_{\mathrm{grand}} = \mathrm{Tr}\exp\left(-\beta\left(\hat{H} - \sum_k \mu_k \hat{Q}_k\right)\right) , \tag{2.63}$$

where we promoted the particle numbers N_k to conserved charge operators $\hat{Q}_k$.[5] The state operator is then likewise given by

$$\rho = \frac{1}{\mathcal{Z}_{\mathrm{grand}}} e^{-\beta\left(\hat{H} - \sum_k \mu_k \hat{Q}_k\right)} , \tag{2.64}$$

which concludes our recapitulation of both classical and quantum statistical mechanics.

2.3.2 Finite temperature

Field theory side

It is well-known how to incorporate finite temperature on the field theory side, for comprehensive reviews see e.g. [81–83]. To wrap it up, the temporal integration in the partition sum is exchanged by an integration over

[5] In quantum mechanics, particle numbers are only defined if there are global symmetries protecting them. Labelling any distinct global symmetries by k, we can derive an associated conserved charge operator $\hat{Q}_k$, which could be a number operator, for example. If there is no particle conservation, e.g. for photons which are not charged, we have to set $\mu = 0$.

imaginary time over a compact region of size β, which turns out to be the inverse temperature, $\beta = 1/k_B T$, with k_B the Boltzmann constant. Depending on the nature of the fields involved, we need to set periodic or antiperiodic boundary conditions for bosons and fermions, respectively. For zero temperature systems, a generic partition function is given by

$$\mathcal{Z} = \int \mathcal{D}[\Phi]\, e^{+i\, S[\Phi]}\,, \tag{2.65}$$

where Φ denotes the entity of field and S denotes the action of the system, given by

$$S[\Phi] = \int \mathrm{d}t \int \mathrm{d}^d x\ \mathcal{L}(\Phi)\,, \tag{2.66}$$

with $\mathcal{L}$ some Lagrangian defining the theory. By exchanging $t \to -i\tau$, we end up with the Euclidean path integral

$$\mathcal{Z}_\beta = \int \mathcal{D}[\Phi]\, e^{-S_E}\,, \tag{2.67}$$

which we already encountered in (2.46) and S_E is the Euclidean action. So far, we did nothing but a Wick rotation, which is always possible for time independent boundary conditions. However, if we compactify the integration regime of imaginary time to $\tau \in [0, \beta)$ by identifying $\tau \sim \tau + \beta$, we need to determine boundary conditions for the fields involved. It turns out that bosonic fields need periodic boundary conditions $\Phi(0) = +\Phi(\beta)$, while fermionic fields require anti-periodic boundary conditions $\Phi(0) = -\Phi(\beta)$ for this compactification to make sense. The path integral becomes

$$\mathcal{Z}_\beta = \int\limits_{\Phi(0)=\pm\Phi(\beta)} \mathcal{D}[\Phi]\ \ e^{-S_E[\Phi]}\,, \tag{2.68}$$

and compactifying the integration regime to $\tau \in [0, \beta]$, where we imposed (anti-)periodic boundary conditions in the path integral as discussed above. S_E denotes the *euclidean* action, given by

$$S_E[\Phi] = \int_0^\beta \mathrm{d}\tau \int \mathrm{d}^d x\ \mathcal{L}(\Phi)\,. \tag{2.69}$$

It's called Euclidean, because in the process of exchanging real time for imaginary time, we effectively also changed the signature of the metric from $\{-,+,+,\ldots\}$ to $\{+,+,+,\ldots\}$. The Euclidean action still contains temporal derivatives of the fields. If we require the fields and operators to be stationary, as they should be in thermal equilibrium, we see can trivially

integrate over the temporal direction, which yields a factor of β. The other factor reduces to an integration of the Hamiltonian density over all spatial dimensions, which yields the Hamiltonian $\hat{H}$ of the system. Hence, we see that (2.67) defines the canonical partition function in the sense of statistical mechanics,

$$\mathcal{Z}_{\text{can}} = \int\limits_{\Phi(0)=\pm\Phi(\beta)} \mathcal{D}[\Phi] \;\; e^{-\beta\, H[\Phi]} = \text{Tr}\left(e^{-\beta\, \hat{H}[\Phi]}\right) . \tag{2.70}$$

With the state operator defined in the usual way

$$\rho = \frac{1}{\mathcal{Z}_{\text{can}}}\, e^{-\beta\, \hat{H}[\Phi]} , \tag{2.71}$$

the free energy of the system is given by

$$F = T \log\left(\mathcal{Z}_{\text{can}}\right) \approx T \log(S_E) , \tag{2.72}$$

where we performed a saddle point approximation for the second equality. The latter, of course, is only possible for weakly coupled systems, which will not be the case in the weak form of the gauge/gravity duality.

Gravity side

On the gravity side of the duality, the incorporation of temperature appear both naturally and astonishing. Since the seminal paper by Hawking [10], it is known that we can assign a temperature to black holes in the semiclassical regime. More precisely, it was shown that black holes emit particles with an emission spectrum matching that of a perfect black body at a certain temperature, called *Hawking temperature* T_H. In an asymptotically flat Schwarzschild geometry, the Hawking temperature is given in terms of the mass of the black hole by

$$T_H = \frac{\hbar c^3}{8\pi k_B G_N M} \tag{2.73}$$

where we used SI units to show the equation in its full glory, combining constants from quantum mechanics, gravitation and thermodynamics altogether. Most remarkable, the temperature of the black hole decreases with its mass, imprinting itself in negative heat capacity leading to instability of the black hole. While evaporating due to the mentioned Hawking radiation, black holes in asymptotically flat geometries are getting hotter and hotter. Their ultimate faith is subject to speculation. Only a full theory of quantum gravity will be able to solve the dynamics as the curvature at the event

horizon enters the regime in which Hawking's semiclassical analysis is not reliable anymore.

For asymptotically curved backgrounds, the situation is different. Especially in asymptotically AdS spaces, the temperature of black holes grows with their mass, so that for negative cosmological constants, black holes can be thermodynamically stable. For the finite temperature generalisation of the AdS/CFT conjecture, the objects responsible for the temperature on the gravity side are actually near-extremal Dp-branes, which can be used in the same fashion as the Dp-branes for the derivation of the original conjecture. These are non-BPS solutions to type IIB supergravity with metric

$$\mathrm{d}s^2 = H(r)^{-1/2}\left(-f(r)\,\mathrm{d}t^2 + \mathrm{d}x^2\right) + H(r)^{1/2}\left(\frac{\mathrm{d}r^2}{f(r)} + r^2\,\left(\mathrm{d}s^2\right)_{S^5}\right) \quad (2.74)$$

with $H(r) = 1+L^4/r^4$ and $f(r) = 1-r_H^4/r^4$. The solution looks familiar from equation (2.33), but has the additional blackening factor $f(r)$ in its tt and rr-components. This yields an event horizon at $r = r_H$, where $g_{tt}(r_H) = 0$. In the same near horizon limit $r \ll L$ and by changing coordinates to $z \equiv L^2/r$ as in the BPS case, the background metric on which perturbative superstring theory is defined is now given by

$$\mathrm{d}s^2 = \frac{L^2}{z^2}\left(-h(z)\,\mathrm{d}t^2 + \mathrm{d}x^2 + \frac{\mathrm{d}z^2}{h(z)}\right) + L^2\left(\mathrm{d}s^2\right)_{S^5}\,, \quad (2.75)$$

where we defined $h(z) = f(L^2/z)$. This is a black hole or black brane in asymptotically AdS space, respectively, depending on whether or not we compactify the x-directions.

One way to see why black holes are thermal objects is by performing the same mathematical procedure as for quantum field theories at finite temperature: We perform a Wick rotation $t \to -i\tau$ and, in addition, have a closer look at what happens near the event horizon at $z = z_H$ by introducing another radial variable $\rho^2 = L^2\left(1 - \frac{z}{z_H}\right)$. The metric becomes

$$\mathrm{d}s^2 = \mathrm{d}\rho^2 + \rho^2\,\left(\frac{4}{z_H^2}\,\mathrm{d}\tau^2\right) + \frac{L^2}{z_H^2}\,\mathrm{d}x^2 + L^2\left(\mathrm{d}s^2\right)_{S^5}\,. \quad (2.76)$$

If we neglect the last two summands of this metric, it looks similar to a flat metric around $\rho = 0$, which is the location of the event horizon. Event horizons are non-local concepts of (super)gravity, meaning that in general we can only find their positions if we know the metric globally. Hence, it should not display any special local behaviour like curvature singularities or topological kinks. However, for a metric of the form $\mathrm{d}s^2 = \mathrm{d}\rho^2 + \rho^2\,\mathrm{d}\phi^2$,

there exists the possibility of a *conical singularity*, at $\rho = 0$, if the angular coordinate is not 2π-periodic. Requiring that the metric at hand is really flat at $\rho = 0$, we find that τ needs to be periodic, $\tau \sim \tau + \beta$ and its period is determined by

$$\left(\frac{2}{z_H}\beta\right)^2 \stackrel{!}{=} (2\pi)^2 \,, \tag{2.77}$$

which yields $\beta = \pi z_H$. Like in thermal field theory, we identify $\beta = 1/T_H$, where T_H is now the Hawking temperature associated with the black hole or brane, and obtain

$$T_H = \frac{1}{\pi z_H} \,. \tag{2.78}$$

We remember that $z = L^2/r$, so z_H really is a length scale, where, however, larger z_H means smaller black holes/branes due to its definition. Due to the relation we just derived, we see that in asymptotic AdS-space, larger black holes have higher temperature. This renders them thermodynamically stable, as their heat capacity, unlike in asymptotically flat spacetimes, is positive.

The conclusion of this section is, that the original AdS/CFT conjecture can be generalised to $\mathcal{N} = 4$ $SU(N)$ Super Yang-Mills theory at finite temperature T if the gravity side of the duality has a black brane with Hawking temperature T_H, which we identify with the field theory temperature, $T \equiv T_H$. Just like the original AdS/CFT correspondence is really an equivalence of the microcanonical partition functions by (2.48), in the canonical ensemble we have to identify the free energies of both theories [16, 84]. Thermal correlators can then be derived by functional derivatives on both sides.

2.3.3 Finite chemical potential

As we already discussed in section 2.3.1, especially for applications in condensed matter theory it is beneficial to apply the grand canonical ensemble, in which we fix the chemical potentials μ_k instead of the conserved charges. To be able to apply this to the AdS/CFT conjecture, first of all we need conserved charge operators $\hat{Q}_k$ on the field theory side which arise from global symmetries labelled by the index k. Here, we want to show how this is done in the simplest case, where we consider a complex scalar operator $\mathcal{O}$ on the field theory side which is charged under a $U(1)$-symmetry.

Field theory side

In this case, a generic toy model for the scalar action on the field theory side could look like

$$S = -\int \mathrm{d}^4x\, \eta^{\mu\nu}\, \partial_\mu \mathcal{O}^\dagger\, \partial_\nu \mathcal{O} + V(\mathcal{O}^\dagger \mathcal{O})\,, \tag{2.79}$$

which is invariant under the global $U(1)$-transformation $\mathcal{O} \to e^{i\phi}\mathcal{O}$, with constant $\phi \in \mathbb{R}$. The conserved current associated to this global symmetry is then readily derived to read

$$J^\mu = \eta^{\mu\nu} \left(\mathcal{O}^\dagger\, \partial_\nu \mathcal{O} - \mathcal{O}\, \partial_\nu \mathcal{O}^\dagger\right)\,, \tag{2.80}$$

which satisfies the continuity equation $\partial_\mu J^\mu = 0$. Upon integrating over the spatial directions, we can define a conserved charge operator $\hat{Q}$ given by

$$\hat{Q} \equiv \int \mathrm{d}^3x\, J^0\,, \tag{2.81}$$

which is conserved in time in the sense that $\partial_t \hat{Q} = 0$. This is the charge operator appearing in the grand canonical ensemble in the discussion of quantum statistical mechanics in section 2.3.1. We can now change to the grand canonical ensemble by fixing the conjugated chemical potential μ to this conserved operator.

In field theory, conserved currents can couple to gauge fields and we can impose the chemical potential by promoting the global $U(1)$-symmetry to a local $U(1)$ gauge symmetry. For this, we introduce a gauge field A_μ and require that its temporal component has a vacuum expectation value $\langle A_0 \rangle = \mu$ around which we may further quantise the gauge field fluctuations. Because in a gauge invariant Lagrangian, the covariant derivative of the charged scalar operator $\mathcal{O}$ is given by $D_\mu \mathcal{O} = \partial_\mu \mathcal{O} + i\, A_\mu \mathcal{O}$, the scalar field obtains an additional term to its potential, which is given by $\tilde{V}(\mathcal{O}^\dagger \mathcal{O}) = \mu^2\, \mathcal{O}^\dagger \mathcal{O}$. So, essentially, changing the chemical potential will shift the probabilities of generating charged particles, like the scalar operator in our example.

Due to this shift in creation and annihilation probabilities, the conserved charge operator for particles charged under the respective symmetry will have an average value $\langle \mathcal{O} \rangle$, which shifts if we change the chemical potential but is free to fluctuate around that expectation value. This is exactly what we expect in the grand canonical potential.

Gravity side

On the gravity side of the duality, we need to incorporate a gauge field A_m, $m \in \{0, \ldots, 4\}$ which is the holographic dual to the conserved (global)

current J^μ on the field theory side. It will have an additional component due to the emerging radial direction. However, this already tell us how to perform gauge fixing in a canonical fashion in the AdS/CFT correspondence: We fix the radial component to vanish, $A_r = 0$, which is done almost exclusively in the literature. A generic toy gravity model dual to the discussion on the field theory side could then look like

$$S = -\int d^5x \sqrt{g} \left(g^{mn} D_m \Phi^\dagger D_n \Phi + \frac{1}{4} F_{mn} F^{mn} + V(\Phi^\dagger \Phi) \right) , \tag{2.82}$$

where the potential V has, a priori, nothing to do with the potential on the field theory side. Asymptotically, a solution for the gauge field equations of motion is given by

$$A_0 = \mu + \rho\, z + \dots \tag{2.83}$$

where μ is just the chemical potential we want to fix. Obviously, on the gravity side, this can now be performed by fixing the boundary conditions of the gauge field to read $\lim_{z\to 0} = \mu$. The other leading order expansion coefficient will in the spirit of what was already discussed in section 2.2.2 be mapped to the vacuum expectation value of the dual operator. This is the conserved current given in (2.80), or actually its temporal component, the charge density ρ. The vacuum expectation value of the conserved charge operator on the field theory side is then given by integrating over the spatial components. By this, we see that q really denotes the charge density. This makes sense, since in this model, the chemical potential $\mu(x)$ is a function over the spatial components, so it could vary along the spatial directions. To obtain the vacuum expectation value of the conserved charge $\langle \hat{Q} \rangle$ right ahead, we could also compute the electric flux of the dual gauge field at the asymptotical boundary directly via

$$\langle \hat{Q} \rangle \equiv \mathcal{C} \equiv \lim_{z\to 0} \int_{S^d} *F = \lim_{z\to 0} \int_{S^d} \sqrt{\gamma} F^{rt} \, . \tag{2.84}$$

This is something we will encounter again in the main part of this thesis, although the electric flux will have a different interpretation in the context of the holographic model of [60].

To close this section, we mention that if we additional impose a fixed background temperature, which is usually the case in the grand canonical ensemble, according to the discussion in section 2.3.2 we will have a black hole in the interior of the dual gravity model. This black hole will now be charged under the gauge field A_m, and the metric is given by the Reissner-Nordström metric. The event horizon of this black hole will add an interior boundary to the system and imposes regularity conditions on the gauge field. In the

static case, by following the same compactification procedure as in section 2.3.2 on the gravity side, we eventually see that regularity of the gauge field at the event horizon requires its norm to be finite, $g^{\mu\nu} A_\mu A_\nu|_{z=z_H} < \infty$. In Schwarzschild-like coordinates g^{tt} is diverging close to the event horizon, $z \to z_H$, so the condition on the gauge field simplifies to $A_t(z_H) \stackrel{!}{=} 0$.

2.3.4 Entanglement entropy

Apart from introducing finite temperature and density to the AdS/CFT correspondence, there is one element of the holographic dictionary which was added some time after Maldacena's original paper [15] but was actually present the whole time. This is about a genuine feature of quantum theories, which is quantum entanglement.

Field theory side

The "Hello World!"-example to quantum entanglement is given by a Hilbert space $\mathcal{H} = \mathcal{H}_A \otimes \mathcal{H}_B$ which is the tensor product of two single spin Hilbert spaces a.k.a. *qubits*. Either spin is in a superposition of up ($|\uparrow\rangle$) or down ($|\downarrow\rangle$) eigenstates to the angular momentum operator S_z in some preferred direction. A specific example of a pure state in this Hilbert space is one of the *Bell states* [85] given by

$$|\Psi\rangle = \frac{1}{\sqrt{2}} \left(|\uparrow\rangle_A \otimes |\downarrow\rangle_B + |\downarrow\rangle_A \otimes |\uparrow\rangle_B \right) , \tag{2.85}$$

which is said to be entangled for the following reason: Consider the respective spins to be located far away where we have two distinct observers, A and B, for simplicity. We prepare the state of both spins to be given by (2.85) and let A measure the spin of his qubit. If the result of the measurement is $|\uparrow\rangle_A$ (or $|\downarrow\rangle_A$), he knows instantaneously, that B will measure $|\downarrow\rangle_B$ (or $|\uparrow\rangle_B$) on his qubit, and vice versa. In this way, both qubits can be prepared such that one can perfectly well predict the measurement of an arbitrary far away observer from local information. This was coined as "spooky action at a distance" by Einstein. However, after the dust settles, it turns out that causality is *not* violated in the sense of faster-than-light information transmission.

One measure of quantum entanglement is given by the *entanglement entropy*. If we have a Hilbert space $\mathcal{H} = \mathcal{H}_A \otimes \mathcal{H}_B$ and we prepared a pure state, represented by a state matrix $\rho = |\Psi\rangle \langle\Psi|$,[6] we can restrict our knowledge

[6] Note, that the ρ could, of course, equally well define a mixed state. In this case however, the entanglement entropy will not be a genuine measure of quantum entanglement anymore, as it also includes the statistical entropy.

to either subsystem A or B by tracing over the other Hilbert space. In this way, we define the *reduced state matrix* ρ_A by

$$\rho_A = \mathrm{Tr}_B \, \rho \,, \tag{2.86}$$

where the partial trace $\mathrm{Tr}_B : T(\mathcal{H}_A \otimes \mathcal{H}_B) \mapsto T(\mathcal{H}_A)$ maps trace-class operators on the composite Hilbert space to trace-class operators on $\mathcal{H}_A$ and is uniquely determined by

$$\mathrm{Tr}_B(O_A \otimes O_B) = O_A \cdot \mathrm{Tr}_B(O_B) \,, \tag{2.87}$$

for any trace-class operators $O_A \in T(\mathcal{H}_A)$, $O_B \in T(\mathcal{H}_B)$ and the right-hand side is scalar multiplication of O_A with a number given by the trace. The entanglement entropy is then defined by

$$S_A = -\mathrm{Tr}_A \left(\rho_A \log(\rho_A)\right) \,, \tag{2.88}$$

which is just the von Neumann entropy of ρ_A. It is a measure for the quantum entanglement between the Hilbert spaces $\mathcal{H}_A$ and $\mathcal{H}_B$. The point is that the initial state matrix ρ is pure and, thus, has vanishing von Neumann entropy. However, by neglecting information from a subspace, we find the reduced state ρ_A to be in a statistical mixture of energy eigenstates, which resembles a thermal state. This way, entanglement entropy really measures our lack of knowledge. We will see at the end of this section that this is likely to be true for any occurrence of entropy in a thermal system.

Coming back to our example (2.85) with the Bell state, we can compute the entanglement entropy between both qubits and find

$$S_A = \log(2) \,, \tag{2.89}$$

which is the maximal possible entanglement entropy between two qubits.

Gravity side

From the field theory side, the computation of entanglement entropy seems straightforward. On the gravity side of the duality, Ryu and Takayanagi proposed in [19] a way to add entanglement entropy to the holographic dictionary. They started from the long known equation for the entropy of a black hole, which is given by the Bekenstein-Hawking formula

$$S_{BH} = \frac{A_{BH}}{4\, G_N} \,, \tag{2.90}$$

where A_{BH} is the area spanned by the event horizon of the black hole and G_N is Newton's constant. In the aftermath of our discussion about the Bell

state above, it is not surprising to find that a black hole carries entropy: Suppose the quantum state of the universe is pure, but part of it collapses to a black hole. Here, we will assume that there exists a quantum description in which the total state stays pure during the entire evolution. According to general relativity, no information inside the event horizon is accessible from the outside. Hence, the event horizon *forces* an outside observer to neglect this information, and the reduced state outside of it must be in a mixed state.

The Bekenstein-Hawking proposal (2.90) can thus be seen as the entanglement entropy between the outside and inside region of a black hole which stems from tracing over the inside states. That this entropy is proportional to the horizon area, however, is not straightforward at first sight, but makes sense as this is just the boundary between the inside and outside. Moreover, it is known that quantum field theories generically satisfy an *area law* for entanglement entropy, which is discussed e.g. in [33, 34].

Another inside comes from the fact that the event horizon is a minimal surface in the spacetime and its Bekenstein-Hawking entropy actually saturates the Bekenstein entropy bound, which gives an upper bound on the possible amount of entropy in a volume of spacetime. All of this led Ryu and Takayanagi to the conjecture that the entanglement entropy is encodes by specific minimal surfaces on the gravity side. In more detail, if we regard the Hamiltonian of the field theory side as a bipartite system $\mathcal{H} = \mathcal{H}_A \otimes \mathcal{H}_B$, where A and its complement B denote spatial regions of the field theory, they suggested in [19] that the entanglement entropy can be computed holographically by

$$S_A = \frac{\min_S (\text{area}(S))}{4\, G_N}\,, \qquad \partial S|_{z\to 0} = \partial A\,, \tag{2.91}$$

where S is an extremal codimension two surface[7], which ends at asymptotic infinity $z = 0$ such that its restriction to the hypersurface $z = 0$ is the boundary between A and its complement on the field theory side. The hypersurface S extends into the bulk, $z \neq 0$, where the bulk extension can a priori be chosen freely. According to (2.91), we have to minimise the area of S over all possibilities for such a surface, which will then be proportional to the entanglement entropy by the same equation. Due to the minimisation

[7] On the field theory side, for applying the Hamiltonian formalism, we must choose a foliation $\mathcal{M} = \mathbb{R} \times M$ of the field theory spacetime into temporal and spatial directions. Further dividing the spatial manifold M into A and B introduces a codimension two surface $\partial A = \partial B$. The same is true on the gravity side: We choose a foliation matching the one on the field theory side and consider spatial slides, which are further divided into two parts by the minimal surface S. So, as an embedding in the whole spacetime, S is codimension two.

problem and the fact that the AdS metric (2.36) diverges at asymptotic infinity, it is easily seen that S really must extend into the bulk and cannot simply stay at $z = 0$. The same idea yields that S_A generically diverges and must be regularised in some way to yield a finite result. The same is true, however, for entanglement entropies in conformal field theories to which Ryu and Takayanagi compared their proposal and found analytic agreement [19].

A first check is to apply this actually to the whole spacetime, i.e. $A = \mathcal{M}$ where $\mathcal{M}$ is the manifold on which the field theory side is defined. If the field theory side is at $T = 0$, the entanglement entropy reduces to the von Neumann entropy of a pure state, which vanishes. On the gravity side, the surface extending the boundary of some $A \neq \mathcal{M}$ in a minimal way into the bulk of the gravity theory will contract further and further as $A \to \mathcal{M}$ until it vanishes along with its area. So, (2.91) gives the right answer.

What happens if we consider the duality at finite temperature? In that case, according to section 2.3.2, we will a have black hole in the bulk of the gravity spacetime. If we start from a finite $A \neq \mathcal{M}$, the minimal surface S in the bulk will *wrap* the black hole in the bulk as $A \to \mathcal{M}$. As we take the limit, S eventually disconnects from the asymptotic boundary and is just given by the event horizon. The proposal (2.91) then gives us the entropy of the whole event horizon, which is (2.90).

How does this make sense on the field theory side? At this point, it is worthwhile to notice again that the von Neumann entropy of a state operator ρ in a pure state always vanishes identically. This means that by neglecting our knowledge about either subsystem, i.e. by applying Tr_B, the reduced state matrix ρ_A of the other system resembles a mixed state and thermodynamic properties like temperature emerge. This, in particular, must always be the case if a pure state in a gravitational theory evolves such that event horizons form. An event horizon, by definition, defines a natural border to our knowledge about a system and after this section, it should not be surprising anymore that one can always associate a temperature with event horizons, be it event horizons of black holes or cosmological event horizons.

It is conversely always possible to *purify* a mixed quantum state by adding another, auxiliary Hilbert space of at least the same size. If we relabel the original Hilbert space to $\mathcal{H}_A$, we can (due to guaranteed properties of density matrices) diagonalise the state matrix of any mixed state in a basis of orthogonal states $\{|i\rangle\}_{i\in\mathbb{N}}$ and obtain

$$\rho = \sum_i p_i \, |i\rangle \langle i| \, , \tag{2.92}$$

for some probabilities p_i, which are normalised such that $\sum_i p_i = 1$. Next, we add the same Hilbert space, $\mathcal{H}_B \sim \mathcal{H}_A$, with a similar basis $\{|i'\rangle\}|_{i'\in\mathbb{N}}$

such that the full Hilbert space is the tensor product $\mathcal{H} = \mathcal{H}_A \otimes \mathcal{H}_B$. One possible purification of the mixed state is then given by

$$|\Psi\rangle = \sum_i \sqrt{p_i}\, |i\rangle \otimes |i'\rangle \ , \tag{2.93}$$

which is a pure state in $\mathcal{H}$ with its density matrix being the projection operator

$$\rho_\Psi = |\Psi\rangle \langle\Psi| \ . \tag{2.94}$$

We say *one* possible purification, because it is not unique and depending on our choice of $\mathcal{H}_B$, there can be infinitely many. This is unique to quantum statistics, because classical system cannot have quantum entanglement or reduced state matrices.

Coming back to the question of how (2.91) makes sense for the AdS/CFT duality at finite temperature, we must notice that the field theory side is now in a mixed state. In equilibrium, the gravity dual is defined on a static black hole metric, which is sometimes called an *eternal* black hole. In figure 2.2 we show the conformal diagram of an eternal black hole in asymptotic Anti de-Sitter space. In analogy with the Kruskal extension for asymptotically flat black hole spacetimes, an eternal black hole in asymptotically AdS features 'another' side, labelled as region II, of the black hole which can be regarded as a wormhole in this context.[8] If we vary the codimension two surface S in the gravity bulk to minimise its area as $A \to \mathcal{M}$, it will eventually wrap the wormhole throat in the sense that it settles at the minimum circumference of the wormhole. If we consider the purification of the thermal field theory, we can now see which subspaces are entangled: It's the spacetime $\mathcal{M}$ on which the conformal field theory (CFT 1) on the field theory side of the duality is defined, and its complement due to purification, $\tilde{\mathcal{M}}$, which is the asymptotic boundary on the other side of the wormhole. The minimal area obtained is also called the *bifurcation surface*, $\mathcal{B}$, due to its special role in the conformal diagram.

An analysis of this kind in the context of gauge/gravity duality was elaborated in [28,86]. Here, the combined Hilbert space $\mathcal{H} = \mathcal{H}_\mathcal{M} \otimes \mathcal{H}_{\tilde{\mathcal{M}}}$ is in the *thermofield double* state

$$|\Psi\rangle = \sum_i e^{-\beta E_i/2}\ |i\rangle \otimes |i'\rangle \ , \tag{2.95}$$

which is just (2.93) for a special choice of the p_i. Upon building the projection operator $\rho_\Psi = |\Psi\rangle \langle\Psi|$ and tracing over $\mathcal{H}_{\tilde{\mathcal{M}}}$, we recover the state matrix (2.61) of the field theory side.

[8] There are no time-like paths through the wormhole for reasonable energy conditions.

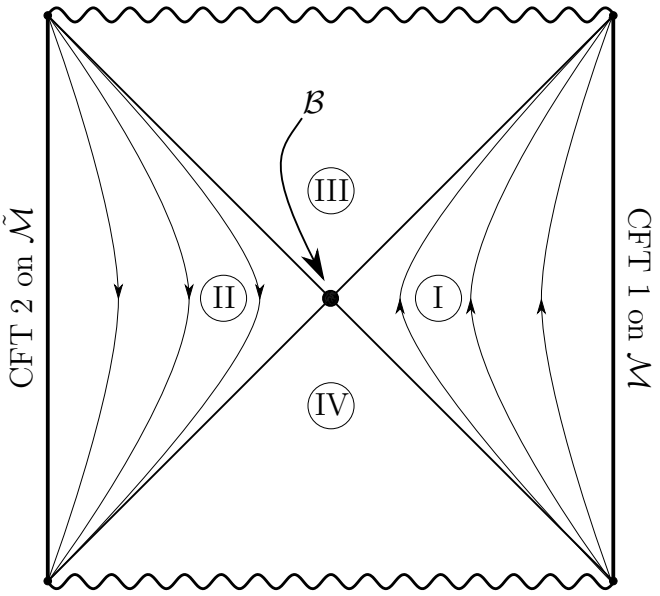

Figure 2.2: A conformal diagram of an eternal black hole in asymptotic AdS spacetime. CFT 1 denotes the conformal field theory in an equilibrium state ρ_A at finite temperature, to which the gravity dual is given by this geometry. CFT 2 lives in a Hilbert space $\mathcal{H}_B$ which is needed to purify ρ_A.

Chapter 3

Holographic Kondo model

"Maybe that pattern is like the pattern in the stock market, the Torah, this 216 number..."

Max – π [6]

The previous chapter gave an overview on various elements of the dictionary of gauge/gravity duality. From this chapter onward, we will focus on a specific application of the correspondence. More precisely, we will consider a magnetic impurity coupled to a strongly interacting bath of electrons and generalisations. To do so, we first introduce the original Kondo model by Jun Kondo [61], its extensions and solution strategies on the field theory side. Afterwards, the holographic Kondo model suggested by Erdmenger et al. [60] will be explained. At the end, we will have a look at possible generalisations, some of which have been worked out in this thesis.

3.1 Kondo model in condensed matter theory

In 1964, Jun Kondo published a seminal paper about a simple model for isolated magnetic impurities coupled to host metals [61], which is called the *Kondo model*. The motivation for this model was to answer the question of why certain metallic alloys with traces of impurities (typically iron) feature a minimum in their electric resistivity at low temperatures [62]. Indeed, the major result of his paper is that impurities with antiferromagnetic coupling to the conduction band actually give rise to a minimum in the electric resistivity due to a logarithmic contribution whose origin is in perturbation theory up to second order in the coupling constant. For this reason, the minimum is synonymously called the *Kondo effect* in the context of the Kondo

model. This section is devoted to explaining the original Kondo model, its implications, different solution strategies and generalisations.

3.1.1 Kondo model and solution techniques

The Hamiltonian of the original Kondo model is given by

$$\begin{aligned} H = H_0 + H_K = \sum_{\vec{k},\sigma} \epsilon_{\vec{k}}\, \psi^\dagger_{\vec{k},\sigma} \psi_{\vec{k},\sigma} + \sum_{\vec{k}\,\vec{k}'} J_{\vec{k}\,\vec{k}'}\, \vec{J}\cdot\vec{S}\,, \\ \vec{J} = \left(\psi^\dagger_{\vec{k}'}\, \vec{T}\, \psi_{\vec{k}}\right)\,, \qquad \vec{S} = \left(\chi^\dagger\, \vec{T}\, \chi\right)\,, \end{aligned} \tag{3.1}$$

where ψ denotes the annihilation operators of the conduction band electrons, $\vec{k}, \vec{k}'$ the electron momenta, σ their spins and $\vec{T}$ the generators of the $SU(2)$ spin symmetry. Spin indices have been suppressed. $J_{\vec{k}\vec{k}'}$ is the coupling between impurity and conduction band. Because the impurity is supposed to be point-like, we can approximate its Fourier transpose by a constant and set $J_{\vec{k}\vec{k}'} \approx J$ for all $\vec{k}$, $\vec{k}'$. Depending on its sign, the coupling is ferromagnetic ($J < 0$) or antiferromagnetic ($J > 0$), respectively.

By applying perturbation analysis at second order in J, Kondo showed [61] that the interaction with the impurity adds a logarithmic term to the resistivity. Incorporating this in $3+1$ dimensions, the resistivity is given by

$$\rho(T) = a\, T^5 + c\, \rho_0 + c\, \rho_1\, \log(T/T_F)\,, \tag{3.2}$$

where T_F is the *Fermi temperature*. The resistivity has a minimum at

$$T_{\min} = (c\, \rho_1 / 5a)^{1/5}\,. \tag{3.3}$$

This minimum in the resistivity is called the *Kondo effect* and is experimentally observed [62]. However, the logarithmic term indicates a divergence of the resistivity as $T \to 0$. Comparison with experiments shows that this is false, the resistivity settles at a finite value. The quest of understanding in which way this happens was coined the *Kondo problem*.

The solution emerges by looking in more detail at the Kondo coupling J. Upon changing the energy scale of the problem, the coupling constant is subject to renormalisation. The temperature of the system provides a natural cutoff in momentum integrals and hence it provides a physical renormalisation scale. Hence, the Kondo coupling J is renormalised if the temperature is shifted, where its running is given to leading order by

$$J(T) = \frac{J}{1 - N_0\, J\, \log(T/T_F)}\,. \tag{3.4}$$

Here, J is the coupling constant at the Fermi temperature T_F and N_0 denotes the electron density at the Fermi surface. For $J > 0$, i.e. in the antiferromagnetic case, the coupling diverges at a finite temperature. This temperature is called the *Kondo temperature*, T_K, and is given by

$$T_K = T_F \, e^{1/N_0 \, J} \, . \tag{3.5}$$

Apparently, the Kondo system becomes strongly coupled around the Kondo temperature, such that perturbation theory ceases to be reliable.

Following the renormalisation group flow in the opposite direction, the effective coupling defined by (3.4) vanishes as $T \to \infty$. So, the impurity decouples from the otherwise free electron gas in the bulk of the field theory. This asymptotic freedom is, along with strong coupling at low energies, the reason why the Kondo model is often regarded as a toy model for quantum chromodynamics (QCD). It was hoped that a solution to the Kondo problem might shed some light on how to deal with strongly coupled QCD.

What happens for $T \lesssim T_K$? Since perturbation theory is not reliable anymore, we must resort to different techniques, some of which will be presented in the following.

Wilson's numerical renormalisation group

To begin with, we should state that the full resolution of the Kondo problem as $T \to 0$ was performed first by Kenneth Wilson [63] with this numerical renormalisation group approach. He numerically computed the full non-perturbative RG flow of the coupling down to zero temperature which actually shows that the divergence of $J(T)$ appears not at the finite Kondo temperature T_K but only at $T = 0$. The divergence at T_K in 3.4 is an artefact of cutting off perturbation theory at finite order in J. Going to higher orders changes the critical temperature at which the coupling diverges. Nevertheless, we will go on to refer to (3.5) as the definition of T_K.

Conformal field theory approach

In [87,88], Affleck and Ludwig proposed an elegant alternative way of deriving the endpoints of the Kondo model's RG flow by applying methods from conformal field theory. Essentially, they performed a partial wave decomposition centred around the impurity and retained only its s-wave. In this way, the system reduces to a 1+1-dimensional conformal field theory. The excitations of the host are given by left- and right-movers $\psi_L(t+r)$, $\psi_R(t-r)$ away from the impurity at $r = 0$, where r is a non-negative radial coordinate measuring the distance from the defect. By enhancing the range of the radial

coordinate to $(-\infty, \infty)$ and mirroring the right-movers defined on $r > 0$ to left-movers ψ_L defined on $r < 0$, they mapped the Kondo model to and chiral model given by the Hamiltonian density

$$H = \frac{v_F}{2\pi}\, \psi_L^\dagger\, i\partial_r\, \psi_L + v_F\, \lambda\, \delta(r)\, \vec{S} \cdot \psi_L^\dagger\, \vec{T}\, \psi_L\,, \tag{3.6}$$

where v_F denotes the Fermi velocity which we set to $v_F = c = 1$ in our setup. At the impurity, matching conditions for the ψ_L-field must be provided and it turns out that at the RG fixed points, i.e. in the UV and the IR of the theory, the only difference is due to these matching conditions which imprints itself in a phase shift. It is important to keep this approach in the back of our heads, as the holographic model presented in the next section will have similar properties.

Large-N ansatz

There are several ways to represent the impurity $\vec{S}$ in the Kondo Hamiltonian (3.1). Above, we chose the totally antisymmetric representation[9], but there are also others. In this case, as written down in equation (3.1), the impurity spin is modelled by *Abrikosov pseudo-fermions*, whose annihilation operator is given by χ. They are auxiliary degrees of freedom constrained to the impurity. In order to project our model back to physical degrees of freedom, the Abrikosov pseudo-fermions must obey a constraint, which is given by the quantisation condition

$$\chi^\dagger \chi = q\,. \tag{3.7}$$

Here, q denotes the number of Abrikosov pseudo-fermions in any state which is also the number of boxes in the Young tableaux of the representation.

The vector symbol on $\vec{S}$ indicates that the original model was intended for a $SU(2)$-symmetry in three dimensions. However, it can obviously be extended to $SU(N)$ by using symmetry generators T^a, $a \in \{1, \dots N^2 - 1\}$ of the fundamental representation of $SU(N)$ instead. The completeness relation of the $SU(N)$ generators is given by

$$T^A_{\alpha\beta}\, T^A_{\gamma\delta} = \frac{1}{2}\left(\delta_{\alpha\delta}\, \delta_{\beta\gamma} - \frac{1}{N}\, \delta_{\alpha\beta}\, \delta_{\gamma\delta}\right)\,. \tag{3.8}$$

If we insert this into the CFT model (3.6), we find that the coupling to the impurity becomes

$$H_K = \frac{\hat{\lambda}}{2}\left(\mathcal{O}\mathcal{O}^\dagger - \frac{q}{N}\psi_L \psi_L^\dagger\right)\,. \tag{3.9}$$

[9] This means that due to its composition, $\vec{S} = \chi^\dagger\, \vec{T}\, \chi$ forms an antisymmetric representation of $SU(2)$ when acting on states.

where we defined $\hat{\lambda} = v_F \lambda$ and the scalar operator $\mathcal{O} = \psi_L^\dagger \chi$, which has conformal dimension $\Delta = 1/2$. The 'double trace'-term $\sim \mathcal{O}\mathcal{O}^\dagger$ is the additional marginally relevant term which is added in a localised fashion to the free chiral current in the holographic model of [60] and is therefore of central interest here.

Most interestingly, upon taking the large-N limit, $N \to \infty$, it was shown that this variation of the Kondo model features a proper phase transition at a critical temperature T_c which is of the same order of magnitude as the Kondo temperature T_K [89–94]. Below the critical temperature, $T < T_c$, the scalar operator $\mathcal{O}$ condenses in terms of mean-field theory, where close to the phase transition its behaviour is given by

$$\langle |\mathcal{O}| \rangle \sim \left(\frac{T_c - T}{T_c} \right)^{1/2} , \tag{3.10}$$

which is characteristic for order parameters in mean-field transitions. Due to its definition, $\mathcal{O} = \psi^\dagger \chi$, the condensation of the scalar operator indicates the formation of a singlet state involving the impurity and the degrees of freedom in the host metal. This singlet state is often referred to as the *Kondo screening cloud*, as the effects of the impurity on the host metal are screened at large distances due to the singlet formation.

This phase transition is a relict of the large-N limit and is not present in the original model. The transition at finite N is rather a cross-over than a phase transition, which is also consistent with the fact that there are no proper phase transitions possible in field theories of dimensionality $d < 3$ [95, 96]. Taking N to infinity is, however, a loop-hole to this theorem. On a computational level, the reason for the phase transition to occur at finite $T \approx T_K$ is given by equation (3.4). This is the one-loop approximation to the running, but as $N \to \infty$, the higher order contributions actually vanish and the coupling diverges at a finite temperature [97].

We cannot expect that the large-N approach to the Kondo model captures all of its phenomenology. One of the most important features of the original Kondo model, namely the logarithmic contribution to the resistivity along with its associated minimum at finite T, is absent in the large-N limit. However, it is a very convenient starting point for holographic model building, which always utilises a large-N limit if we want to have a classical theory of gravity on the gravity side of the duality. Moreover, the gauge/gravity conjecture only works for conformal field theories, which may include (marginally) relevant operators, varying only the low energy behaviour of the theory. This is the case in the model at hand and in the next section, we will show how the authors of [60] used those features as a guideline in order to build a holographic model which shows strikingly similar phenomenology.

3.1.2 Summary

In this section, we laid the foundations to understand the holographic Kondo model of [60], which will be described in the following section. We encountered the various phenomenological features of the original Kondo model (3.1) and its variations in the CFT and large-N approaches. Essentially, we found that

- The original Kondo model leads to a logarithmic contribution to the resistivity, captured in (3.2), from which the minimum in the resistivity at finite temperature (3.3) follows.

- We can simplify the model to a 1+1-dimensional conformal field theory described by (3.6) by applying an s-wave reduction. The Kondo interaction is a marginally relevant deformation of the CFT in this ansatz and the UV and IR fixed points can be found analytically.

- Additionally taking the large-N limit reveals itself in a phase transition at $T_c \approx T_K$ instead of a cross-over. The composite scalar operator $\mathcal{O} = \psi_L^\dagger \chi$ condenses at low temperatures, indicating the formation of a singlet state between the host metal excitations and the auxiliary degrees of freedom localised at the impurity.

3.2 The holographic model

After the review of the Kondo model in field theory in the previous section, we will now introduce the main framework for the holographic approach to the Kondo model in this thesis. It is given by the holographic Kondo model of Erdmenger, Hoyos, O'Bannon and Wu [60]. This work describes one possible way of incorporating Kondo-like impurities in holography, starting from type IIB string theory. The latter admits several distinct sorts of D-branes, among which there are D3-, D5-, and D7-branes. All of those are used in order to find a tractable holographic model resembling the mixed large-N conformal field theory ansatz described at the end of the previous section.

The D3-branes are used in the same manner as in the original AdS/CFT-correspondence. It is their number, N, of coincident D3-branes which will be sent to infinity in the large-N limit. The D7-branes intersect the D3-branes in two dimensions, and mainly set the stage for a 1+1-dimensional worldvolume theory, to which we can restrict our attention and which, in a way, is an analogy to the s-wave reduction in the conformal field theory

coordinates	0	1	2	3	4	5	6	7	8	9
N_3 D3-branes	•	•	•	•	–	–	–	–	–	–
N_7 D7-branes	•	•	–	–	•	•	•	•	•	•
N_5 D5-branes	•	–	–	–	•	•	•	•	•	–

Table 3.1: Embedding of N_3 D3-, N_5 D5-, and N_7 D7-branes as used by the authors of [60] in order to derive a holographic model of the Kondo effect from type IIB string theory.

ansatz for the Kondo model. By intersecting with the D7-branes, the D5-branes introduce an impurity in this lower-dimensional world, which will turn out to represent the Kondo impurity.

In the following, we will describe this interplay of D-branes in more detail, before we follow the authors of [60] and restrict our attention to a holographic bottom-up model, which captures the essential ingredients of the top-down model, but is more tractable. We focus on the most important features of this model and prepare the reader to understand the generalisations of the holographic Kondo model of [60], which will be presented in the following chapter.

3.2.1 From type IIB string theory to the Kondo model

In their top-down approach, the authors of [60] consider type IIB superstring theory with several D-branes in the setup. The configuration of D-branes in this model is summarised in table 3.1. In the open string picture to this set of D-branes, we have to consider the world-volume theories of all of these D-branes. There are open string stretching from any Dp- to any Dq-brane, which are labelled (p, q)-strings, where $q, p \in \{3, 5, 7\}$. We will apply a low-energy limit like in the original AdS/CFT correspondence, so we can restrict our attention to strings confined to the intersections of the D-branes, as those of finite length are massive and can be integrated out.

Here, the weak form of the correspondence will be used, so we have to send the number of D3-branes to infinity, $N_3 \to \infty$. Apart from the presence of the other D-branes, this gives us the original AdS/CFT model of Maldacena [15]. The intersection between the D3- and D7-branes introduces another sector of strings, whose worldvolume theory is given by chiral Weyl fermions ψ_L governed by

$$S = \frac{1}{\pi} \int \mathrm{d}^2x \, \psi_L^\dagger (i\partial_x - A_-)\psi_L \,, \tag{3.11}$$

where A_- is a component of the $\mathcal{N} = 4$ $SU(N_3)$ gauge field restricted to the intersection. As is apparent from the notation, the ψ_L will be modelling

the left-movers in the conformal field theory approach to the Kondo model in (3.6). A conserved current is formed out of the Weyl fermions, $J^a = \psi_L^\dagger T^a \psi_L$, where the T^a are the generators of the spin symmetry $SU(N_3)$. A conserved chiral current is holographically dual to a Chern-Simons field of equal rank and level, whose action is to leading order given by

$$S_{CS} = -\frac{N_3}{4\pi} \int \mathrm{Tr} \left(A \wedge \mathrm{d}A + \frac{2}{3} A \wedge A \wedge A \right) , \tag{3.12}$$

where the integration is over AdS_3.

The D5-branes intersect with the D3-branes in the temporal dimension x_0. In the 1+1-dimensional D3/D7-brane intersection, they introduce an additional defect, whose worldvolume action supports fermions which are charged under $SU(N_3) \times U(N_5)$. The action is given by

$$S = \int \mathrm{d}x_0 \, \chi^\dagger (i\partial_0 - A_0 - \phi_9) \chi \, , \tag{3.13}$$

where the scalar ϕ_9 encodes fluctuations of the embedding of the D5-branes in the x_9-direction, in which they are not fixed, see table 3.1. There is a conserved $U(N_5)$-current $S^a = \chi^\dagger \, T^a \, \chi$.

On the gravity side, this current is dual to a $U(N_5)$ gauge field a with field strength $f = \mathrm{d}a + a \wedge a$. Its action is given by

$$S_a = -N_5 \, T_5 \left(\int \mathrm{d}^6 x \sqrt{\det(X_5^* g + f)} - \int (X_5^* C_{(4)} \wedge f) + \dots \right) , \tag{3.14}$$

where the $C_{(4)}$-form field is one of the form fields appearing in type IIB string theory, X_5 is the embedding of the D5-brane and X_5^* denotes the pullback with respect to this embedding. It sources the gauge field, which produces some quantised electric flux in the AdS_2-subspace spanned by the D5-brane embedding.

Finally, the intersection of the D5- and D7-branes introduces a tachyonic scalar operator, which transforms bifundamental under $U(N_5) \times U(N_7)$, but is a singlet under the $SU(N_3)$-symmetry of the D3-branes' worldvolume theory. This is the scalar which corresponds to the operator $\mathcal{O} = \psi_L^\dagger \chi$ discussed in the large-N approach to the Kondo model in section 3.1. On the gravity side, it is dual to a complex scalar field Φ on the AdS_2 hypersurface.

3.2.2 Holographic bottom-up Kondo model

After explaining its origins in type IIB string theory, the authors of [60] restrict their attention to a holographic bottom-up model which is built upon

the same essential ingredients: A $2+1$-dimensional gravity theory with a defect hypersurface dual to a $1+1$-dimensional field theory which has a $0+1$-dimensional defect, represented by the hypersurface in the holographic model. We will often refer to this hypersurface as the *defect hypersurface* in the following. The numbers of D-branes are fixed to be given by $N_5 = 1 = N_7$ and the large-N_3 limit is imposed, $N_3 \to \infty$. Note, that according to the discussion in the previous section, this sends the rank of the spin symmetry, $SU(N_3)$, of the impurity to infinity. As there will be no confusion by doing so, we will relabel the number of D3-branes by N in the following.

From the top-down model, we find that the essential field content on the gravity side is given by a Chern-Simons field A in the $2+1$-dimensional bulk, which is dual to the chiral current in the conduction band of the field theory model. A complex scalar field Φ as well as an additional $U(1)$-gauge field a are constrained to the hypersurface. The electric flux $\mathcal{C}$ of the gauge field encodes the representation of the impurity. The complex scalar is suggested to be dual to the composite operator $\mathcal{O} = \psi^\dagger \chi$ and is hence charged under both the gauge field a and the Chern-Simons field A.

This already concludes the field content of the holographic model. Its action in the probe limit is then given by

$$S_{\text{tot}} = S_{CS} + S_{2d}\,, \tag{3.15}$$

$$S_{CS} = -\frac{N}{4\pi}\int \text{Tr}\left(A\wedge \mathrm{d}A + \frac{2}{3}A\wedge A\wedge A\right)\,, \tag{3.16}$$

$$S_{2d} = -N\int \mathrm{d}^2x\sqrt{\gamma}\left(\gamma^{\mu\nu}D_\mu\Phi^\dagger D_\nu\Phi + \frac{1}{4}f_{\mu\nu}f^{\mu\nu} + V(\Phi)\right)\,, \tag{3.17}$$

where γ is the induced metric on the $1+1$-dimensional hypersurface, $f = \mathrm{d}a + a\wedge a$ is the field strength tensor of a, V is the potential of the scalar, to be defined below, and $D_\mu = \partial_\mu - ia_\mu + iA_\mu$ is the covariant derivative of the complex scalar.

In principle, the action also includes the Einstein-Hilbert action

$$S_{EH} = \frac{1}{2\,\kappa_N}\int \mathrm{d}^3x\,\sqrt{g}(R - 2\Lambda)\,, \tag{3.18}$$

where g denotes the metric in the $2+1$-dimensional bulk. For now, we will assume that the matter content does not backreact to the metric, i.e. we are in the probe limit with respect to the metric. This is also consistent with the fact that $N_5/N \to 0$ in the large-N limit if we keep $N_5 = 1$ fixed. Accordingly, the defect hypersurface is fixed at a certain position, which we can choose to be $x = 0$ throughout the bulk due to translational symmetry.

Later on, especially in chapter 4, we will describe how backreaction of the impurity to the metric can be incorporated in this bottom-up model. The upshot is that the embedding profile becomes non-trivial.

If we want to mimic the Kondo model on the field theory side of this bottom-up model, we must incorporate a finite temperature into the model. According to the holographic dictionary, we hence need to impose a static background metric at a finite temperature, which in 2+1 dimensions is given by the BTZ spacetime [98] with metric

$$\mathrm{d}s^2 = \frac{L^2}{z^2}\left(-f(z)\mathrm{d}t^2 + \frac{\mathrm{d}z^2}{f(z)} + \mathrm{d}x^2\right) , \tag{3.19}$$

where $f(z) = 1 - z^2/z_H^2$, $t, x \in (-\infty, +\infty)$ and $0 \leq z \leq z_H$. The temperature is then given by the Hawking temperature, which for this metric reads $T = (2\pi\, z_H)^{-1}$. The scalar potential,

$$V(\Phi) = M^2\, \Phi^\dagger \Phi \,, \tag{3.20}$$

is chosen to consist of a mass term only, although we will discuss the necessity of extensions in the following sections, too.

As we can see, the bottom-up model (3.15) - (3.17) closely resembles holographic models of superconductors, see e.g. [56, 57]. Indeed, we will observe a very similar phenomenology: The model features a phase transition at low temperatures, below which a scalar condensate will form. So, in a way, the bottom-up model described above is a holographic superconductor on a AdS_2 submanifold. The interpretation, of course, will be different as this holographic model is dual to a strongly coupled version of the Kondo model. Nevertheless, we will refer to the phases by this analogy with superconductors. That is, we say that we are in the *normal* phase if $T > T_c$ and in the *condensed* phase if $T < T_c$.

From the action, the equations of motion are readily derived. They read

$$\epsilon^{n\mu\nu} F_{\mu\nu} = \delta(x)\sqrt{g}\, J^n \,, \tag{3.21}$$

$$\partial_\mu \left(\sqrt{\gamma}\, \gamma^{\mu\rho}\, \gamma^{\nu\sigma}\, f_{\rho\sigma}\right) = -\sqrt{\gamma}\, J^\nu \,, \tag{3.22}$$

$$\nabla_\mu J^\mu = 0 \,, \tag{3.23}$$

$$\gamma^{\mu\nu}\, D_\mu\, D_\nu\, \Phi = \partial_\Phi V(\Phi) \,, \tag{3.24}$$

where the conserved current reads

$$J^\mu = -i\, g^{\mu\nu} \left(\Phi^\dagger \left(D_\nu\, \Phi\right) - \Phi \left(D_\nu\, \Phi\right)^\dagger\right) . \tag{3.25}$$

The boundary expansions of the scalar can be derived from the probe limit. That is, we set the scalar to zero and solve the gauge field's equation of

motion. The solution is given by

$$a_\mu = \frac{Q}{z} + \mu \,. \tag{3.26}$$

Here, μ denotes the chemical potential and Q is equal to the asymptotic electric charge of the hypersurface, which encodes the representation of the impurity. Inserting this solution in the equation of motion of the scalar, 3.24, we can derive its asymptotic solution by assuming the ansatz $\Phi \sim z^p$, where p is to be derived. At leading order in z, this yields

$$p_{1/2} = \frac{1}{2}\left(d \pm \sqrt{d^2 + 4(M^2 - Q^2)}\right) \,, \tag{3.27}$$

where $d = 1$ in this case. We already encountered this formula in (2.43). In contrast to higher dimensional holographic models, the charge of the gauge field alters the asymptotics of the scalar field, which is why the combination $M^2 - Q^2$ appears.

In the conformal field theory approach to the Kondo model, we saw that the conformal dimension of the scalar operator is given by $\Delta = 1/2$. Hence, we need to set $M^2 - Q^2 = -1/4$ if we want to draw an analogy. Unfortunately, this means we need to set the scalar mass exactly to the stability bound given by the Breitenlohner-Freedman bound [79]. In general, this yields additional logarithmic terms in the boundary expansion of the scalar field which will follow us throughout the rest of the thesis. To leading order, the expansion is given by

$$\Phi = \sqrt{z}\,(A \log(\Lambda z) + B) + O(z^{3/2}) \,, \tag{3.28}$$

where A and B are complex expansion coefficients and we had to introduce an arbitrary energy scale Λ for dimensional reasons in the logarithmic term.

Up to this point, we introduced a scalar degree of freedom with the appropriate conformal dimension. Now, we have to choose boundary conditions on the gravity side. In order to model the Kondo impurity on the field theory side, we need to introduce the Kondo interaction in our model. This is done by adding a double-trace boundary term $\hat{\lambda} \int \mathrm{d}t\, \mathcal{O}(t)\mathcal{O}^\dagger(t)$ to the action, which resembles the term appearing in (3.9) in the large-N approach. As shown in [68, 97], the vacuum expectation value of the scalar operator is given by

$$\langle \mathcal{O} \rangle = -N\, B^\dagger \,. \tag{3.29}$$

Hence, the boundary term reads $S_{bnd} = \hat{\lambda} \int_\partial \mathrm{d}t\, B^\dagger(t)\, B(t)$, and following [97], the scalar field needs to satisfy special boundary conditions given by

$$A = \hat{\lambda}\, B \,. \tag{3.30}$$

For convenience, we will define the absolute values, as well as the real and imaginary parts, of the scalar expansion coefficients as

$$A = \alpha_1 + i\alpha_2, \qquad |A| = \alpha, \tag{3.31}$$
$$B = \beta_1 + i\beta_2, \qquad |B| = \beta, \tag{3.32}$$
$$\hat{\lambda} = \kappa_1 + i\kappa_2, \qquad |\hat{\lambda}| = \kappa, \tag{3.33}$$

which will become important for different decompositions of the scalar field. Especially, we want the coupling, $\hat{\lambda}$, to be real, so $\kappa_2 = 0$ and (3.30) becomes

$$\alpha_1 = \kappa_1\beta_1, \qquad \alpha_2 = \kappa_1\beta_2\,. \tag{3.34}$$

Phenomenology in equilibrium

In equilibrium, we can choose the phase of the scalar to vanish which sets $\beta_2 = 0 = \alpha_2$, and the real parts of the different expansion coefficients are given by their absolute values α, β and κ.

First, we consider what happens if we rescale the arbitrary energy scale Λ introduced in (3.28). As the scalar field cannot change, we can look at the expansion at another energy scale, say $\tilde{\Lambda}$, and compare coefficients:

$$\tilde{\phi} = \sqrt{z}\left(\tilde{\beta}\tilde{\kappa}\log(\tilde{\Lambda}z) + \tilde{\beta}\right) + O(z^{3/2}) \tag{3.35}$$
$$= \sqrt{z}\left(\tilde{\beta}\tilde{\kappa}\left(\log(\Lambda z) + \log\frac{\tilde{\Lambda}}{\Lambda}\right) + \tilde{\beta}\right) + O(z^{3/2}) \tag{3.36}$$
$$= \sqrt{z}(\underbrace{\tilde{\beta}\tilde{\kappa}}_{=\kappa\beta}\log(\Lambda z) + \underbrace{\tilde{\beta}\left(\tilde{\kappa}\log(\tilde{\Lambda}/\Lambda + 1)\right)}_{=\beta}) + O(z^{3/2})\,. \tag{3.37}$$

The running of the coupling κ is hence described by

$$\Lambda \to \tilde{\Lambda}\,, \tag{3.38}$$
$$\beta = \tilde{\beta}\left(1 + \tilde{\kappa}\log(\tilde{\Lambda}/\Lambda)\right)\,, \tag{3.39}$$
$$\beta\kappa = \tilde{\beta}\tilde{\kappa}\,, \tag{3.40}$$
$$\Rightarrow \qquad \kappa = \frac{\tilde{\kappa}}{1 + \tilde{\kappa}\log(\tilde{\Lambda}/\Lambda)}\,, \tag{3.41}$$

which is precisely the running of the Kondo coupling in the original model, given by (3.4). As mentioned, this is the exact renormalisation of the coupling in the large-N limit [97] which justifies its appearance here.

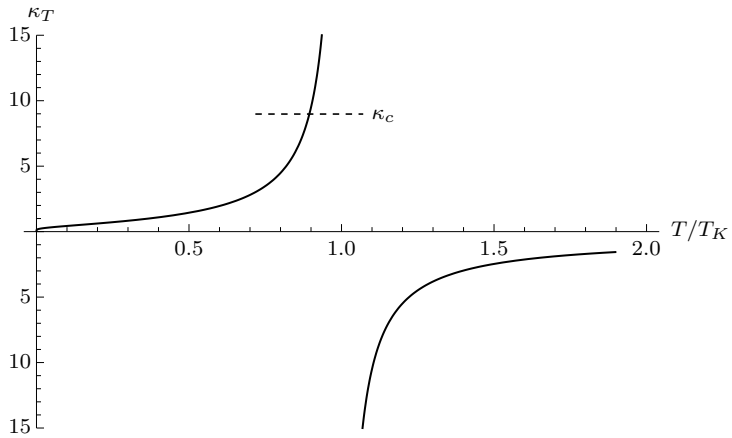

Figure 3.1: Running of the holographic Kondo coupling κ_T as a function of T/T_K.

To define the renormalisation group flow of κ as a function of Λ, we necessarily have to define a starting point $\tilde{\kappa} = \kappa(\tilde{\Lambda})$. There are two choices, $\tilde{\kappa}$ either being positive or negative. The latter, antiferromagnetic, case is the phenomenologically interesting one, as it provides asymptotic freedom when $\Lambda \to \infty$ and a strong coupling regime for small values of Λ, which mimics the Kondo model. Actually, the coupling diverges as

$$\Lambda \to \Lambda_{crit} = \tilde{\Lambda} \exp\left(1/\tilde{\kappa}\right). \tag{3.42}$$

Although the critical energy scale Λ_{crit} directly depends on the starting point of the RG flow, it is invariant under the rescalings (3.38) and (3.41). We want to look at the system at finite temperature, so we define a characteristic temperature scale T by $\tilde{\Lambda} = 2\pi T$. The coupling now diverges at a temperature given by

$$T_K = \frac{\tilde{\Lambda}}{2\pi} \exp(1/\tilde{\kappa}) \tag{3.43}$$

which we call the Kondo temperature, due to the analogy with eq. (3.4). In this analysis, T_K is the only dimensional quantity aside from the chemical potential μ, which will be considered later on. Hence, every instance of $(\tilde{\Lambda}, \tilde{\kappa})$ leading to the same T_K by means of eq. (3.43) is equivalent in the sense that they are different starting points for the same trajectory of the renormalisation group flow. Keeping that in mind, we can choose T_K to start with. We then replace the energy scale at which we define the coupling by $\tilde{\Lambda} = 2\pi T$, which sets a temperature scale at which the system is observed. To keep in mind that the coupling is now referred to at a temperature scale,

we relabel it to $\kappa_T \equiv \tilde{\kappa}$ and end up at

$$\frac{T}{T_K} = \exp(-1/\kappa_T)\,. \tag{3.44}$$

In this way, we found an easy relationship between the holographic Kondo coupling, κ_T, the temperature of the system, T, and the characteristic energy scale, T_K.

In the original Kondo model, there is a cross-over transition approximately located around the Kondo temperature T_c. In the large-N Kondo model, however, this smooth cross-over becomes a proper second order phase transition, taking place at a critical temperature $T_c \approx T_K$, which is approximately the Kondo temperature.

Indeed, the holographic Kondo model of [60] features such a second order phase transition, too. It can be found analytically by looking at the quasinormal modes of the scalar field in the normal phase. If we regard the coupling parameter κ_T as the independent variable, setting the state of the system, we find that there exists a critical value κ_c, below which the scalar field has an unstable quasinormal mode in the normal phase.

In order to find this unstable mode, the authors of [60] employed a perturbation analysis of the equation of motion for the absolute value of the scalar field around the trivial solution. In [68], this analysis was refined in a way to correctly derive all two-point functions of the system. Without going into the details, we simply state the most important result for this thesis. One can perturb the scalar field around its trivial solution and require (3.30) to be satisfied. By going to momentum space, the coefficients in (3.30) depend on the complex frequency rather than time. If we want the equations of motions for the perturbations to be satisfied, we find a constraint, given by

$$\frac{1}{\kappa_T(\omega)} = H\left(-\frac{1}{2} + iQ - i\frac{\omega}{2\pi\, T}\right) + H\left(-\frac{1}{2} - iQ\right) + \log(2)\,. \tag{3.45}$$

Here, the H are the Harmonic numbers, the ω denote quasinormal modes of the scalar operator, Q is the electric flux of the gauge field, and $\kappa_T(\omega)$ is the parameter showing up in the boundary conditions of the scalar field. In order to find the quasinormal modes in the normal phase, we need to find all ω's for which (3.45) is satisfied if we set $\kappa_T(\omega)$ to a fixed value, which is restricted to be real, so that the Kondo coupling is real. For each choice, there will be infinitely many values of ω solving the equation. These are the quasinormal modes of the system at a temperature T, set by κ_T using (3.44).

For temperatures above a critical temperature T_c, all of these modes will have a negative imaginary part. However, at $T = T_c$, one of them vanishes. If

we go below T_c, this mode goes into the upper halfplane and hence indicates an instability of the trivial solution. By setting $\omega = 0$ in (3.45), we are able to find the critical value of κ_T, which is given by

$$\kappa_c = \left(H\left(-\frac{1}{2} - iQ\right) + H\left(-\frac{1}{2} + iQ\right) + \log(2) \right)^{-1} \approx 8.98 \tag{3.46}$$

The critical temperature T_c is now easily found by applying (3.44) to the critical value of κ_T, and we find

$$\frac{T_c}{T_K} = \exp(-1/\kappa_c) \approx 0.895\,. \tag{3.47}$$

In the condensed phase, we cannot solve the perturbation equation analytically anymore, and need to resort to numerical methods. The output in the static analysis will be a list of lists of parameter values for α, β and κ. Each of its entries will be of the form $(\alpha, \beta, \kappa_T)$, denoting solution values for the parameters. We use (3.44) to obtain temperatures from the respective value of κ_T, and normalise the dependent coefficients to T_c.

Thus, we can find the dependence of α, β or combinations on the temperature. For $\kappa_T\,\beta/\sqrt{T_c}$, the result is shown in 3.2, where we identified $\beta \sim \langle\mathcal{O}\rangle$ by equation (3.30). There is a second order phase transition at a critical temperature $T = T_c$, below which the scalar field condenses. This is modelled by fitting a function of the form $a(1 - T/T_c)^b$ to the points close to $T/T_c = 1$, which is shown as a dashed line. The fitted parameters are given by $a \approx 0.296$ and $b \approx 0.501$. At low temperatures, $\kappa_T\,\langle\mathcal{O}\rangle/\sqrt{T_c}$ deviates slightly from the fitted curve. Note that this is a recomputation of the same result in [60]. It is worthwhile to notice that $\alpha = \kappa_T\beta$ as shown in figure 3.2 appears to stay finite as $T \to 0$.

However, the vacuum expectation value of the scalar operator is given by $|\langle\mathcal{O}\rangle| \sim \beta$ [68]. Its behaviour in the condensed phase is shown in figure 3.3. Again, we fit $a(1 - T/T_c)^b$ to the points close to $T/T_c = 1$. The fitted parameters are given by $a \approx 0.0134$ and $b \approx 0.503 \approx 1/2$. This is not obvious from the linear plot, but is revealed in the double logarithmic subplot close to T_c. The exponent, b, is the critical exponent[10] of the order parameter, $|\langle\mathcal{O}\rangle|$, of the phase transition and $b = 1/2$ indicates mean-field behaviour of the scalar field near the phase transition. This is expected for the phase transition in the large-N Kondo model.

[10] Usually, one denotes the critical exponent of the order parameter by β. Here, however, this notation would obviously be confusing due to our naming conventions in the holographic Kondo model, i.e. $\beta \equiv |\langle\mathcal{O}\rangle|$.

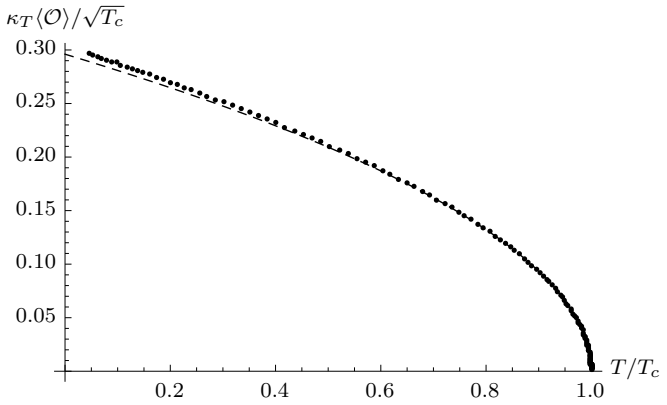

Figure 3.2: Shown is $\kappa_T \langle\mathcal{O}\rangle/\sqrt{T_c}$ vs. the temperature of the system.

In contrast to the combination $\kappa_T \langle\mathcal{O}\rangle$, the vacuum expectation value itself clearly diverges as $T \to 0$. This is physically meaningful and reflects the fact that the potential used in [60] does not provide a bound for the scalar condensation. To be reliable at low temperatures, we would need to stabilise the scalar potential, e.g. by introducing a ϕ^4 term. This is beyond the scope of this thesis. The reason to mention it already at this point is that it will turn up later both in section 4 and 5.

Apart from the phase transition, the holographic Kondo model of [60] also features a phase shift of the Chern-Simons field across the defect. This is in accordance with what is expected from the field theory side.

3.2.3 Generalisations of the holographic model

Having an overview of the holographic Kondo model of [60], certain possible generalisations immediately follow. First of all, so far we only described the static limit. However, it is perfectly reasonable to consider a time dependent coupling as this could model tuning, or quenching, the coupling parameter. This is feasible to realise in experimental settings [99], which was one of the main motivations to investigate it. We report on this generalisation in chapter 5.

Moreover, defects in a quantum field theory yield a possibly interesting behaviour of the entanglement around the impurity. Especially, we are able to define the notion of impurity entropy, which is the difference of entanglement entropy of symmetric patches around the defect with the defect present or not, respectively. It gives a measure on how much the defect influences the environment around it. Since the Kondo problem is is essentially solved by

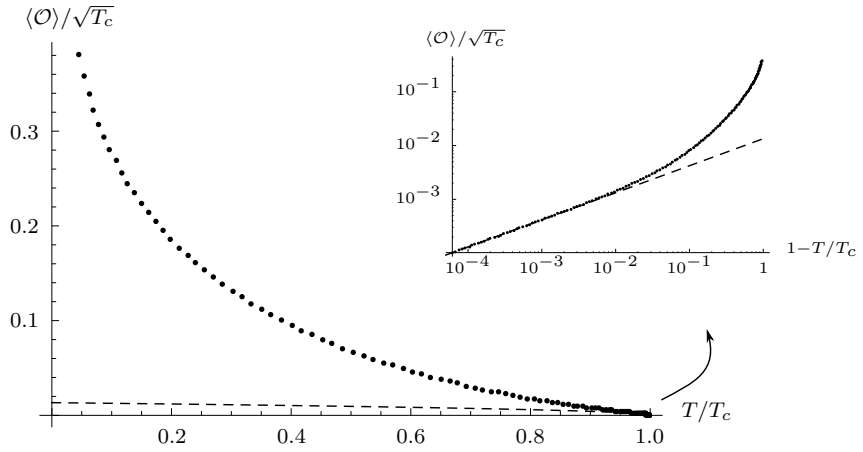

Figure 3.3: Shown is $\beta/\sqrt{2\pi\, T_c} \sim \langle\mathcal{O}\rangle/\sqrt{2\pi\, T_c}$ vs. the temperature T/T_c of the system.

a cloud of conduction electrons forming a singlet state with the impurity, we expect the defect to have a large influence on the entanglement entropy of the surrounding band.

We know from section 2.3.4 that the entanglement entropy is encoded in the geometry of the holographic dual. More precisely, it is dual to the area of minimal surfaces in the bulk by equation 2.91. So, if we want to compute entanglement entropy, we need to compute the backreaction of the impurity to the geometry in the bulk for different condensates. It turns out that there is a well-known way to compute it, which goes by the name Israel junction conditions. Those give rise to additional equations of motions for the embedding of the defect hypersurface, in which its extrinsic curvature is coupled with the singular energy-stress constrained to the hypersurface. In chapter 4, we will describe in detail, how to set up the system in order to incorporate backreaction. Then we compute the impurity entropy at different temperatures and compare to the literature.

Ultimately, we would like to merge time dependence and backreaction in order to holographically model the spatio-temporal evolution of the Kondo screening cloud. This could be compared to [100], and we will outline an ansatz of how to achieve this in a linearised fashion in the end of chapter 5.

There are other possible generalisations, which we do not try to solve in this thesis. One of them is to introduce another defect and couple the two defects by RKKY interactions, which has been performed in [101]. Essentially, the $U(1)$ gauge symmetry of the gauge field on the defect hypersurface is promoted to a $U(2)$ symmetry which captures the relevant effect. In the phase

diagram, the relative strength of the Kondo coupling between the impurities and the conduction band, and the coupling between the two impurities compete and determine the phase in which the model settles in equilibrium. Although first steps were taken, the challenge of finding a tractable holographic model of a Kondo lattice is left for future research.

3.2.4 Summary

The holographic Kondo model of [60] establishes a gauge/gravity duality between a mixture of the large-N and conformal field theory approach to the Kondo problem as described in section 3.1. Starting from a D-brane model in type IIB string theory, a more tractable bottom-up model is developed which retains only the essential ingredients. The impurity is mapped to a defect hypersurface embedded into a 2+1-dimensional bulk manifold on which the gravity dual is defined. The chiral current $\psi_L^\dagger T^a \psi_L$ finds its dual in a Chern-Simons field defined throughout the bulk. It decouples from the brane and can in principle be integrated after solving the equations of motion on the hypersurface, which sources the Chern-Simons field. The field content on the hypersurface features a gauge field a as well as a complex scalar Φ which are dual to the impurity representation and the scalar operator $\mathcal{O} = \psi_L^\dagger \chi$ on the field theory side. The scalar condenses via a mean-field transition at a critical temperature $T_c \approx T_K$ in the large-N ansatz for the Kondo model. The logarithmic behaviour of the resistivity at high temperatures is absent, which is an artefact of the large-N ansatz, and could likely be restored by $1/N$-corrections. In this case, it is also expected that the mean-field transitions smoothens to a cross-over. Generalisations dealt with in the next chapters 4 and 5 are given by considering backreaction of the field content on the hypersurface to the bulk geometry as well as time dependence in the form of quenching the Kondo coupling κ_T.

Chapter 4

Static backreaction

"This is insanity, Max!"

Sol – π [6]

This section describes the first generalisation of [60], which considers backreaction of the defect hypersurface to the geometry and was published in [1, 2]. Although this formalism was developed for the holographic Kondo model, it is possible to extend it to similar systems in gauge/gravity duality with boundaries on the field theory side, as we are free to choose the field content on the hypersurface. Similar approaches have already been worked out [65], however most of the time the authors deal with constant tensions on the hypersurface. Such setups go by the name of boundary conformal field theories (BCFT) and defect conformal field theories (DFCT), depending on whether the singular point is being regarded as a proper boundary to the system of a defect, i.e. the bulk manifold is extending to both sides. Due to our symmetry assumptions, this will only change the equations of motion by a factor of 2.

In the context of the holographic Kondo model, we find that for a vanishing scalar field, the gauge field on the defect hypersurface is yielding such a constant tension. This is expected for temperatures above the critical temperature, $T > T_c$, see section 3.2.2. Here, we will motivate the usage of geodesic normal flows, described in more detail in appendix A, with which we can construct constant tension solutions in our setting for arbitrary tensions. The tensions can be translated into the asymptotic electric flux $\mathcal{C}$ of the gauge field and hence only depend on the representation of the defect spin on the field theory side. These analytic solutions will be the starting point for our numerical analysis and represent the normal phase in which the scalar condensate vanishes.

4.1 A framework for backreaction

In this section, we will introduce the general framework for static backreaction in the bottom-up version of the holographic Kondo model. We begin by taking the same action as in (3.15), and add the Einstein-Hilbert action in order to incorporate backreaction to the geometry. This yields

$$S = S_{EH} + S_{CS} + S_{2D} =: S_{EH} + S_M \,, \tag{4.1}$$

$$S_{EH} = \frac{1}{2\kappa_N} \int \mathrm{d}^3x \sqrt{g} \left(R - 2\Lambda\right) \,, \tag{4.2}$$

$$S_{CS} = -N \int \left(A \wedge \mathrm{d}A + \frac{2}{3} A \wedge A \wedge A \right) \,, \tag{4.3}$$

$$S_{2D} = -N \int \mathrm{d}^2x \sqrt{\gamma} \left(\gamma^{\mu\nu} \left(D_\mu \Phi^\dagger D_\nu \Phi + D_\nu \Phi^\dagger D_\mu \Phi \right) /2 \right. \tag{4.4}$$

$$\left. + \frac{1}{4} f_{\mu\nu} \gamma^{\mu\alpha} f_{\alpha\beta} \gamma^{\beta\nu} + V(\Phi^\dagger \Phi) \right) \,, \tag{4.5}$$

where $\kappa_N = 8\pi\, G_N$ is the gravitational coupling and we have rewritten the action of the scalar such that the symmetry of the indices becomes apparent. The scalar curvature R is defined in the usual way from the metric g, whereas γ denotes the induced metric on the hypersurface. It depends on the embedding of the hypersurface and we will come back to it further below. The equations of motion for the scalar and gauge field on the hypersurface are readily derived for a generic embedding. They read

$$D_\mu D^\mu \, \Phi = \partial_{\Phi^\dagger} V \,, \tag{4.6}$$

$$\frac{1}{\sqrt{\gamma}} \partial_\mu \sqrt{\gamma} f^{\mu\nu} = J^\nu \,, \tag{4.7}$$

where the covariant derivative D is defined by

$$D_\mu \Phi = \nabla_\mu \Phi + i\, A_\mu \, \Phi - i\, a_\mu \, \Phi \,, \tag{4.8}$$

with ∇ the Levi-Cevita connection with respect to the induced metric γ, and J denotes the conserved current due to global phase rotations of the scalar, given by

$$J_\mu = -i \, \left(\Phi^\dagger (D_\mu \Phi) - \Phi (D_\mu \Phi)^\dagger \right) \,. \tag{4.9}$$

Note that in the definition of the covariant derivative (4.8), we already made a choice of the charges of the scalar w.r.t. the gauge field a and the Chern-Simons field A.

In the bottom-up holographic Kondo model, the magnetic defect on the field theory side was chosen to be represented as a codimension one hypersurface on the gravity side of the duality. Here, we will stick with this form of representing the impurity. Upon varying the action w.r.t. the bulk metric g, we recover the field equations of general relativity

$$R_{mn} - \frac{1}{2} R\, g_{mn} = \kappa_N\, T_{mn}\,, \tag{4.10}$$

where T_{mn} is the energy-stress tensor in the bulk manifold, and is given by

$$T_{mn} = \frac{-2}{\sqrt{g}} \frac{\delta S_M}{\delta g^{mn}}\,. \tag{4.11}$$

Apart from the hypersurface, the only possible source of energy-stress in the bulk is the Chern-Simons field A. This field, however, is topological, which means that the variation of its action w.r.t. the bulk metric g vanishes identically. This becomes apparent by the fact that the CS action does not involve the metric g at all. Moreover, gravity in 2+1 dimensions has no propagating degrees of freedom. So the metric in the bulk must be given by a vacuum solution. To stay compatible with the original model, we will choose a BTZ black brane as the background. Its metric in Poincare coordinates is still given by equation (3.19). Hence, the temperature of the environment surrounding the defect is given by $T = 1/2\pi z_H$.

The Chern-Simons field is flat in the bulk manifold and can be neglected for the backreaction as was shown in the appendix of [1]. After determining the field configurations of the other fields, one can use its equation of motion to integrate it.

Next, we turn our attention to the hypersurface. The Einstein field equations (4.10) are still applicable in the vicinity of defects in spacetime, that is codimension one hypersurfaces carrying localised non-vanishing energy-stress. In this case, the Einstein equations have to be satisfied in the smooth geometry away from the hypersurface, and are replaced by the so-called *Israel junction conditions* for the metric and its normal derivative at the hypersurface. We need to split our bulk manifold into two parts: The manifolds $\mathcal{N}_-$ and $\mathcal{N}_+$ located to the "left-" and the "right-hand side" of the defect hypersurface $\mathcal{D}$, which they share as a common boundary. This is sketched in figure 4.1. The position of the hypersurface $\mathcal{D}$ is given by a priori independent embeddings

$$\mathcal{X}_\pm : \mathcal{D} \hookrightarrow \mathcal{N}_\pm : (t, z) \mapsto (t, z, X_\pm(t, z))\,, \tag{4.12}$$

where we assumed the coordinate frame on the defect to be induces from

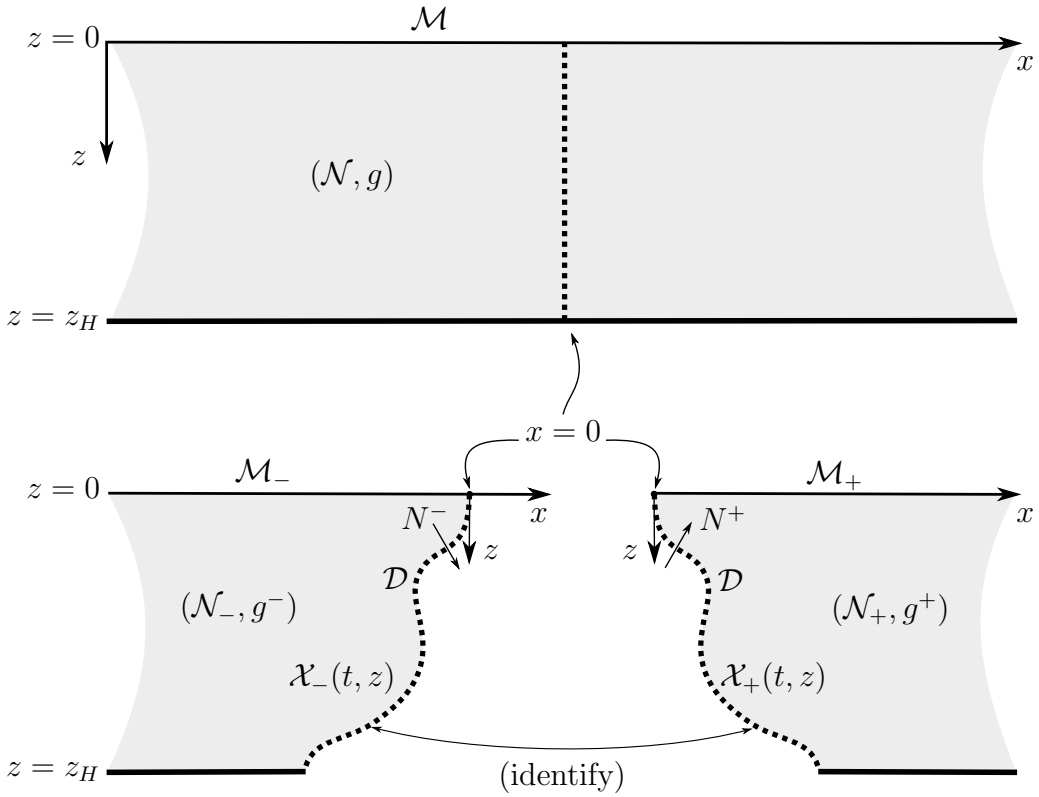

Figure 4.1: Visualisation of the manifold splitting for applying the Israel junction conditions (4.17). *Above*: The geometry without backreaction follows from the trivial, totally geodesic embedding $X = 0$. *Below*: In order to apply the junction conditions, we need to make the defect hypersurface a boundary of two distinct manifolds $\mathcal{N}_+$, and $\mathcal{N}_-$, respectively. We identify points on the different boundaries, and require the induced metric to be unique on the hypersurface. Furthermore, the normal vectors on the defect are defined such that N_- points out of $\mathcal{N}_-$, and N_+ points into $\mathcal{N}_+$.

the ambient geometry.[11] That is, we choose the hypersurface coordinates t and z to be inherited from the bulk manifold, which works as long as the embedding functions $X_\pm$ are differentiable with respect to t and z everywhere in the bulk. This assumption holds true for the energy-stress content in our model, see [1].

With the defect hypersurface $\mathcal{D}$ embedded into $\mathcal{N}_\pm$ by regular embeddings $\mathcal{X}_\pm$, we can compute both the induced metrics and extrinsic curvatures w.r.t. either embedding. The induced metrics are given by pulling back g with respect to $\mathcal{X}_\pm$ and read

$$\gamma_{(\pm)} \equiv (\mathcal{X}_\pm)_* g = \begin{pmatrix} g_{tt} + (\partial_t X_\pm)^2 g_{xx} & (\partial_t X_\pm)(\partial_z X_\pm) g_{xx} \\ (\partial_t X_\pm)(\partial_z X_\pm) g_{xx} & g_{zz} + (\partial_z X_\pm)^2 g_{xx} \end{pmatrix} . \tag{4.13}$$

The extrinsic curvatures of the embeddings $\mathcal{X}_\pm$ are defined by

$$\mathcal{K}_\pm(U,V) = g(\nabla_V U, N_\pm) = -g(U, \nabla_V N_\pm) , \quad \forall U, V \in T\mathcal{D} , \tag{4.14}$$

where $N_\pm \in T\mathcal{N}_\pm$ is a normed vector field normal to the hypersurface and U, V are vector fields which are normed and tangential to the hypersurface $\mathcal{D}$ in the vicinity of $\mathcal{D}$. Their extension to the bulk of $\mathcal{N}_\pm$ is arbitrary and has no impact on the exterior curvatures at $\mathcal{D}$. Our sign convention is that N_- (N_+) is pointing out of (into) $\mathcal{N}_-$ ($\mathcal{N}_+$), see figure 4.1. Defined via (4.14), the extrinsic curvatures $\mathcal{K}_\pm$ are tensors in the ambient geometry. Their information content remains equivalent upon projection onto the hypersurface $\mathcal{D}$ by pulling them back via $(\mathcal{X}_\pm)_*$. The projected extrinsic curvatures are given by

$$\begin{aligned} (\mathcal{X}_\pm)_* \mathcal{K}_\pm \equiv (K_\pm)_{\mu\nu} =& \frac{\partial(\mathcal{X}_\pm)^m}{\partial\xi^\mu} \frac{\partial(\mathcal{X}_\pm)^n}{\partial\xi^\nu} \nabla_m (n_\pm)_n \\ =& -(n_\pm)_m \left(\frac{\partial^2(\mathcal{X}_\pm)^m}{\partial\xi^\mu \partial\xi^\nu} + \Gamma^m_{nk} \frac{\partial(\mathcal{X}_\pm)^n}{\partial\xi^\nu} \frac{\partial(\mathcal{X}_\pm)^k}{\partial\xi^\nu} \right) , \end{aligned} \tag{4.15}$$

where ξ^μ are the coordinates on the hypersurface, Γ^m_{nk} are the Christoffel symbols w.r.t. the ambient metrics $g_\pm$ and $n_\pm$ are the normalised 1-forms dual to the normal vectors $N_\pm$. The similarity of the expression in the last pair of brackets to the geodesic equation is notable and no coincidence. In fact, if the extrinsic curvature vanishes, i.e. $K_{\mu\nu} = 0$, the embedding is called "totally geodesic". The name comes from any geodesic w.r.t. the induced

[11] In general, the coordinates on the hypersurface can be independent from the ones in the ambient geometry. With the choice of induced coordinates, however, the identification of the points on the hypersurface with their location on the boundary of the ambient geometry simplifies.

metric γ on the hypersurface being also a geodesic w.r.t. the ambient metric g in this case. Likewise, any geodesic w.r.t. g in $\mathcal{N}$ starting on $\mathcal{D} \subset \mathcal{N}_\pm$ tangential to $\mathcal{D}$ stays in $\mathcal{D}$.

Having defined the extrinsic curvatures $K_\pm$, we can look at the junction conditions at $\mathcal{D}$ implied by the Einstein field equations (4.10). The original approach by Israel [102] is to split the content of the entire energy stress tensor T in $\mathcal{N}$ into three components by defining

$$T \equiv \Theta(-s)\, T_- + \delta(s) S + \Theta(s)\, T_+ \,, \tag{4.16}$$

where Θ is the Heaviside step distribution, δ the Dirac distribution and s is defined such that the hypersurface is located at $s = 0$. The energy-stress tensor splits into the parts $T_\pm$ defined in the smooth geometries $g_\pm$ away from the defect and *surface energy-stress tensor* S localised on $\mathcal{D}$. We require the induced metric γ to be the same with respect to both embeddings $\mathcal{X}_\pm$, that is, the metic $g = \Theta(-s)\, g_- + \Theta(s)\, g_+$ is imposed to be continuous. Inserting this decomposition into (4.10), and decomposing the Ricci curvature R_{mn} w.r.t. to the local foliation given by the coordinate s, we can compare the coefficients in front of the Θ- and δ-distributions. The coefficients of the Θ-distributions yield that Einstein's equation must still be satisfied in $\mathcal{N}_\pm$, as expected. The components of the Dirac distribution, however, vanish if and only if

$$[K_{\mu\nu} - \gamma_{\mu\nu}\, K] = -\kappa_N\, S_{\mu\nu} \,, \tag{4.17}$$

where for any tensor $A_\pm$ defined via the embeddings $\mathcal{X}_\pm$, the bracket $[A] \equiv A_+ - A_-$ defines its jump across the hypersurface. Hence, (4.17) tells us that the jump between the extrinsic curvatures $K_\pm$ is given by the amount of singular energy-stress S localised on the defect hypersurface $\mathcal{D}$. In appendix A, we emphasise that in a particular coordinate system normal to the hypersurface, the extrinsic curvature is given by $K_{\mu\nu} = -\partial_s \gamma_{\mu\nu}/2$, with s being the same parameter used in the splitting above.

Thus, while requiring the metric g to be continuous around $\mathcal{D}$, codimension one sources of energy-stress introduce a jump in its derivative normal to $\mathcal{D}$. So, the metric itself is in the differentiability class $\mathcal{C}^0$ around $\mathcal{D}$.

The junction conditions (4.17) were first shown in coordinate independent manners by Werner Israel [102], and are thus often called *Israel junction conditions*, a terminology to which we will refer throughout this thesis. They provide the equations of motions for the a priori unknown embeddings $\mathcal{X}_\pm$ and depend on the localised field content on $\mathcal{D}$. If the ambient manifold is vacuum, these equations are supplemented by constraints in the form of

$$\nabla_\mu S^{\mu\nu} = 0 \,, \tag{4.18}$$

$$\{K_{\mu\nu}\}\, S^{\mu\nu} = 0 \,, \tag{4.19}$$

where $\{ A \} \equiv (A_- + A_+)/2$ is the mean of quantities defined w.r.t. the embeddings $\mathcal{X}_\pm$. The first equation (4.18) imposes the divergence of the surface energy-stress tensor to vanish. Although vanishing divergence is natural for a field theory on its own, this form of the divergence does not necessarily hold true if the theory is constrained to a boundary of an ambient theory. Due to the coupling of the defect energy-stress tensor $S_{\mu\nu}$ to the one in the bulk, T_{mn}, the surface energy-stress tensor can actually feature a divergence, which originates in energy-stress flowing from the hypersurface into the bulk and vice versa. In this case, the right-hand side of equation (4.18) would not vanish. In the case at hand, however, both the Chern-Simons field and gravity in 2+1 dimensions contain no local energy-stress. Both theories are purely topological, so there is no possibility of energy-stress flowing from the defect to the bulk geometry in the holographic Kondo model of [60].

Equipped with the proper equations of motion for the embedding, the missing piece is the surface energy-stress tensor itself. It is defined in the same way as a stress-tensor in a smooth manifold by variation of the action with respect to the induced metric γ by

$$S_{\mu\nu} \equiv \frac{-2}{\sqrt{\gamma}} \frac{\delta S_{2D}}{\delta \gamma^{\mu\nu}} \,, \tag{4.20}$$

where S_{2D} is the action of the defect surface as defined in 4.5. By applying the product rule, along with $\delta\sqrt{\gamma} = -\sqrt{\gamma}\,\gamma_{\mu\nu}\,\delta\gamma^{\mu\nu}$, we find

$$\frac{-2}{\sqrt{\gamma}} \frac{\delta S_{2D}}{\delta \gamma^{\mu\nu}} = \gamma_{\mu\nu}\,\mathcal{L}_{2D} - 2\,\frac{\partial \mathcal{L}_{2D}}{\partial \gamma^{\mu\nu}} \,, \tag{4.21}$$

which is more convenient for actual computations. The defect Lagrangian is split into $\mathcal{L}_{2D} = \mathcal{L}_\Phi + \mathcal{L}_a + \mathcal{L}_V$ with the parts given by

$$\frac{\partial \mathcal{L}_V}{\partial \gamma^{\mu\nu}} = 0 \,, \tag{4.22}$$

$$\frac{\partial \mathcal{L}_\Phi}{\partial \gamma^{\mu\nu}} = \frac{-N}{2} \left(D_\mu \Phi^\dagger D_\nu \Phi + D_\nu \Phi^\dagger D_\mu \Phi \right) \,, \tag{4.23}$$

$$\begin{aligned} \frac{\partial \mathcal{L}_a}{\partial \gamma^{\mu\nu}} &= (-N)\,\frac{\partial}{\partial \gamma^{\mu\nu}} \left(\frac{1}{4}\, f_{ij}\, \gamma^{i\alpha}\, f_{\alpha\beta}\, \gamma^{\beta j} \right) \\ &= \frac{-\mathcal{N}}{2} \left(f_{\mu j}\, \gamma^{j\beta}\, (-f_{\beta\nu}) \right) \,. \end{aligned} \tag{4.24}$$

In total, the surface energy-stress tensor is computed to read

$$\begin{aligned} S_{\mu\nu} = &- N\gamma_{\mu\nu} \left(D_\alpha \Phi^\dagger\, D^\alpha \Phi + \frac{1}{4} f_{\alpha\beta}\, f^{\alpha\beta} \right) \\ &+ N \left(D_\mu \Phi^\dagger D_\nu \Phi + D_\nu \Phi^\dagger D_\mu \Phi \right) + N f_\mu{}^\beta\, f_{\beta\nu} \,, \end{aligned} \tag{4.25}$$

where we emphasised the symmetry in its indices.

As we investigate static backreaction in this chapter, we will drop the time dependence in the embedding from now on. Then, we can further simplify the geometric framework by taking into account an apparent symmetry. It comes along with the fact that the Chern-Simons field A is the only field which carries a handedness into the splitting of the whole manifold into $\mathcal{N}_\pm$. However, as written above, the Chern-Simons field decouples from the defect. Hence, it is safe to assume that the embeddings $\mathcal{X}_\pm$ obey a mirror symmetry around the defect. In other words, if we choose the coordinate system and embedding functions $X_\pm$ as in (4.12), the embedding functions $X_\pm$ satisfy

$$X_+(z) = -X_-(z)\,, \tag{4.26}$$

where we dropped time dependence. This symmetry prolongs to the exterior curvatures $K_\pm$ via (4.14) and yields

$$K_{(+)\mu\nu} = -K_{(-)\mu\nu}\,, \tag{4.27}$$

$$[K_{\mu\nu} - \gamma_{\mu\nu}K] = 2\left(K_{(+)\mu\nu} - \gamma_{\mu\nu}K_{(+)}\right)\,, \tag{4.28}$$

$$\{K_{\mu\nu}\} = 0\,. \tag{4.29}$$

Especially, the last symmetry implies that one of the constraints, (4.19), is always satisfied in a symmetric setup like this. Further more, (4.28) allows us the restrict our attention to one side of the defect, e.g. $\mathcal{N}_+$, by plugging it into (4.17). The resulting equations of motion for the embedding are then given by

$$K_{\mu\nu} - \gamma_{\mu\nu}K = -\frac{\kappa_N}{2}\,S_{\mu\nu}\,, \tag{4.30}$$

where we already dropped the (+)-sign indicating the origin of the extrinsic curvature. Due to the symmetry (4.28), this should not cause any confusion anymore and we will stick to this notation for the rest of the thesis. After solving (4.30), we can easily obtain the embedding on the (−)-side by applying (4.26).

Note that equation (4.30) is just the Neumann boundary condition for general relativity on a manifold with boundary that carries boundary degrees of freedom. Actually, this can be seen more directly by deriving the Israel junction conditions from an action approach, see e.g. [103]. If we want to write down an action for gravity on a divided geometry with boundaries as shown in figure 4.1, we must add the Gibbons-Hawking-York boundary term to the action in order to render the variational problem meaningful. In [103], this was done and the junction conditions are then derived by varying this action with respect to the embedding. The same von Neumann condition was

used e.g. by [64, 65] which considered BCFTs without additional degrees of freedom, but with a constant boundary tension $S_{\mu\nu} = -\lambda\gamma_{\mu\nu}$. We will come back to a similar model in section 4.3, where we will find that the normal phase is perfectly well described by a constant tension on the hypersurface.

Due to the similarity with Neumann boundary conditions in the symmetric case, our model can be regarded as a holographic gravity dual both to a defect conformal field theory (DCFT), as well as to a boundary conformal field theory (BCFT) as emphasised in [1]. In fact, this simplification reminds us of the mathematical trick deployed by Affleck and Ludwig [87, 88]. They started with dropping any interactions between the Kondo impurity and the host degrees of freedom but the s-wave after a partial wave decomposition. For the latter, we need to define a centre of the geometry by $r = 0$, where $r \in [\,0, \infty)$ is some radial coordinate. In the s-wave decomposition, the current in the host metal decouples into its left- and right-moving components, which are chiral. The mathematical trick is then to enhance the range of r to $-\infty < r < +\infty$ and map the right-moving current to a left-moving current in $r \in (-\infty, 0\,]$.

The top-down model of [60], however, starts already at this point: The D-brane construction shown in table 3.1 leads to left-moving chiral currents on the field theory, defined throughout $x \in (-\infty, +\infty)$, which is the boundary radial coordinate similar to r above. In our framework for backreaction, we just showed that we may restrict our attention again to $x \in [\,0, +\infty)$ due to symmetry reasons. During this process we considered only to the field content on the hypersurface, which is symmetric under this mapping, as the Chern-Simons field in the bulk of the gravity dual decouples from the hypersurface. To complete the reduction to $\mathcal{N}_+$, however, we certainly would need to map the Chern-Simons field A in $\mathcal{N}_-$ to some equivalent object in $\mathcal{N}_+$. Although the full analysis is not performed in this thesis, we may speculate that this object would be a Chern-Simons field of opposite chirality in $\mathcal{N}_+$, which completes the analogy with the conformal field theory approach of [87, 88] to the Kondo model.

4.2 Holographic defect entropy

If we succeed in computing the embeddings of the defect surface described by eq. (4.17), how do we extract the corresponding defect entropy? In section 2.3.4, we reviewed a well-known proposal how to compute entanglement entropy holographically. Here, we'll use this proposal to define a holographic way of computing defect entropies for models similar to what we described above in the sense that the impurity is extending on a defect hypersurface

into the bulk of the gravity dual.

The defect entropy S_D is defined in the following way: We assume that the field theory side of a holographic duality contains a defect and define an area A symmetrically around the defect, where ℓ denotes the radius of the boundary ∂A to the impurity. We can compute the entanglement entropy $S(\ell)$ of A using the holographic description, i.e. (2.91).

Afterwards, we subtract the holographic entanglement entropy $S_0(\ell)$ of A in the same theory, but without any defect. In our approach to holographic models of impurities, this is simply the same as using the trivial embedding $X = 0$. Hence, the geometry without any defect is given by the BTZ black hole at the same temperature and the entanglement entropy of A is given by [65]

$$S_0(\ell) = S_{BH}(\ell) = \frac{c}{3} \log\left(\frac{1}{\epsilon\,\pi T}\sinh(2\pi\, T\,\ell)\right), \tag{4.31}$$

where ϵ denotes a cutoff in the form of a grid constant, which is necessary to render the result finite, ℓ denotes the distance from the impurity, and c is the central charge of the conformal field theory. The difference between $S(\ell)$ and $S_0(\ell)$ can only be affected by the presence of the defect and its entanglement with the environment. We denote this difference as the *defect* or *impurity entropy*, which is given by

$$S_D(A) = S(A) - S_0(A)\,. \tag{4.32}$$

The nontriviality in our case comes from the holographic description of the defect. Instead of smearing out the defect in the bulk, i.e. having a smooth holographic dual[12], we follow the authors of [60] and choose a singular representation in the sense that the defect on the field theory side maps to a defect hypersurface in the bulk of its gravity dual. Although the dual metric is required to be continuous, its derivative normal to the hypersurface (which, by definition, is the extrinsic curvature) will have a jump, determined by the Israel junction conditions [102], as discussed in section 4.1.

This can be dealt with by taking equation (2.91) serious: We solve an optimisation problem for minimal surfaces across a hypersurface connecting two manifolds subject to gluing conditions. Luckily, for the 2+1-dimensional case, the minimal surfaces are given by geodesics and the restriction of this optimisation problem to geodesics was already solved in [107].

[12] For approaches in which the defect smears out into a smooth geometry in the bulk, see e.g. [104–106] for Janus solutions. It should be noted at this point that Janus solutions are more compatible with proper top-down approaches to impurities which can be embedded in string theory.

So, in our case the formula for holographic entanglement entropy (2.91) reduces to refraction conditions for the geodesics at the defect hypersurface. Let the geodesics in the spatial submanifolds of $\mathcal{N}_\pm$ (see figure 4.1) be given by

$$\gamma_\pm(\tau) = \left(\gamma_\pm^z(\tau), \gamma_\pm^x(\tau)\right) , \tag{4.33}$$

where τ is some affine parameter. Assuming $\gamma_-(0) = \gamma_+(0)$ being located on the defect hypersurface $\mathcal{D}$ and applying variational methods, the authors of [107] found that at the hypersurface the geodesics need to satisfy

$$g_-\left(\dot\gamma_-(0), t\right) \stackrel{!}{=} g_+\left(\dot\gamma_+(0), t\right) , \quad \forall t \in T\mathcal{D} , \tag{4.34}$$

in order to minimise their total length for any starting points in $\mathcal{N}_-$ and ending points in $\mathcal{N}_+$. Of course, apart from the hypersurface, the geodesics need to solve the geodesic equation as the metrics $g_\pm$ are smooth.

We assume a static geometry in $d+1$ dimensions, so the geodesics will have d components. The refraction conditions (4.34) are $d-1$ matching conditions for a codimension two defect hypersurface $\mathcal{D}$. Adding the normalisation of the geodesic tangents $||\dot\gamma_\pm|| = 1$, we find a total of d constraints for d components. Hence, starting with a geodesic γ_- in $\mathcal{N}_-$, which eventually hits $\mathcal{D}$ at $\gamma_-(0)$ with velocity $\dot\gamma_-(0)$, we are guaranteed to find the outgoing geodesic starting at $\gamma_+(0) = \gamma_-(0)$ and velocity $\dot\gamma_+(0)$ by solving (4.34).[13]

For the case of symmetric ambient manifolds $\mathcal{N}_\pm$ in the sense of equations (4.26)-(4.29), it was shown in [108] that the geodesics need to approach $\mathcal{D}$ orthogonally in order to satisfy the refraction conditions, i.e.

$$g_-\left(\dot\gamma_-(0), t\right) = 0 = g_+\left(\dot\gamma_+(0), t\right) , \quad \forall t \in T\mathcal{D} . \tag{4.35}$$

Hence, together with the normalisation constraint, we find that we need to solve for the geodesics whose initial velocity is given by the normal of the defect hypersurface. Note, that this only holds for minimal surfaces associated with the entanglement entropy of regions A *symmetric* around the defect, which, however, is the scope of this thesis.

So, by requiring symmetric embeddings in the sense of (4.26), we can compute the entanglement entropy of a symmetric patch A as follows: We restrict ourselves to the (+)-side of the divided manifold as discussed at the end of section 4.1 and solve for the respective embedding via (4.30) and the equations of motion for the field content on the hypersurface. Afterwards, for each point on $\mathcal{D}$, we compute the geodesic starting normal to the hypersurface at that point and moving into the bulk. Due to (4.26), the corresponding

[13] Here, we neglect the possibility that there could be phenomena like total reflection at some critical angle, which will not relevant for our discussion.

geodesic in the other half of the manifold, $\mathcal{N}_-$, is simply given by changing the sign of the x-component of the geodesic we just solved for. The important part, its proper length, is the same as for the computed geodesic, so essentially we just need to take that twice in order to find the entanglement entropy via (2.91).

Note, that we do not need to renormalise the proper length of the geodesics as we subtract the divergent parts at asymptotic infinity automatically via the definition of the defect entropy (4.32). The divergence appears as the leading order term close to $z = 0$ in the proper length, which is both independent of the temperature and the asymptotic position $\ell = \gamma_+^x(z = 0)$.

There is one more observation, that simplifies the analysis of the defect entropy dramatically. It is the fact, that while our embeddings $\mathcal{X}_\pm$ are in principal arbitrary (numerical) solutions to (4.17), the background metrics in the ambient geometries, $g_\pm$, are constant by construction and still given by the BTZ metric (3.19). This is due to having no propagating degrees of freedom in our 2+1-dimensional model with only topological fields in the 2+1-dimensional bulk.

Moreover, the geodesics in this metric are known analytically, see e.g. [109]. So instead of computing numerical solutions to the geodesic equation for each starting point on the defect $\mathcal{D}$, we just need to fit the point and its normal with the known solutions, which is faster and exact. This way, the only source of numerical uncertainty entering our results of the defect entropy (4.32) is given by numerical errors in the embeddings themselves. To suppress those as much as feasible, we apply pseudospectral methods by computing the embeddings and its derivatives on a Chebyshev-Gauss-Lobatto grid. For the details of the numerical approach, we refer the reader to appendix B.

4.3 Background solution: The normal phase

Solving the coupled equations for the scalar and gauge field seems intractable. Hence, we need to resort to numerical methods. In order to do so, we typically need an initial guess to seed the solution algorithm. In this section we will describe how to find an analytic solution in case of a vanishing scalar field, which luckily is also the case for temperatures at or above the critical temperature, $T \geq T_c$. Of course, we need to assume that the system still has a phase transition, which will turn out to be true.

In the normal phase, the scalar field is trivial, $\Phi = 0$, and the only energy-stress on the hypersurface originates in the gauge field a. The electric flux

of a d-form in D dimensions is in general defined by

$$\mathcal{C} = \int_{S^{D-d-1}} *f_{d+1}\,, \tag{4.36}$$

where $*$ denotes the Hodge star. According to the dictionary discussed in chapter 3, its asymptotic limit as $z \to 0$ is dual to the representation of the defect, which is hence given by

$$\mathcal{C} \equiv \sqrt{\gamma}\, f^{tz}\big|_{z\to 0}\,. \tag{4.37}$$

If the scalar field vanishes and we are interested in static solutions, the equation of motion for the gauge field reduces to

$$\partial_z \underbrace{\left(\sqrt{\gamma} f^{zt}\right)}_{=\mathcal{C}} = 0\,, \tag{4.38}$$

which already tells us that the electric flux is constant along the hypersurface, i.e. $\sqrt{\gamma} f^{tz} = \mathcal{C}$ everywhere. This is intuitive, since there is no charged field which could screen the flux. We have found a background solution for the gauge field, which still depends on on the induced metric and hence the embedding. In order to find out what this implies for the junction conditions, which are the equations of motion of the embedding, let's have a look at the energy-stress due to the background solution of the gauge field. Following our analysis above, the energy-stress tensor for vanishing scalar is given by

$$S_{\mu\nu} = -\frac{\mathcal{N}}{4}\left(f_{\alpha\beta}\, f^{\alpha\beta}\right)\gamma_{\mu\nu} + \mathcal{N} f_\mu{}^\beta\, f_{\nu\beta} = \frac{\mathcal{N}}{4}\, f_{\alpha\beta}\, f^{\alpha\beta}\,, \tag{4.39}$$

where in the last equality we used that $f_\mu{}^\beta\, f_{\nu\beta} = \gamma_{\mu\nu} f_{\alpha\beta}\, f^{\alpha\beta}/2$ which holds in our case of a 1+1-dimensional, diagonal metric γ. Applying $\sqrt{\gamma} f^{tz} = \mathcal{C}$ then yields

$$S_{\mu\nu} = -\frac{\mathcal{N}}{2}\,\mathcal{C}^2 \gamma_{\mu\nu}\,. \tag{4.40}$$

This is, remarkably, setting a constant tension on the hypersurface, since the energy-stress tensor is proportional to the induced metric, $S_{\mu\nu} \sim \gamma_{\mu\nu}$. In appendix A, we show that in such cases, there is a construction to generate solutions of the Israel junction conditions if we have a valid initial solution of constant tension.

To wrap it up, it works by following the geodesic normal flow of the hypersurface. To begin with, we can find a valid solution to the equations of motion of the field content on the hypersurface by imposing the gauge field to vanish, too. A possible solution for the embedding consistent with our

boundary conditions, $X(z=0)=0$, is then given by setting $X^{(0)}(z)=0$ in (4.12). In this case, all of our assumptions in appendix A hold true and we can apply the flow construction. To do this, we have to define a vector field which is normal to the hypersurface, normed, and for each starting point on the hypersurface, the integral curve of that point along the vector field satisfies the geodesic equation. We define new embeddings $\mathcal{X}^{(s)}:\mathcal{D}\hookrightarrow\mathcal{N}$ as the set of points which we obtain by following the normal geodesic at each point on the initial hypersurface $\mathcal{X}^{(0)}$ for a proper length s. After following the geodesic normal flow for an arc length s, the embedding function $X_+=X^{(s)}$ is given by

$$X^{(s)}(z)=-z_H\,\mathrm{artanh}\left(\frac{\sinh(s/L)}{\sqrt{(z/z_H)^2+\sinh^2(s/L)}}\right)\,. \tag{4.41}$$

Upon integrating the equation of motion (4.7) for the gauge field with vanishing scalar field and an embedding given by (4.41), we find the analytic solution

$$a_t^{(s)}=\frac{\mathcal{C}\,L^2}{z_H}\cosh(s/L)\left(\cosh(s/L)-\sqrt{(z/z_H)^2+\sinh^2(s/L)}\right)\,. \tag{4.42}$$

In order to eliminate the auxiliary variable s, we can plug equations (4.41) and (4.42) into the Israel junction conditions and find

$$\tanh\left(\frac{s}{L}\right)=\frac{L}{4}\,\kappa_N\,\mathcal{N}\,\mathcal{C}^2\,. \tag{4.43}$$

At this point, we should keep in mind that s can have either sign. According to our convention, the normal vector field is pointing out of the bulk manifold $\mathcal{N}$, such that its volume grows if $s>0$, which is indeed the case as can be seen from (4.43). A sketch of the geodesic normal flow construction is shown in figure 4.2, where we see how the embedding changes as we increase the parameter $s>0$, initially starting at the trivial and totally geodesic embedding with $s=0$.

The extrinsic curvature K_s and the induced metric γ_s as functions of the parameter s are readily derived to read

$$\gamma_s=\left(\frac{L\cosh(s/L)}{z_b}\right)^2\left(-f(z_b)\,\mathrm{d}t^2+f^{-1}(z_b)\,\mathrm{d}z^2\right)\,, \tag{4.44}$$

$$K_s=\frac{-L\sinh(s/L)\cosh(s/L)}{z_b^2}\left(-f(z_b)\,\mathrm{d}t^2+f^{-1}(z_b)\,\mathrm{d}z^2\right)\,, \tag{4.45}$$

where z_b denotes the point on the trivial embedding $X = 0$, from which we start following the normal geodesic for an arc length s to find the embedding X_s. The induced metric and extrinsic curvature obviously satisfy

$$K_s = -\tanh(s/L)\,\gamma_s/L\,, \tag{4.46}$$

which is shown in appendix A to hold in more generality than in the context presented here.

From (4.43), we can already tell our first analytic result regarding the defect entropy. We remember from section 4.2, that the minimal surfaces whose area give us the defect entropy have to start normal to the defect hypersurface. As we just have seen, the embeddings for vanishing scalar fields are generated by using the same geodesics. Hence, the defect entropy S_D as defined by (4.32) will simply be proportional to the arc length $s = L\,\mathrm{artanh}\,(L\,\kappa_N\,\mathcal{N}\,\mathcal{C}^2/4)$ used in our construction above. This will describe the overall offset of S_D for any choice of $\mathcal{C}$, κ_N, and $\mathcal{N}$.

Moreover, equation (4.43) puts a constraint on the matter content on the defect hypersurface. As the tanh function takes its values between -1 and $+1$, the allowed range of values for the parameters $\mathcal{N}$, $\mathcal{C}$, $\mathcal{L}$, and κ_N is restricted to

$$0 \leq L\,\kappa_N\,\mathcal{N}\,\mathcal{C}^2 \leq 4\,, \tag{4.47}$$

where we already took into account that the appearing product of parameters is always positive. To the best of the authors knowledge, there is no such constraint on the Kondo model on the field theory side. Investigating its physical reason would be very interesting, but is left for future research.

This concludes the analysis of the normal phase in the static backreaction of the holographic Kondo model. In the next section, we will start from this background solution and describe the system's behaviour in terms of the temperature T as it drops below the critical temperature T_c, at which point the scalar field becomes non-trivial.

4.4 The condensed phase

So far, we could track the equations analytically as the scalar field was vanishing. However, our model features similar phenomenology as the original holographic Kondo model [60]. Especially, we have a phase transition between the normal and the condensed phase at a critical temperature $T_c \approx T_K$ below which the scalar field becomes non-trivial. Via the duality, this means the scalar operator $\mathcal{O}$ on the field theory side condenses. We are not able to discuss this case analytically anymore and need to apply numerical methods.

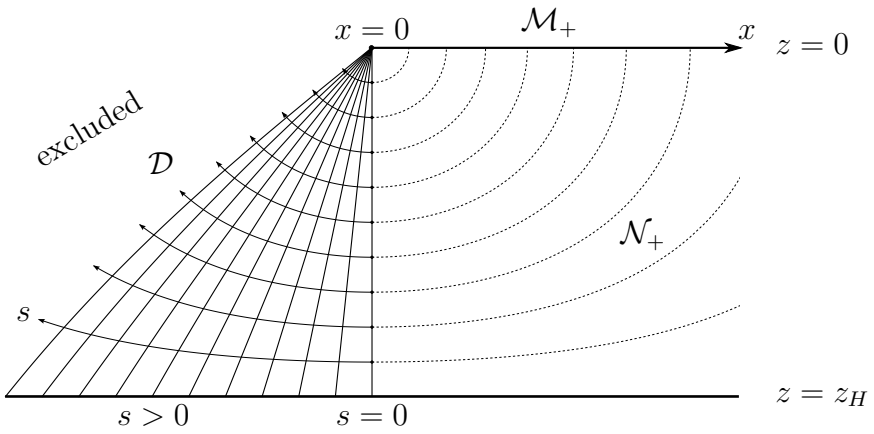

Figure 4.2: Geodesic normal flow of the embedding $\mathcal{D}$ in the (+)-part of the geometry. More volume is added to $\mathcal{N}_+$ as the parameter s is increased.

In the end, this will mean that for temperatures $T < T_c$ in the condensed region, we can only provide numerical embeddings and defect entropies. In this section, we will give an overview on the computational approach and refer to appendix B for further details.

4.4.1 Reduction of the equations of motion

Solving the equations of motion for the field content on the brane and the embedding means solving equations (4.6), (4.7) and, after imposing the mirror symmetry, (4.30). However, the Israel junction conditions (4.30) is a tensor equation, so it provides $(d+1)^2$ equations for a $d+1$-dimensional defect. In our case, these are three independent equations for one independent function X, so there is some redundancy. Usually, we would try to solve the equation of motion with highest derivatives of X. The surface energy-stress tensor S is built from intrinsic objects on the hypersurface only and the only occurrence of the embedding is in the induced metric. It is shown in (4.13) and carries only first derivatives of X. Indeed, for our static setup, only the zz-component features derivatives of the embedding function. Looking at (4.15), we find that the component of K carrying second derivatives in X is the zz-component, whereas in the tt-component only first derivatives appear. However, the combination $K_{\mu\nu} - \gamma_{\mu\nu} K$ inverses this behaviour and the second derivatives appear in the tt-component. So we would solve the equations of motions of the scalar and gauge field, and the tt-component of the junction conditions. The left-over zz-component is a constraint equation, including *only* the first derivative of X.

Fortunately, we find that this constraint is exactly solvable for $X'(z)$. There are four solutions, but we can sort out three of them by requiring the solution to be real and having $X'(0) < 0$ in order to match our analytic background solution (4.42). The left-over solution is given by equation (B.4) in appendix B.

In the equations of motion for the scalar and gauge field, the embedding only appears via the induced metric and, hence, only in the form of its first derivative. So, an alternative approach is to solve the Israel junction conditions for $X'(z)$ and plug the solution into the rest of the equations. This way, we can reduce the set of equations of motion from three ODEs for Φ, a_t and X to two ODEs for Φ and a_t, only. After solving this set of equations, we can obtain X by applying the numerical solutions for Φ and a_t in the solution of the constraint, which yields $X'(z)$, and integrate it starting from $z = 0$ to the horizon. The integration constant yields $X(z = 0)$, which we set to zero to match the defect being located at $x = 0$ on the field theory side.

4.4.2 Boundary analysis

We need to get away from the asymptotic boundaries in order to solve the equations numerically, as they present singular points of the set of differential equations. Hence, we expand the equations order by order in the radial coordinate at asymptotic infinity and at the event horizon, and solve for the coefficients. The respective leading and next-to-leading order coefficients cannot be determined by this procedure. For each field, one of them will represent a boundary condition to be chosen. The other one will only be revealed after integrating the equations of motion numerically in the whole domain. However, any remaining coefficient can be solved in terms of the leading and next-to-leading order coefficients.

After the reduction mentioned in the previous section, we are left with only two fields, Φ and a_t. The boundary expansions of those fields to leading order at asymptotic infinity ($z = 0$) are, like in [60], given by

$$\Phi(z) \sim \alpha\sqrt{z}\log z + \beta\sqrt{z} + O(z^{3/2})\,, \tag{4.48}$$

$$a_t \sim \frac{Q}{z} + \mu + c_1\log(z) + c_2\log(z)^2 + c_3\log(z)^3\,, \tag{4.49}$$

where the c_i are next-to-next-to-leading order coefficients, and can be solved in terms of α, β, Q and μ. Q itself is already determined by the normal phase solution (4.42) of the gauge field. Its value is given by

$$Q = -\mathcal{C}\,L^2\,\cosh(s/L)\,, \tag{4.50}$$

which is completely constrained by choosing the electric flux $\mathcal{C}$ and applying (4.43). The mass of the scalar field needs to be fixed such that the scalar field is right at the Breitenlohner-Freedman stability bound [79]. Only then, the conformal dimension of the scalar operator maps to $\Delta = 1/2$ via the holographic dictionary. This is accomplished by setting

$$M^2 = \frac{4\,Q^2\,\cosh^2(s/L) - 1}{4\,L^2\,\cosh^2(s/L)}\,, \tag{4.51}$$

which, again, is fixed by applying (4.50) and (4.43). This concludes the expansions at asymptotic infinity.

At the event horizon, the fields need to satisfy regularity conditions. These essentially come from the fact that the event horizon is a tautological construct and cannot be determined locally. Subsequently, a local field theory ought not behave in any weird way around an event horizon and especially the fields involved cannot diverge. However, in a time dependent analysis we find that there are irregular modes for the fields.

In a static setup, the event horizon falls together with the apparent horizon, which is locally detectable. In this case, we can define boundary conditions on the event horizon. Essentially, they follow from applying a boundary analysis of the fields around the location of the horizon. Unlike in the case of the asymptotic boundary, only one coefficient per field is left undetermined.

So in contrast to the asymptotic boundary, the boundary conditions at the event horizon need not to be imposed by hand, but follow from the special nature of this boundary. For each field, one of the leading order coefficients is constrained and, in the case at hand, given by

$$\Phi'(z_H) = -\frac{L^2\,M^2\,\Phi(z_H)}{2\,z_H}\,, \tag{4.52}$$

$$a_t(z_H) = 0\,, \tag{4.53}$$

$$X'(z_H) = \kappa_N\,\frac{2\,L^4\,M^2\,\Phi(z_H)^2 - z_H^4\,a_t'(z_H)^2}{4\,L^3}\,. \tag{4.54}$$

Thus, we can arbitrarily choose $\Phi(z_H)$, $a_t'(z_H)$ and $X(z_H)$ to integrate all fields from the horizon and obtain valid solutions throughout the bulk. However, the fields eventually need to satisfy the imposed boundary conditions at asymptotic infinity, which reduces the solution space. Of course, we need not to impose the condition (4.54) for the embedding if we eliminated it from the set of independent fields by reducing the set of equations of motion, as explained in section 4.4.1.

4.4.3 Computational strategy

We are left to solve the equations of motion for the field content on the hypersurface given by (4.6) and (4.7), which only depend on Φ and a_t after replacing any occurrence of X' and X'' by the solution from the constraint. The further procedure is the same as it would be without embedding. We compute the asymptotic and horizon expansions of the fields, which due to having the scalar field exactly at the Breitenlohner-Freedman bound, contains logarithmic terms at asymptotic infinity. The order of the highest logarithmic term is increasing with the order of the expansion variable, which is z. For computational convenience, we need to define numerical values for the parameters $\mathcal{C}$, Q, κ, L and z_H. Otherwise, the doing the expansions at asymptotic infinity takes too long. For the plots in the next section 4.5 we choose

$$\kappa_N = 1,\ L = 1,\ z_H = 1 \quad \text{and} \quad \mathcal{C} = 1/2. \tag{4.55}$$

Note that the values for L and z_H can always be achieved due to scale invariance of the equations of motion. The value for the electric flux $\mathcal{C}$ was chosen to be consistent with the computations in [60]. As we will see below, the results are surprisingly close.

After computing the expansions to a convenient order, we define cutoffs ϵ_{bnd} and ϵ_{hor} near the asymptotic boundary and the event horizon. We choose

$$\epsilon_{bnd} = 10^{-3} \quad \text{and} \quad \epsilon_{hor} = 1 - 10^{-1}\,, \tag{4.56}$$

which resembles the appearance of logarithmic terms near asymptotic infinity, which makes the approximation error grow faster as we go away from the singular point. At the horizon, the expansions are analytic and there is not much precision lost by going away from the horizon.

Between the cutoffs and the boundaries, we know the solutions of the equations of motion approximately due the expansions. Between the cutoffs, we solve the equations numerically by applying the shooting method. That is, for each field we choose the two leading order coefficients and use the expansions to obtain the field values and their derivatives at ϵ_{bnd}. For each field, we have one asymptotic boundary condition. For the gauge field component, this is fixing Q via (4.50). The scalar field still has the same boundary conditions as in the original model of [60], which are given by (3.30). Hence, one of the leading order coefficient can be chosen freely.

Of course, we need to fix those in order to obtain e.g. the vacuum expectation value of the scalar operator, given by $\beta \sim \langle \mathcal{O} \rangle$. To do this, we numerically integrate the equations of motions in the numerical domain, given one fixed coefficient and one variable coefficient for each field. As we reach the

horizon cutoff ϵ_{hor}, we are able to obtain the coefficients of the horizon expansion for each field. We check how much the horizon conditions (4.54) are violated and correct the variable boundary coefficients in a direction which improves the misalignment. This is done by infinitesimally varying them, repeating the above steps, and looking at the mismatch for each variation. From this we can compute a numerical gradient which tells us the optimal direction of the next choice for the boundary coefficients. We change the boundary coefficients accordingly and reiterate until the mismatch drops below a numerical threshold. The final set of boundary coefficients corresponds to the numerical solution for the choices of the fixed boundary coefficients we made. Afterwards, we choose another set of fixed coefficients and start from the beginning.

In our computations, we used Q and μ as fixed boundary coefficients. Although they both appear in the expansion of the gauge field a_t, the discussed procedure works just as fine. We start from the normal phase in which μ is given by

$$\mu_c = \frac{\mathcal{C}\, L^2\, \cosh^2(s/L)}{z_H}\,, \tag{4.57}$$

which is obtained by expanding (4.42) as a series in z and comparing with (4.49). Then, we take a range of values for $\mu > \mu_c$ which will correspond to solutions in the condensed phase, i.e. $T < T_c$, and compute the numerical solutions for each of them. As we want to obtain the embedding profiles of the solutions in order to compute the entanglement entropy, we need to store the whole solution profiles of Φ and a_t.

Having found numerical solutions for Φ and a_t, we can use them in equation (B.4) to numerically integrate $X'(z)$ and find $X(z)$. Its value at the asymptotic boundary is fixed to $X(0) = 0$, which is the only integration constant we need to provide and is physically sensible. With these embedding profiles, we can apply the discussion of section 4.2 and find the defect entropies for any symmetric regions A around the defect by following the respective geodesics starting normal to the hypersurface.

At this point, we are done with the computations and can investigate the results. Further details about the actual implementation of what was discussed in this section are provided in appendix B.

4.5 Analysis of the results

In the previous sections, we discussed the framework for static backreaction in a holographic Kondo model, along with the computational approach to solve for the field content, the embeddings and eventually the defect entropy.

In this section, we will analyse the numerical results and compare them to the literature.

As the final result, we obtain is the defect entropy S_D as a function of the region A which lies symmetrically around the defect located at $x = 0$. More specifically, the parameter entering the defect entropy is the radius ℓ at which the boundary ∂A of the region A is located. $S_D(\ell)$ will turn out to be a monotonically decreasing function, which will be interpreted in terms of a g-theorem, stating that the defect entropy decreases as we follow a renormalisation group (RG) flow from higher to lower energies. The RG flow comes along with the fact that as we increase the radius ℓ of ∂A, we effectively measure the defect entropy at growing length scales i.e. at lower energies.

Another kind of RG flow is provided by fixing the interval radius around the impurity and changing the temperature T of the system. As the temperature sets a typical scale at which the impurity interacts with its environment, higher temperatures mean higher energy scales in the RG flow. This is also done in the literature about Kondo physics, see eg. [110], to provide a cutoff in the momentum integration. Hence, it corresponds to a physical renormalisation scale.

As anticipated from the behaviour of the model in the probe limit (see [60] and chapter 3), the system features a phase transition at a critical temperature $T_c \approx T_K$. For $T < T_c$, the scalar field and hence the scalar operator condenses, i.e. $\langle \mathcal{O} \rangle \neq 0$. Remarkably, the dependence of this condensate on the temperature is almost exactly the same as for the system without backreaction, which is shown in figure 4.3. When looking at this figure, we should keep in mind that the numerical values of the boundary expansions and fields actually *did* change. However, the final result does not seem to be affected after reducing the numbers to meaningful quantities, i.e. normalising e.g. with respect to the critical temperature T_c. To show this, we have a look at the critical value of κ_T, which is decreases by around 10% to

$$\kappa_c \approx 8.161\,, \tag{4.58}$$

if we include backreaction. This differs from the result without backreaction, $\kappa_c \approx 8.98$ in (3.46), much more than the results shown in figure 4.3, for example. Unfortunately, an explanation for this invariance is lacking so far.

Coming back to the discussion in section 3.2.2, we see in figure 4.4 that the condensate $\langle \mathcal{O} \rangle \sim \beta$ itself is still diverging as $T \to 0$. This is not surprising, as we did not stabilise the scalar potential, which is left for future research.

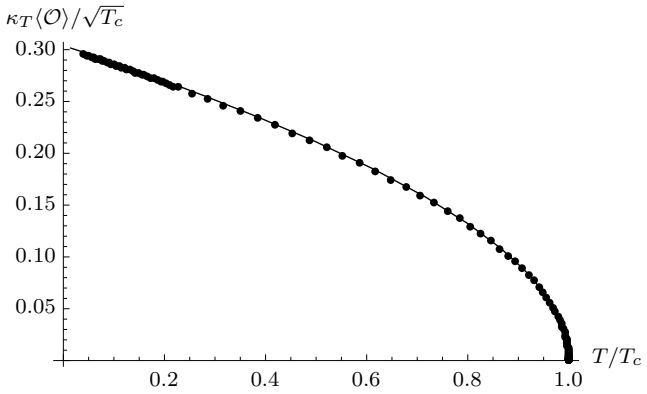

Figure 4.3: Shown is the combination $\kappa_T \langle\mathcal{O}\rangle\sqrt{T_c}$ as a function of the temperature T of the system. The dots denote numerical data including backreaction while the line is an interpolation from the data without backreaction, c.f. section 3.2.2.

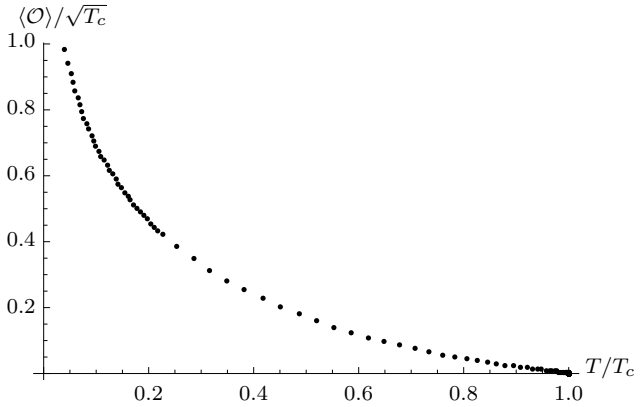

Figure 4.4: Shown is the condensate $\langle\mathcal{O}\rangle$ as a function of the temperature T of the system. Like in [60], the condensate divergences as $T \to 0$, which is due to the potential being unbound from below.

4.5.1 Embeddings at different temperatures

As outlined in section 4.4.3, once we found the numerical solutions of Φ and a_t throughout the hypersurface for various temperatures, we use equation (B.4) to integrate the embedding profiles. More details about the numerical approach are found in appendix B. The embeddings are shown in figure 4.5, where each embedding is drawn in a colour indicating the temperature. Red is for temperatures close to $T = T_c$, while blue graphs are closer to $T = 0$.

We can lower the temperature until $T/T_c \approx 0.04$ where our numerics become unstable. This, once more, is most likely due to the fact that we did not stabilise the scalar potential, which results in stiff equations of motions at low temperatures that are hard to integrate.

From their graphs, we see that the embeddings never cross each other. Moreover, although not shown in figure 4.5, the geodesics starting at different values of z on each embedding never cross each other, too. This puts a non-trivial constraint on the shape of the embeddings and can probably be derived from energy conditions on the brane, which, however, is left for future research. The implications of this are two-fold: Firstly, if the geodesics would cross each other, there would at least be two geodesics where one starts lower in the bulk, at a larger value of z, but asymptotically ends up at a value of x which is closer to the impurity at $x = 0$ then the other geodesic. This would imply a cusp in the entanglement entropy, and thus in the impurity entropy, as a function of the distance ℓ from the impurity. Secondly, one result of this computation, that the impurity entropy satisfies a g-theorem, would probably be spoiled. We will describe the g-theorem further below in section 4.5.3. Finally, a follow-up result about a holographic g-theorem for complexity, published in [111], would likely be spoiled by this, too.

4.5.2 Defect entropy

As described in section 4.2, the entanglement and impurity entropies are holographically dual to the renormalised lengths of geodesics starting normal at an embedding for a specific temperature. Those geodesics starting deeper in the bulk, i.e. at larger values of the radial coordinate z will asymptotically end up at a larger distance ℓ from the impurity. For a given starting position and a starting velocity, the desired geodesics are known analytically, see e.g. the appendix of [109]. We use their formulae to compute the distances ℓ to the defect at $x = 0$ at which all the geodesics on the Chebyshev-Gauss-Lobatto grid in z on the respective embedding end up, as well as their arc lengths. From their lengths, we subtract the geodesic which ends up at the same distance ℓ but starts perpendicular to the trivial embedding $X = 0$.

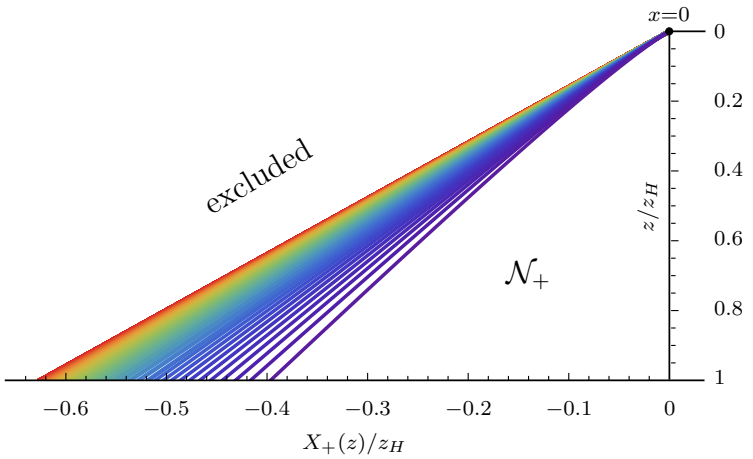

Figure 4.5: Shown are various embeddings of the defect hypersurface, where the temperature is encoded in the embeddings' colours. Red graphs denote temperatures close to the critical temperature $T = T_c$, while blue graphs are those closer to zero temperature $T = 0$. The embedding at lowest temperature is at $T/T_c \approx 0.04$. Embeddings at different temperatures never cross each other and they all end up at $x = 0$ with the same slope.

This serves two purposes: Firstly, we automatically renormalise the geodesic lengths to finite values. The diverging parts near the asymptotic boundary at $z = 0$ are the same for any geodesic and thus the divergent parts cancel exactly if we subtract the proper length of any two geodesics ending up at $z = 0$. Secondly, this is just the definition of the impurity entropy (4.32) if we normalise the resulting difference by the factor $1/4G_N$ in (2.91). The resulting function $S_D(\ell) = S(\ell) - S_0(\ell)$ is an interpolation from the discrete set $\{\{l_i, S_D(l_i)\}|i = 0 \dots n\}$ where n corresponds to our choice of the number of starting points, i.e. the size of the Chebyshev-Gauss-Lobatto grid on the embeddings.

The defect entropies $S_D(\ell)$ are shown in figure 4.6 as functions of the distance ℓ for various temperatures. Here, we replaced the factor of G_N appearing in the Ryu-Takayanagi formula by the central charge c of the field theory away from the defect by using the Brown-Henneaux formula $c = 3\,L/2\,G_N$. As we can see, the defect entropies all start at the same constant value as $\ell \to 0$, which we denote by $S_D^* = S_D(0)$. Furthermore, those close to the critical temperature T_c, denoted by red graphs, essentially stay close to S_D^*. This constant is just given by the constant arc length s used for the construction of the background embedding with the scalar field

vanishing as described in section 4.3. It is given by

$$S_D^* = L\,\mathrm{artanh}\left(L\,\kappa_N\,\mathcal{C}^2\,\mathcal{N}/4\right) = \mathrm{artanh}(1/16) \approx 0.0626\,, \tag{4.59}$$

for our choices of $L = 1$, $\kappa_N = 1$, $\mathcal{C} = 1/2$ and $\mathcal{N} = 1$ for the numerics.

If we subtract the impurity entropy at asymptotically large distances, $S_D(\infty)$, from the respective graphs, they all vanish for large ℓ by construction. In a logarithmic plot of the resulting curves, shown in figure 4.7, two distinct features are revealed. On the one hand, the impurity entropy decays exponentially to its asymptotic value at large ℓ, which imprints itself in the linear behaviour at large ℓ in the logarithmic plot. On the other hand, the decay constant is always given by

$$\ell_* = 1/\pi T\,. \tag{4.60}$$

The black line, which is also shown in figure 4.7, represents this falloff of the form $S_D(\ell) \sim e^{-\ell/\ell_*}$, where the constant factor is chosen arbitrarily for representational purpose.

The interpretation is straightforward: On the one hand, if we keep the temperature fixed, the impurity entropy decreases as we investigate the impurity at larger and larger distances ℓ. This is known as the *screening* of the impurity, which is why the singlet state forming below T_c is also referred to as the *Kondo screening cloud*. On the other hand, keeping the distance ℓ fixed and lowering the temperatures, the impurity entropy also decreases more and more. Again, the interpretation is that at the impurity is screened more at lower temperatures. In both cases, the impurity entropy decreases as the energy scale ε at which the system is probed becomes smaller, where either $\varepsilon \sim T$ or $\varepsilon \sim 1/\ell$.

4.5.3 Zero temperature and a holographic g-theorem

Although it is impossible to tell exactly what happens at $T = 0$ from our numerics, it could be extrapolated that, eventually, the impurity entropy decreases to

$$\lim_{T\to 0} S_D(\ell \to \infty) = 0\,. \tag{4.61}$$

This is probably a little ambitious to see in figure 4.6, but is more digestive if one looks at the values of $S_D(\ell \to \infty)$ as a function of T/T_c in figure 4.8. This is known as *critical screening* and is in fact the case for the original Kondo model as was shown in the conformal field theory approach in [87]. Here, the ground state of the Kondo model differs from the UV only by a change from Ramond to Neveu-Schwarz boundary conditions. In both cases,

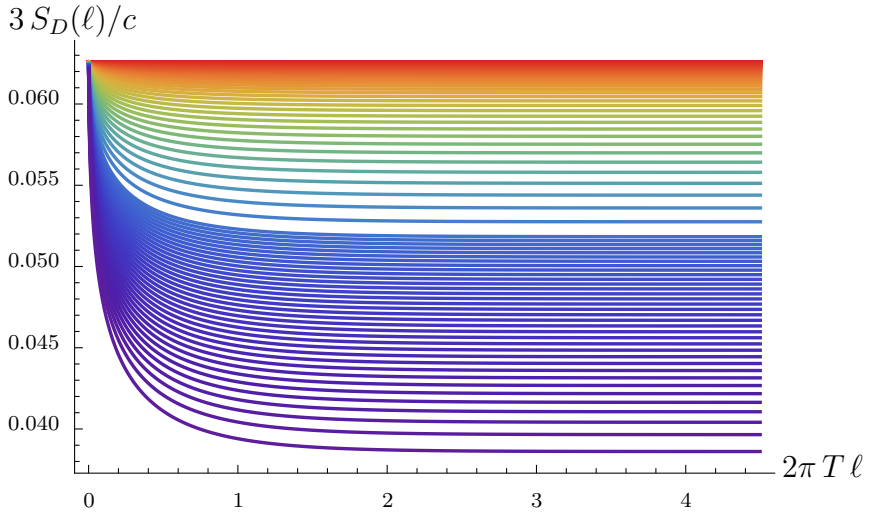

Figure 4.6: Shown is the impurity entropy $3\,S_D(\ell)/c$ vs. radius $2\pi\,T\cdot\ell$ of symmetric patches around the defect for various temperatures. The red graphs denote the embeddings close to $T = T_c$, while the blue ones are close to $T = 0$. We see that for fixed radius $2\pi\,T\cdot\ell$, the impurity entropy is a monotonically decreasing function of T.

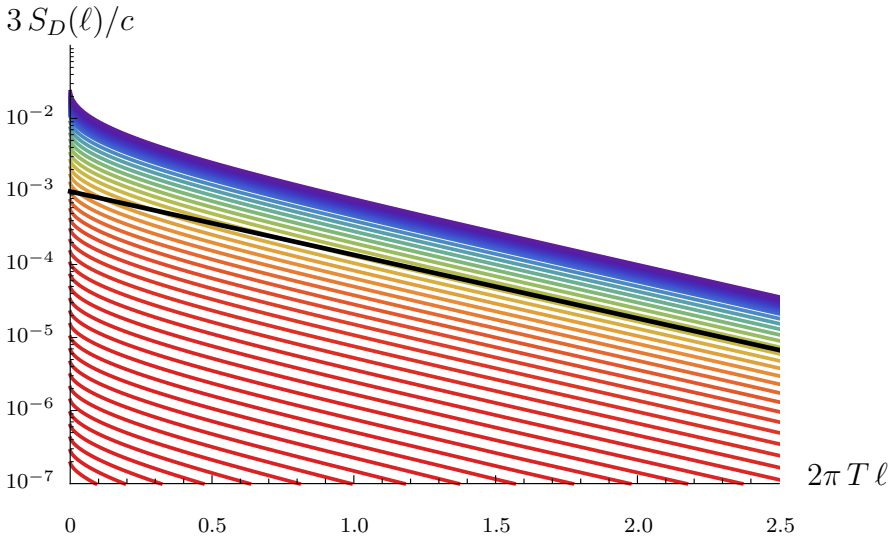

Figure 4.7: A logarithmic plot the impurity entropy $3\,S_D(\ell)/c$ vs. radius $2\pi\,T\cdot\ell$ of the patch around the defect after subtracting the $\ell\to\infty$ limit of the impurity entropy for each temperature separately. The temperature is encoded in the colour of the graphs, red is closer to $T = T_c$ and blue is closer to $T = 0$. The slope of the thick black line represents results from field theory, which match quite well for large ℓ.

the impurity is absent at the fixed point, in the sense that it is critically screened in the IR ($T = 0$) and that the Kondo coupling features asymptotic freedom in the UV.

In our setup, this limit cannot be achieved due to the following considerations: The impurity entropy is defined by (4.32), $S_D(\ell) = S(\ell) - S_0(\ell)$, so it is zero if and only if at $T = 0$, we find $S(\ell \to \infty) = S_0(\ell \to \infty)$. This, however, cannot be true. The $\ell \to \infty$ limit of $S_D(\ell)$ is readily seen to be proportional to the proper geodesic length from the horizon limit of the embedding, $X(z_H)$, to the trivial embedding $X_0(z_H) = 0$. So to obtain $S_D(\ell \to \infty) = 0$ at zero temperature, the embedding needs to end at $X(z_H) = 0$.

Our embeddings all start $X(0) = 0$ with negative slope $X'(0) < 0$ determined by the boundary conditions (4.54) of the gauge field, only. Thus, the embedding function must be negative close to the asymptotic boundary. In order to reach $X(z_H) = 0$, it would need to turn around and have positive slope $X'(z) > 0$ afterwards. This, however, is excluded due to energy conditions on the brane, which was shown in [1].

The lesson is, once more, that we cannot reach the $T \to 0$ limit in this model. If possible at all, we would certainly need to stabilise the scalar potential by at least a Φ^4-term. This will certainly have effects at low temperatures, which can be seen from the fact that the derivative of the potential w.r.t. the scalar field, $\partial_\Phi V(\Phi)$ appears in the horizon conditions (4.52) and (4.54).

Apart from this, our results show a behaviour of the impurity entropy which is known as the g-theorem in field theory. It states that the boundary entropy $\log(g)$ monotonically decreases as one drags the system from the UV to the IR. The boundary entropy is proportional to the number of boundary degrees of freedom, so the take-home message is that those degrees of freedom are screened as the system is cooled down. It was proven for 1+1-dimensional setups in [112], where the renormalisation group flow took the temperature of the system as the energy scale. In this case, the theorem states that

$$\frac{\partial}{\partial \log(T)} S_D(\ell \to \infty) > 0\,, \tag{4.62}$$

which is obviously the case if looking at figure 4.8. As we already mentioned, the same result holds true in our system if we identify $1/\ell$ with the renormalisation group energy scale.

The holographic g-theorem was already considered in [64, 65], in which an ad hoc identification of g was given by

$$\log(g) \sim -\operatorname{arsinh}\left(\frac{X(z)}{z}\right)\,. \tag{4.63}$$

If the null energy condition is satisfied, an assumption of this form guarantees the validity of the g-theorem. In our case, the null energy condition is of course also satisfied, so the formula would equally well work in our setup. However, our numerics show that it also holds true without an identification of this kind.

To end this section, we should mention that a closely related result was presented in [111], in which a similar theorem was considered for a conjectured holographic dual of *computational complexity* $\mathfrak{C}$. The computational complexity of a quantum state is, roughly stated, given by the minimal amount of *simple* gate operations needed to prepare the quantum state[14], which is represented by the dual geometry. It was conjectured in [113, 114] and [115] that this complexity finds a holographic dual which is either proportional to the volume of a codimension one region or the integrated action of certain codimension zero patches in the bulk of the gravity dual. The result of [111] is that along the renormalisation group flow from the UV (high temperatures) to the IR (low temperatures), the holographic complexity monotonically decreases.

This can be seen in figure 4.5 as follows: At $T = T_c$, the embedding is given by the analytic expression (4.41), which is the most left curve in figure 4.5. In the condensed phase, $T < T_c$, the scalar field on the hypersurface is non-trivial and the hypersurface starts bending to the right. The ambient geometry, g_+, is fixed throughout this process whereas the boundary to the geometry, given by the hypersurface, changes. So, more and more of the geometry is cut away at lower temperatures, effectively taking away volume of the spacetime. On the other side of the hypersurface, the same happens due to the symmetry established in (4.26). Hence, the volume loss of both sides does not cancel, but is rather doubled. As was mentioned earlier, the embeddings shown in figure 4.5 never cross each other, so the volume loss is monotonic. Assuming that the on-shell action is semi-positive, the computational complexity $\mathfrak{C}$ decreases monotonically in either case as the temperature is lowered, thus proving the claim. The discussion in [111] investigates this behaviour in much more detail by considering energy conditions of the field content constrained to the hypersurface, too.

[14] In more detail, one defines a priori a minimal but universal set of linear operators, called *quantum gates*. They act on the Hilbert space $\mathcal{H}$, which is the tensor product of some n qubits. Universality means in this context that any quantum operator can be approximated arbitrarily well with a circuit composed of these gates, only. One possibility for such a universal set is given by the Toffoli, Hadamard, phase-shift, ancillary, and erasure gates, where the latter two are only needed for non-unitary operations. The complexity $\mathfrak{C}(|\Psi\rangle)$ of any quantum state $|\Psi\rangle \in \mathcal{H}$ is then defined as the minimum number of such operations to prepare the state starting from $|0\rangle^{\otimes n}$ up to some predefined precision.

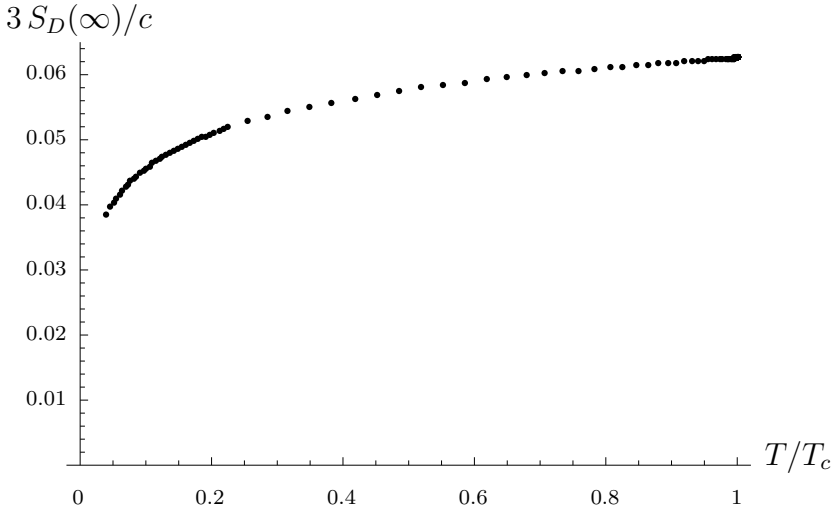

Figure 4.8: Shown are the asymptotic values of the impurity entropy $S_D(\ell \to \infty)$ vs. the temperature T/T_c, hinting towards the possibility of a zero temperature limit $\lim_{T\to 0} S_D(\ell \to \infty) = 0$.

4.6 Summary

In this chapter, we described a framework to incorporate backreaction of the defect to the geometry of the gravity dual in the holographic Kondo model of [60]. This framework is readily generalisable to different holographic models of field theories with impurities. The essential assumption is that the defect is represented by a codimension one hypersurface in the bulk. The basic idea is to split the geometry in two halves at the defect and impose the Israel junction conditions in order to glue them back together. The junction conditions match the amount of energy-stress localised on the hypersurface to the jump of the exterior curvatures of its embeddings on either side.

We applied this framework to the holographic Kondo model of [60] to compute the embeddings along with the configurations of the field content on the hypersurface at various temperatures. This allowed us to compute the impurity entropy due to the holographic correspondence of certain minimal surfaces and entanglement entropy. The impurity entropy is screened away from the defect and converges to an asymptotic value at large radii. This asymptotic value depends on the temperature, but the impurity entropy always approaches it exponentially fast, where the damping scale is given by $\ell_* = 1/\pi T$. Furthermore, the impurity entropy satisfies a g-theorem, which states that the impurity entropy decreases as the temperature of the system is lowered.

Chapter 5

Quenches in the probe limit

"Or maybe it's genius! I have to get that number."

Max – π [6]

In this chapter, we will deal with a completely different extension of the holographic Kondo model [60], which is time dependence. Unlike in the previous chapter about back-reaction, we will go back to the probe limit, but look at time dependent boundary conditions for the Kondo coupling κ. This will allow us to quench the system from the condensed phase to the normal phase, vice versa, and within each phase almost arbitrarily. We extract the behaviour of boundary coefficients of the gauge field and the scalar field numerically, and extract the time scales with which the system thermalises to equilibrium. Although this chapter does not include proper renormalisation and analysis of the 1-point functions, we are able to compare with results from Erdmenger et al. [68]. The authors of this paper compute the quasinormal modes of the system in a semi-analytic way by solving perturbations around the equilibrium in both phases. In contrast to that, our numerical analysis allows the investigation of the model far from equilibrium. The late-time behaviour is determined by the quasinormal modes, which coincide with the ones derived in [68].

Moreover, we can quench the Kondo coupling onto the critical value at which the phase transition takes place. This way, are able to analyse the critical dynamics of the holographic Kondo model.

The original results presented in this chapter were published in [4]. Many details about the numerical approach have already been published by M. Strydom in [67], who wrote most of the Mathematica code used for this analysis. A main difference to [67] is that we changed the gauge in order to compare with the results in [68]. Although it appears that another gauge choice should

make no difference, the involved gauge transformation appears to be a large gauge transformation, altering the fields at asymptotic infinity.

5.1 Time dependent boundary analysis

The model investigated in this chapter stays the same as in the original holographic Kondo model discussed in chapter 3. Once more, the Chern-Simons field decouples from the defect, such that the relevant part of the action is simply given by

$$S_{2d} = -\mathcal{N} \int \mathrm{d}^2x \sqrt{\gamma} \left(\gamma^{\mu\nu} D_\mu \Phi^\dagger D_\nu \Phi + \frac{1}{4} f_{\mu\nu} f^{\mu\nu} + V(\Phi) \right) , \tag{5.1}$$

which is just (3.17). Due to the probe limit, the background metric γ is fixed to the induced metric of the BTZ black brane

$$\mathrm{d}s^2 = \frac{L^2}{z^2} \left(-f(z)\, \mathrm{d}t^2 + \frac{\mathrm{d}z^2}{f(z)} \right) , \tag{5.2}$$

with f the blackening factor, given by $f(z) = 1 - (z/z_H)^2$. The temperature of the black brane Hawking radiation, and thereby the temperature of the system on the field theory side, is related to the black brane radius by $T = (2\pi\, z_H)^{-1}$. The equations of motions are just given by (3.22) and (3.24),

$$\frac{1}{\sqrt{\gamma}} \partial_\mu \sqrt{\gamma} f^{\mu\nu} = J^\nu , \tag{5.3}$$

$$D_\mu D^\mu \, \Phi = \partial_{\Phi^\dagger} V , \tag{5.4}$$

However, since in the time dependent setup we cannot expect the phase of the scalar to be vanishing anymore, we apply another splitting of the scalar into its real and imaginary parts,

$$\Phi(t, z) = \phi_1(t, z) + i\, \phi_2(t, z) . \tag{5.5}$$

Introducing the double trace operator $\hat{\lambda}\, \mathcal{O}\mathcal{O}^\dagger$ on the field theory side induces new boundary conditions for the scalar field, as described in chapter 3 and pioneered in [97]. The Kondo coupling $\hat{\lambda}$ is related to the expansion coefficients of the scalar field. The first order expansion (3.28) is still valid in the time dependent setup, however we show its explicit form for our scalar splitting by

$$\begin{aligned} \phi_1(t, z) &= \sqrt{z}\, (\alpha_1(t)\, \log \Lambda z + \beta_1(t)) + O(z^{3/2}) , \\ \phi_2(t, z) &= \sqrt{z}\, (\alpha_2(t)\, \log \Lambda z + \beta_2(t)) + O(z^{3/2}) . \end{aligned} \tag{5.6}$$

For our splitting and coupling constant $\hat{\lambda} = \kappa_1 + i\,\kappa_2$, the relationship (3.34) remains the same,

$$\alpha_1(t) = \kappa_1(t)\,\beta_1(t), \qquad \alpha_2(t) = \kappa_1(t)\,\beta_2(t)\,, \tag{5.7}$$

although the coefficients now explicitly carry time dependence, and we set $\kappa_2 = 0$ due to reality of the coupling. Then, we define κ_T from κ_1 by following the exact same procedure as in section 3.2. The higher order expansions of the fields are more involved than the static analysis. They were carried out by a program published by Strydom in [67], which we needed to adapt for our purposes.

The reason for adapting the code lies within the gauge fixing in this model. In holography, we commonly choose the radial gauge for the gauge field,

$$a_z = 0\,, \tag{5.8}$$

as this is a natural choice due to the radial direction being the emergent holographic direction. Thus, we are left with the temporal component a_t and its equation of motion, which is the t-component of (5.3). This fixes the gauge only up to a function of t, as explained in more detail in appendix C.

In this thesis, we do *not* utilise this residual gauge freedom to fix the phase of the scalar asymptotically, as was done in [67]. There, the phase of the scalar was chosen to vanish asymptotically, which yields $\beta_2 = 0$. It was found that, due to the asymptotics of the gauge field in AdS_2, obtaining this result requires a *large gauge transformation* which alters the physics. Since we want to compare e.g. with the results of [68], in which such a large gauge transformation was not applied, we leave the scalar's phase free throughout the bulk.

The model as described above can easily be reduced to the static model of [60], described in section 3.2, by setting any occurring temporal derivatives to zero. Especially, the model still features a phase transition at a critical temperature $T_c \approx T_K$ which transfers to a critical coupling $\kappa_c = 1/\log(T_K/T_c)$, where T_K denotes the Kondo temperature. For our choice of the representation, $\mathcal{C} = 1/2$, the numerical value for the critical coupling is given by

$$\kappa_c \approx 8.9796\,, \tag{5.9}$$

which, of course, is the same number as in (3.46).

5.2 Computational strategy

At first sight, solving the equations of motion (5.3) and (5.4) seems straightforward. The overall approach is:

(i) Compute the boundary expansions of the fields at the event horizon and asymptotic infinity up to some convenient order,

(ii) restrict the computational domain to the region $\mathcal{R}_{\text{num}} = [\varepsilon_{\text{bnd}}, \varepsilon_{\text{hor}}]$ between two cutoff parameters at the event horizon and asymptotic infinity, and

(iii) compute the fields in $\mathcal{R}_{\text{num}}$ numerically by providing boundary conditions at ε_{bnd} and ε_{hor} which originate from an approximation of the fields by applying the respective boundary expansions up to the cutoffs.

In the case at hand, however, the procedure is surprisingly involved. The reason is that we need to fix the scalar field's mass to saturate the Breitenlohner-Freedman bound in order to obtain the correct scaling dimension for the dual operator as discussed in 3.2.2. This induces many logarithmic terms in the boundary expansion, as we already encountered in the static backreaction in chapter 4. In the time dependent setting presented in this chapter, even more logarithmic terms can be turned on and solving for all the coefficients becomes tedious.

So, especially step (i) becomes much harder. Fortunately, the algorithm introduced in [67] is capable to find the coefficients order by order in an expansion around the asymptotic boundary. However, finding the right cutoff values in (ii) and evolving the fields by supplying approximate boundary values from the expansions in (iii) is tricky, because it is numerically hard to distinguish between terms which only differ in their logarithmic power.

In order to address these issues, we replace the dependent variables a_k and ϕ_i, where k denotes the left-over component of the gauge field after fixing the gauge, by substituted fields $\tilde{a}_k$ and $\tilde{\phi}_i$. Those are built by subtracting the boundary terms of the respective fields up to a convenient order:

$$\tilde{a}_k \equiv a_k - s_a \,, \tag{5.10}$$

$$\tilde{\phi}_i \equiv \phi_i - s_{\phi,i} \,, \tag{5.11}$$

where the subtracted terms s_a and $s_{\phi,i}$ are given by

$$s_a = \frac{Q}{z} + \mu(t) + O\left(z^1\right) \,, \tag{5.12}$$

$$s_{\phi,i} = \sqrt{z}\left(\alpha_i(t)\log(z) + \beta_i(t)\right) + O\left(z^{3/2}\right) \,, \tag{5.13}$$

and the O symbols denote higher order terms. The substituted fields $\tilde{a}_k$ and $\tilde{\phi}_i$ are replacing the original fields in the equations of motion. This way, we

transfer the dependency of the system on the involved boundary coefficients $\mu(t)$, $\alpha_i(t)$ and $\beta_i(t)$ from the fields themselves to the equations of motion.

Moreover, with a static event horizon due to the probe limit, there is no need to use the cutoff at the horizon and appropriate horizon conditions. Instead, we choose our discretisation scheme in the radial direction as an expansion of the fields in Chebyshev polynomials and choose a point *inside* the event horizon as the boundary of the computational domain $\mathcal{R}_{\text{num}}$. As Chebyshev polynomials build a complete set of regular functions and the computational domain includes the event horizon, we implicitly require regularity at the horizon. The metric has the feature that the future lightcone tilts into the event horizon once we cross it. This way, points in the event horizon cannot affect points outside and ingoing boundary conditions are satisfied automatically.

The temporal direction is discretised on an evenly distributed grid, which sets bounds on the temporal resolution. Especially, as we did not implement an adaptive temporal grid, we need to know which frequencies have to be resolved before we start the run. Without a semi-analytic analysis of the quasinormal modes, this can only be done by trial and error. We perform perturbative Gaussian quenches over a fixed background value for the Kondo coupling κ_0, given by

$$\kappa_T(t) = \kappa_0 \left(1 + a \exp\left(-s^2 (t - t_0)^2\right)\right) , \tag{5.14}$$

where v_0 is the time around which the quench is centred, the parameter s is describing the steepness of the quench, and a is the ratio of maximal amplitude to background amplitude of the coupling. Quenches like this kick the system slightly out of equilibrium and we can find the respective quasinormal mode at κ_0 by fitting the ring-down of the fields to a quasinormal behaviour. In addition to that, quenches starting in the normal phase feature another quasinormal-like behaviour at early times. Here, the perturbation is exponentially growing in time, with a time constant which can be read off analytically from performing perturbation theory around the normal phase, in which the scalar vanishes. Finally, the steepness parameter s of the quench itself is setting a temporal scale. In order to set the temporal resolution properly, we must ensure that the smallest time scale from above is resolved by the temporal grid.

The time evolution scheme is chosen to be Crank-Nicolson-like, as already described in [67]. For some more details about the numerical evolution scheme, we refer the reader to appendix C.

5.3 Classification of quenches

Before we explain how to extract the quasinormal modes from the numerical data in the next section, we will show the different classes of quenches which have been investigated. This will be necessary in order to get a feeling about the timescales involved and which quasinormal modes are important in which region. We investigate two main types of quenches:

(a) Quenches, in which the asymptotic values of κ_T are equal, and

(b) quenches, in which the asymptotic values of κ_T differ.

For the sake of simplicity, we use differentiable functions in both cases, although the algorithm explained in more detail in appendix C is actually capable of dealing with instantaneous quenches. For (a), we apply a Gaussian shape for the coupling of the form

$$\kappa_T(t) = \kappa_0 \left(1 + a \exp\left(-s^2 (t - t_0)^2\right)\right) , \tag{5.15}$$

which we already encountered in (5.14). In the case of (b), we apply a tanh form of the quench, given by

$$\kappa_T(t) = \kappa_i + (\kappa_f - \kappa_i) \left(\frac{1}{2} \tanh\left(s\,(t - t_0)\right) + \frac{1}{2}\right) , \tag{5.16}$$

which interpolates smoothly between the initial value, κ_i, and the final value, κ_f, where the steepness and midpoint of the quench is determined by s and t_0, respectively.

Of course, for numerical reasons, we need to start at a finite time t_i, which we always set to $t_i = 0$, and end at another finite time, which we denote by t_f. Hence, we have $\kappa_T(0) \neq \kappa_i$ and $\kappa_T(t_f) \neq \kappa_f$ in general. However, due to the exponential convergence of the Gaussian and Tanh functions to their asymptotic values, we do not run into numerical problems if we set $t_0 \gg 0$, such that these equalities are at least approximately satisfied. For this purpose, we usually set $t_0 \approx 5/s$.

Before we go on to show how to extract the numerical quasinormal modes from the computed evolution of the fields, we conclude this section with a quick overview of the different quenches we can apply in general.

Quenches from the normal to the condensed phase

Here, we start with an initial value of $\kappa_i = \kappa_T(-\infty) \approx \kappa_T(0) > \kappa_c$ and end at $\kappa_T(t_f) \approx \kappa_T(+\infty) < \kappa_c$. Initially, the scalar field vanishes as we

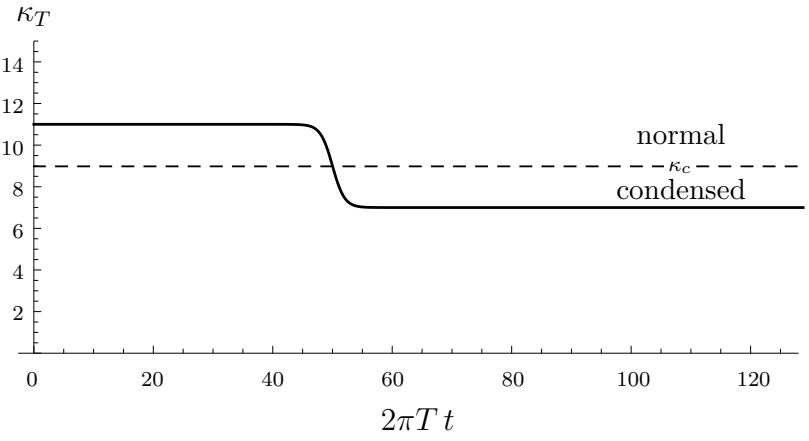

Figure 5.1: Quench profile for κ_T as given by eq. (5.16) with parameters $\kappa_i = 11$, $\kappa_f = 9$, $s = 1/2$, and $2\pi T\, t_0 = 50$.

start in the normal phase. After the quench, a vanishing scalar field is still a metastable solution to the equations of motion. Due to this, the time scale at which the scalar field responds to the quench is generically detached from the time scale of the quench itself. Instead, it is given by the time scale of the unstable quasinormal mode described by figure 5.10 for $\kappa_T < \kappa_c$. Determining the unstable quasinormal modes of the normal phase was the main reason to use this type of quench. The time scale at which the scalar settles to its equilibrium configuration is, on the other hand, given by the lowest lying quasinormal mode at the equilibrium value, κ_f. A generic example of quenches of the type normal to condensed is shown in figure 5.1.

Quenches within the condensed phase

Here, κ_T has its initial and final values within the condensed region, $\kappa_i = \kappa_T(-\infty) \approx \kappa_T(0) < \kappa_c$ and $\kappa_T(t_f) \approx \kappa_T(+\infty) < \kappa_c$. The initial response of the scalar correlates with the time scale of the quench. Asymptotically, the time scale at which the scalar settles to equilibrium is given by the lowest-lying quasinormal mode around the equilibrium value. Examples for both Gaussian and Tanh-like quenches of this type are shown in figure 5.2. This type of quench was mainly used to determine the quasinormal modes in the condensed phase.

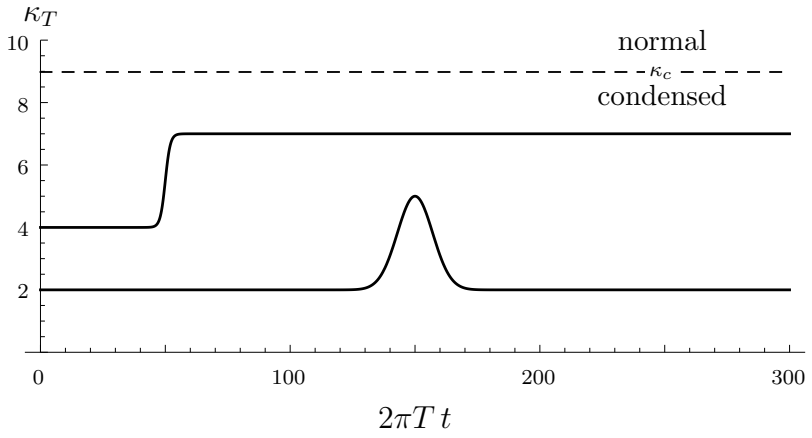

Figure 5.2: Gaussian and Tanh quench profiles within the condensed phase. The Gaussian profile is given by eq. (5.15) with $\kappa_0 = 2$, $s = 1/100$, and $2\pi T\, t_0 = 150$. The Tanh profile is given by eq. (5.16) with $\kappa_i = 4$, $\kappa_f = 7$, $s = 1/2$, and $2\pi T\, t_0 = 150$.

Quenches from the condensed to the normal phase

In this case, we start with $\kappa_i = \kappa_T(-\infty) \approx \kappa_T(0) < \kappa_c$ in the condensed region and end up at $\kappa_T(t_f) \approx \kappa_T(+\infty) > \kappa_c$ in the normal phase. The scalar field always vanishes asymptotically, but the time scale of the decay depends on κ_f and can be given analytically, see figure 5.10. A generic quench of this type is shown in figure 5.3. We used quenches like this to extract the quasinormal modes of the normal phase and compared them to the analytic results to evaluate the performance of the numerics.

Quenches onto the critical coupling

The last, and most special, case of quenches we investigate are those for which the final value of κ_T is right at the critical value κ_c. As we will see in section 5.6, the system features *critical dynamics* in this case. This means that the thermalisation will no longer yield a time scale appearing in an exponential falloff, but rather a polynomial falloff with the polynomial exponent to be determined. The quench profile (5.16) is adapted to logarithmic space,

$$\kappa_T(t) = \kappa_i + (\kappa_f - \kappa_i)\left(\frac{1}{2}\tanh\left(s\,\log(t/t_0)\right) + \frac{1}{2}\right)\,, \tag{5.17}$$

and is shape-invariant in logarithmic space upon changing the midpoint t_0. Furthermore, and in contrast to the usual quenches of the type (5.15) and (5.16), the steepness parameter s does not carry a dimension in this type of

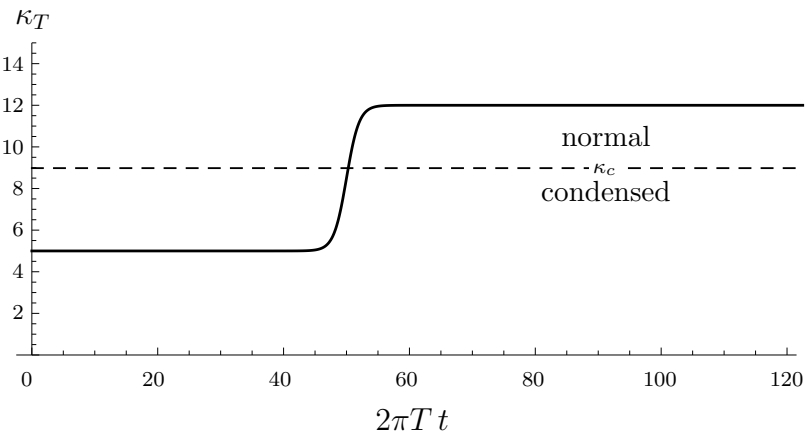

Figure 5.3: Generic quench profile for quenches from the condensed to the normal phase. The coupling $\kappa_T(t)$ is given by eq. (5.16) with parameters $\kappa_i = 5$, $\kappa_f = 12$, $s = 1/2$, and $2\pi T\, t_0 = 50$.

quench. Hence, the time dependence of κ_T itself does *not* introduce a time scale. A generic example for this type of quench is shown in figure 5.4. The behaviour involved in this case will be investigated in section 5.6.

5.4 Extraction of quasinormal modes

The goal of the time dependent analysis is to extract the thermalisation time $\tau_{\rm th}$ after various quenches in either phase. We can define $\tau_{\rm th}$ by different conventions, but the most convenient one is to define them in terms of the damping time scales of any fields in the setup, which are given by the inverse of the imaginary part of the lowest-lying quasinormal mode $\hat{\omega}$ of any observables in the system. Any quasinormal modes can be decomposed into their real and imaginary parts,

$$\hat{\omega} = \hat{\omega}_R + i\,\hat{\omega}_I\,, \tag{5.18}$$

so the thermalisation time $\tau_{\rm th}$ will be given by

$$\tau_{\rm th} = \frac{1}{|\hat{\omega}_I|}\,. \tag{5.19}$$

Let us derive this relation in more detail, as it is an essential assumption for the time dependent analysis. The solutions of the evolution equations at late time, i.e. near the equilibrium values of the respective fields, can always be approximated by a coupled set of linear, second order, hyperbolic evolution

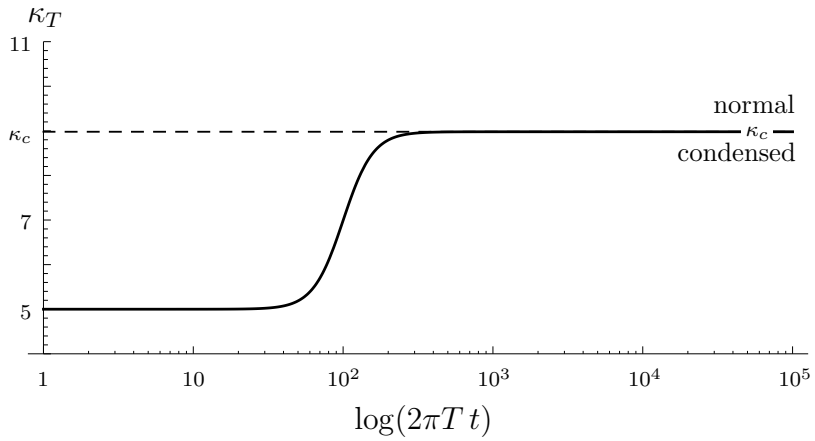

Figure 5.4: Generic quench profile for quenches from the condensed to the normal phase. The coupling $\kappa_T(t)$ is given by eq. (5.17) with parameters $\kappa_i = 5$, $\kappa_f = \kappa_c$, $s = 5$, and $2\pi T\, t_0 = 100$.

equations. The solutions to such differential equations are always given by a sum over the quasinormal modes, which have the form

$$f^{(i)}(t) = \sum_k a_k\, e^{-i\,\omega^{(i,k)}\,t}\,, \tag{5.20}$$

where the $f^{(i)}$ are not necessarily the original degrees of freedom, but might be redefinitions. Expanding the ω_k's into their real and imaginary parts, we end up with

$$f^{(i)}(t) = \sum_k a_k\, e^{\omega_I^{(i,k)}\,t}\, e^{i\,\omega_R^{(i,k)}\,t}\,. \tag{5.21}$$

Each quasinormal mode with $\omega_I < 0$ will decay at a time scale $1/|\omega_I^{(k)}|$. Assuming that all quasinormal modes have negative imaginary part, the field is well-described by the quasinormal mode which is closest to the real axis, i.e. which has the smallest imaginary amplitude. We will denote this quasinormal mode with a hat, $\hat{\omega}$. All other quasinormal modes will become negligible at some point, as their imaginary part is larger in magnitude and, hence, they are damped away exponentially faster.

If any of the quasinormal modes has a positive imaginary part, $\omega_I^{(k)} > 0$, the field will exponentially diverge from its equilibrium value. This can be the case at phase transitions, for example, and we will encounter this kind of unstable quasinormal mode below.

We will restrict our attention to the thermalisation time of the scalar operator $\langle\mathcal{O}\rangle \sim -\beta^\dagger$, where both sides depend on time. As we split the

scalar field into real and imaginary part, the coefficients we want to fit are real and, hence, we take the real part of (5.21) as our model for the fitting function,

$$f(t) = f_0\, e^{\hat{\omega}_I\, t}\, \cos\left(\hat{\omega}_R\, t + \varphi\right)\,, \tag{5.22}$$

where we neglected any quasinormal mode with larger imaginary amplitude than $\hat{\omega}$. The fitting parameters are thus given by $\hat{\omega}_R$, $\hat{\omega}_I$, f_0 and φ, where the last two are not of interest and will be discarded.

Note, that we will take the same function to fit the behaviour in the case of quenches from the normal to the condensed phase. In this case, we deal with unstable quasinormal modes, i.e. $\hat{\omega}_I > 0$. In the linear regime, close to the *initial* equilibrium values of the fields, the linearisation of the equations is still sensible, so we expect quasinormal behaviour, although an exponentially increasing one.

Numerically, we fit (5.22) to the data by discretising it on the same temporal grid as the numerical data and minimising the square error. We do this in logarithmic space, i.e. rather on the logarithmic absolute values of the coefficients $\log(|f^{(i)}(t)|)$ than on the linear ones. The reason is simply that otherwise the errors at late times become exponentially suppressed, and the initial behaviour has larger weight in the optimisation problem. On the other hand, we actually would like to extract the late time behaviour as detailed as possible, and suppress the initial behaviour. We expect that other quasinormal modes than $\hat{\omega}$ are still turned on initially, which might affect the goodness of fit. Actually, we will be able to see those higher quasinormal modes in our analysis, although the accuracy of the fit is too poor in order to extract those modes reliably. In the following, we will show some exemplary quasinormal modes and the respective fits for different types of quenches.

Quenches from the normal to the condensed phase

The quenches from the normal to the condensed phase show two different regimes of interest for our analysis. Firstly, at late times, they feature the quasinormal modes of the condensed phase. Hence, we can use them to determine those, although mainly this was done by using Gaussian quenches within the condensed phase. However, they also show the unstable quasinormal modes of the normal phase. Actually, this is our only way of numerically determining the latter. Although we can perform quenches within the normal phase, we will not be able to fit the quasinormal modes, as the overall amplitude of the scalar field does not change much.

In figures 5.5 and 5.6, we show an exemplary quench of this type and the corresponding evolution of the scalar field. The coupling κ_T, shown in figure 5.5a, starts at $\kappa_i = 9 > \kappa_c$ in the normal phase but close to the

phase transition, and ends up at $\kappa_f = 1$ deep in the condensed phase. The steepness parameter is set to $s = 1/10$ and the midpoint of the quench is located at $t_0 = 50/2\pi T$. As we can see in figure 5.5b, the scalar field rises to macroscopic size only some time after the quench has reached its final value. This indicates a separation of time scales: The time scale of the quench does not govern the initial evolution of the scalar field.

This is due to the fact that the trivial static configuration $\Phi = 0$ is always a possible solution to the equations of motion. However, it is not the global minimum of the free energy, as is the case in the normal phase. In the condensed phase, a non-trivial solution $\Phi \neq 0$ is the global minimiser of the free energy.

In figure 5.5c, we show the fitted quasinormal behaviour of the form described by (5.22) with $\hat{\omega}_I > 0$ to the simulated real part of the scalar field. In contrast to the linear plot, the logarithmic presentation reveals that the scalar responds to the change in the coupling immediately, in terms of its unstable mode being turned on. It then follows its exponentially increasing quasinormal behaviour until the system is not in a linear regime around the initial equilibrium anymore, and finally settles to the new equilibrium. In order to fit the unstable mode numerically, the data to which (5.22) is fitted, is cut to the region in which the approximation is valid.

Figure 5.6a shows the evolution of the absolute scalar expectation value. A log plot of its deviation from the initial equilibrium is shown in figure 5.6b, and from the final equilibrium in figure 5.6c. As we can see, unlike the real and imaginary parts of the scalar field, its absolute value does neither in the normal phase, nor in the condensed phase feature a real part in the quasinormal frequency $\hat{\omega}$. This imprints itself in a pure exponentially damped behaviour, without real-time oscillations.

Quenches of this type have been performed for various values from the normal into the condensed phase. The fit results of $\hat{\omega} = \hat{\omega}_R + i\hat{\omega}_I$ for the quasinormal behaviour of the real and imaginary parts in the initial, exponentially increasing era are shown as red dots in figure 5.10b in the upper half-plane. Those in the lower half-plane are given by $\hat{\omega}_I < 0$, and come from fitting the asymptotic behaviour in quenches from the condensed to the normal phase, described below.

It is crucial to remember that the quasinormal behaviour of the real and imaginary parts of the scalar are giving us the lowest lying quasinormal mode for the operator $\langle \mathcal{O}^\dagger \rangle$, whereas the behaviour of the absolute values gives us the one for $\langle |\mathcal{O}| \rangle$, which are different. In particular, only the absolute value of the vacuum expectation value is gauge-invariant, a topic to which we will refer in the analysis of the critical behaviour, too.

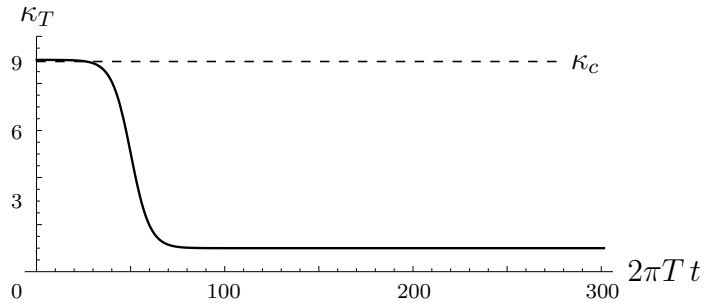

(a) Quench profile for κ_T as given by eq. (5.16) with parameters $\kappa_i = 9$, $\kappa_f = 1$, $s = 1/10$, and $2\pi T\, t_0 = 50$.

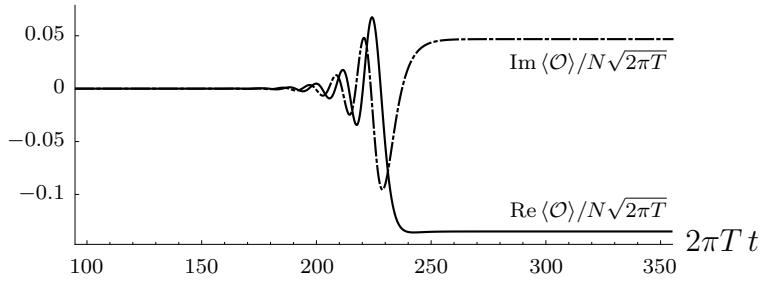

(b) Time evolution of the real and imaginary parts of $\langle\mathcal{O}\rangle$.

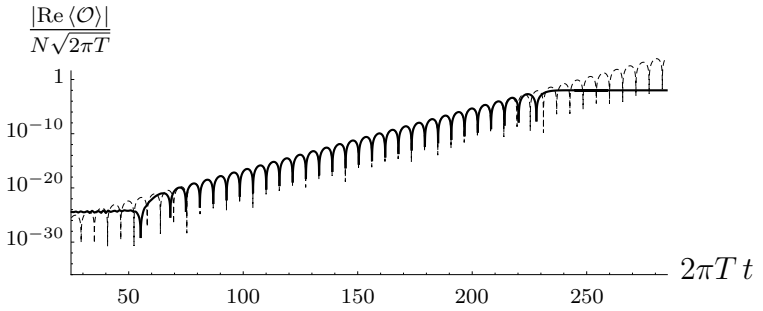

(c) Comparison of the data to a fitted quasinormal mode behaviour (dashed line) in a log plot. The data to be fitted was restricted to the region $t \in (100, 200)$.

Figure 5.5: Exemplary numerical evolution of the real and imaginary parts of the scalar operator (b) for a quench of the coupling κ_T from the normal to the condensed phase (a). We can see that the scalar gains macroscopic size only after the quench has finished, indicating a separation of time scales. In (c), we show the fitted quasinormal behaviour to the simulated data, which fits very good during the exponential era after the quench.

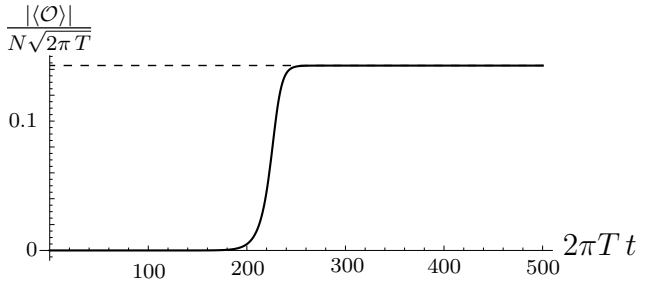

(a) The absolute value of the scalar expectation value. The dashed line indicates the equilibrium value at asymptotic late times.

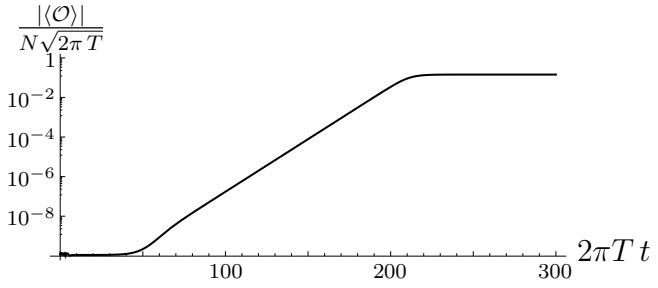

(b) Log plot of (a). The exponential rise of the scalar field is determined by the unstable quasinormal mode of the scalar in the normal phase. Unlike the real and imaginary parts, see figure 5.5b, it does not feature real-time oscillations.

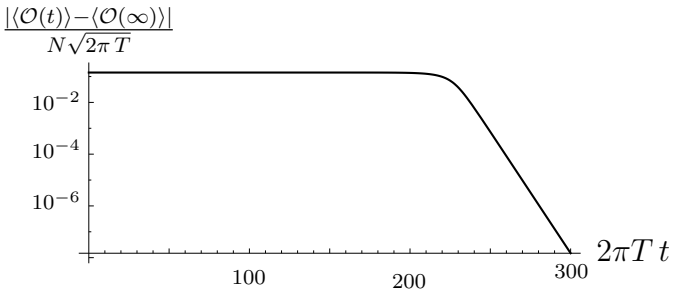

(c) Log plot for the deviation to the equilibrium value at late times, determined by the quasinormal mode of the new coupling $\kappa_f = \kappa_T(\infty)$.

Figure 5.6: Exemplary numerical evolution of the scalar operator (a) for a quench from the normal to the condensed phase. Note the different time scales involved due to the instability mode (b) and the quasinormal ringdown to the final equilibrium (c).

Quenches from the condensed to the normal phase

If we reverse the behaviour of the coupling κ_T in the previous subsection, we obtain quenches from the condensed to the normal phase. These type of quenches have mainly been performed in order to numerically extract the quasinormal modes of the normal phase.

In figure 5.7, we show an example for the evolution of the fields after such a quench, where we used a Tanh profile as described by equation (5.16) with $\kappa_i = 8$, $\kappa_f \approx 10.7$ and $t_0 = 500$. The scalar starts at macroscopic values in the condensed phase and we require the phase to vanish initially, which is shown in figure 5.7a. After the quench at $t_0 = 500$, both fields are disturbed.

Remarkably, as shown in 5.7b, the scalar field follows its late time quasinormal behaviour almost immediately. There is no intermediate truly nonlinear behaviour, which justifies our identification of the thermalisation time scale $\tau_{\text{th}} = (\hat{\omega}_I)^{-1}$ with the inverse of the imaginary part of the lowest lying quasinormal *omêga*. Apart from the damping by $\hat{\omega}_I$, the lowest lying quasinormal mode in the normal phase features an oscillation, i.e. $\hat{\omega}_R \neq 0$. Similar to the unstable mode shown in figure 5.6, the absolute value of the scalar operator $\langle|\mathcal{O}|\rangle$ lacks these real time oscillations, however.

Quenches within the condensed phase

As an example for quenches within the the condensed phase, we display the evolution of the scalar field after a Gaussian quench in figure 5.8. The chosen quench profile in shown in subfigure 5.8a, along with the parameters defining the quench. The macroscopic response of both the imaginary and real part is shown in subfigure 5.8b.

A very important results of the analysis of the quasinormal modes in the condensed phase is depicted in subfigure 5.8c: Here, the deviation of the real and imaginary parts from their asymptotic value at late times is plotted. In contrast to its behaviour in the normal phase, the lowest lying quasinormal mode in the condensed phase shows *no* oscillatory behaviour in the sense of a non-vanishing real part. Indeed, this is true for all temperatures in the condensed phase: $\hat{\omega}_I^{\text{cond}} = 0$.

According to [68, 116], this hints towards the Kondo resonance in the spectrum at low temperatures. In [68] it was analytically shown that this is to be expected at least in the vicinity of the phase transition of the holographic model of [60], which we use here, too. In our numerical analysis, we find that it holds true for all temperatures $0 < T < T_c$.

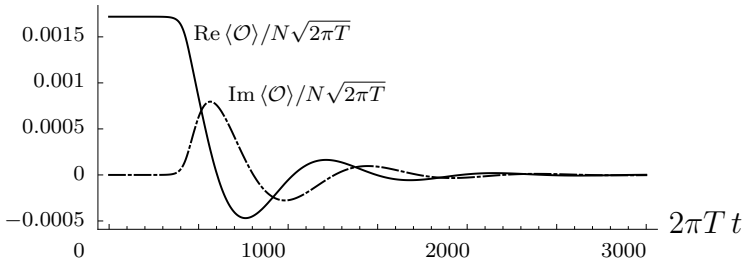

(a) Time evolution of the real and imaginary parts of $\langle\mathcal{O}\rangle$.

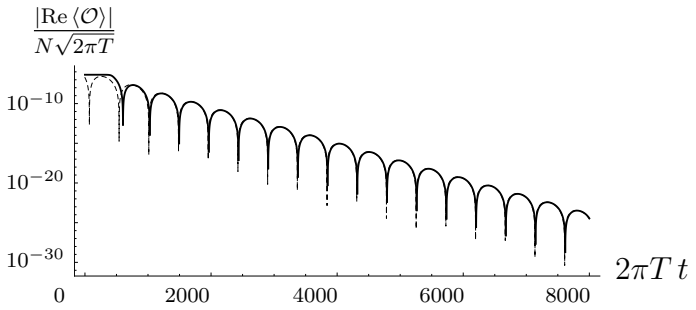

(b) Time evolution of the deviations of the real and imaginary parts of $\langle\mathcal{O}\rangle$ from their late time equilibrium values shown in a log plot. Apparently, there is no real part in the lowest lying quasinormal mode $\hat{\omega}$.

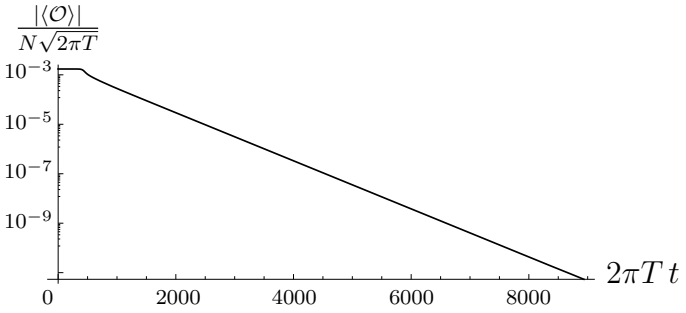

(c) Time evolution of the deviations of the real and imaginary parts of $\langle\mathcal{O}\rangle$ from their late time equilibrium values shown in a log plot. Apparently, there is no real part in the lowest lying quasinormal mode $\hat{\omega}$.

Figure 5.7: Shown is an exemplary evolution of the scalar field after a Tanh quench from the condensed into the normal phase. In subfigure 5.7b, we find that the onset of the quasinormal mode behaviour is almost immediately after the quench.

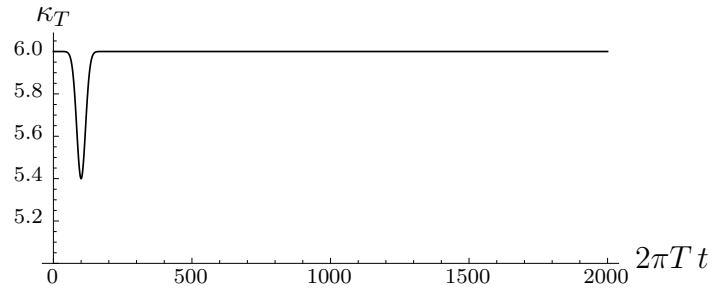

(a) Quench profile for κ_T as given by eq. (5.15) with parameters $\kappa_0 = 6$, $a = -3/5$, $s = 1/500$, and $2\pi T\, t_0 = 100$.

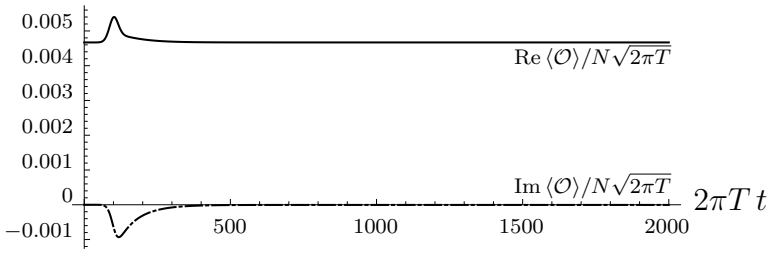

(b) Time evolution of the real and imaginary parts of $\langle\mathcal{O}\rangle$.

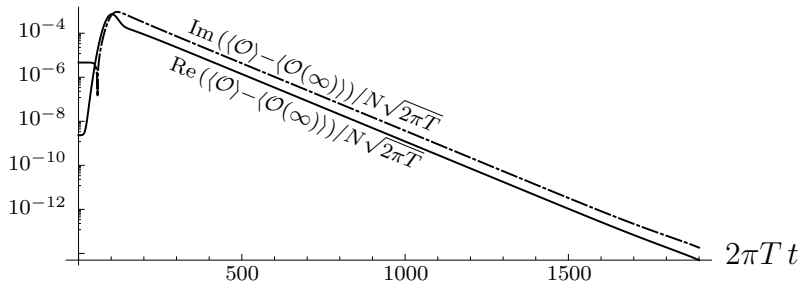

(c) Time evolution of the deviations of the real and imaginary parts of $\langle\mathcal{O}\rangle$ from their late time equilibrium values shown in a log plot. Apparently, there is no real part in the lowest lying quasinormal mode $\hat{\omega}$.

Figure 5.8: Exemplary numerical evolution of the real and imaginary parts of the scalar operator (b) for a Gaussian quench of the coupling κ_T within the condensed phase (a). In contrast to the quasinormal modes of the normal phase, see 5.5c, even the quasinormal modes of the real and imaginary parts of the scalar have no real part in their frequency. We do not show the fits to the data, as they are simply straight lines mimicking the behaviour at late times.

Extraction of next-to-leading order quasinormal modes

At this point, we would like to mention that our numerical analysis is in principle capable of extracting higher order quasinormal modes, too. Instead of fitting a single quasinormal mode as described by equation (5.22) to the data, we can try to fit a mixture model of the type given by (5.21), including several independent modes. Numerically, it is hard to do all of this at once, because the algorithms usually need a good seed a.k.a. initial guess close to the real solution in order to converge. This is due to the problem at hand being non-convex. Moreover, a mixture as described by (5.21) of n quasinormal modes involves $4n$ parameters, which are given by the modes' amplitudes, real and imaginary parts of the frequencies, and their phases, respectively. Searching numerically for the minimal residuum in a high-dimensional search space suffers from the *curse of dimensionality*. So this approach is unfeasible in general.

Here, however, we show that an iterative approach is tractable. Instead of trying to fit all modes at once, we iteratively subtract the lowest-lying quasinormal mode from the data. Let $f(t)$ be the data we obtained from our evolution algorithm. We subtract its lowest-lying quasinormal mode $f^{(0)}_{QNM}(t)$ and label the resulting curve as $\delta^{(1)}f(t)$. Doing this iteratively, we define

$$\delta^{(i)}f(t) \equiv \delta^{(i-1)}f(t) - f^{(i-1)}_{QNM}(t)\,, \tag{5.23}$$

where $\delta^{(0)}f(t) \equiv f(t)$. In figure 5.9, we show $\delta^{(2)}\beta_1(t)$, which is the resulting data after performing this operation for two steps on the data shown in figure 5.5c. Remarkably, we find oscillating quasinormal modes at next-to-next-to leading order although the lowest-lying quasinormal modes' frequencies always have vanishing real parts in the condensed phase. We can fit this behaviour by either one or two quasinormal modes, which gives reasonable results as shown in figures 5.9a and 5.9b.

The approach described here remains a proof-of-concept, as the fitting needed to be carefully initialised by hand in order for the algorithm to find a minimiser. This, however, is not feasible to perform on a larger dataset with several time dependent field coefficients to be fitted.

5.5 Quasinormal mode analysis

The previous sections gave an overview about the different types of quenches we use, the typical evolution of the scalar operator after such quenches, and how to extract the quasinormal modes by fitting. In this section, we go on and present the numerical values of the quasinormal modes which have been

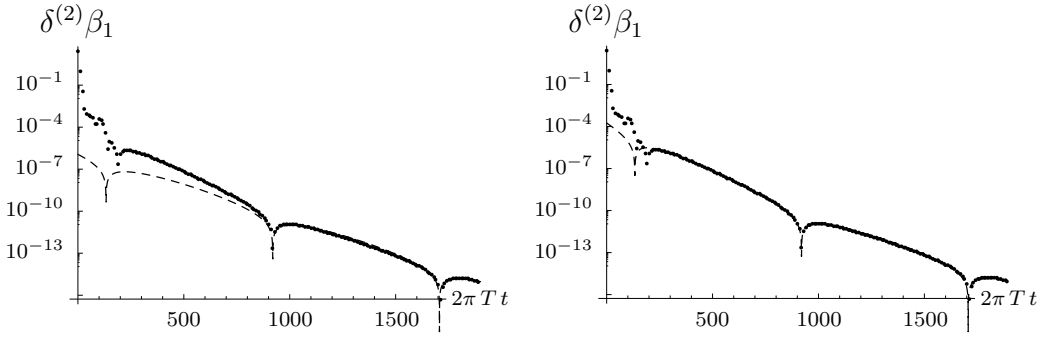

(a) Fitting one mode (b) Fitting two modes

Figure 5.9: Shown is the behaviour of $\delta^{(2)}\beta_1$ (dots), after subtracting the two lowest-lying quasinormal modes. Apparently the next lowest lying quasinormal mode has a non-vanishing real part. We can fit the late time behaviour by one additional (a), or two additional (b) quasinormal modes (dashed lines).

obtained by performing many of such quenches and fitting the respective behaviour. First, we justify our numerics by a comparison of the numerical results with known analytic results in the normal phase. Then, we analyse the behaviour of the lowest lying quasinormal mode in the condensed phase as a function of the temperature of the system.

5.5.1 Quasinormal modes in the normal phase

In section 3.2.2 we saw that the quasinormal modes in the normal phase are implicitly given by equation (3.45). In order to obtain their values, we have to solve (3.45) for ω, where we obtain multiple solutions. Those semi-analytic results can be extracted up to arbitrarily high precision. The lowest lying quasinormal mode $\hat{\omega}$, i.e. the one with smallest absolute imaginary value, will be the one which describes the behaviour of the scalar operator at late times.

We can extract $\hat{\omega}$ numerically by considering both the late time behaviour after quenches from the condensed phase into the normal phase as well as the early time behaviour after quenches from the normal to the condensed phase, as explained in section 5.4. Having found $\hat{\omega}$ both semi-analytically due to solving (3.45) and numerically due to the temporal evolution of the fields, we are able to compare. This way, we would immediately see if the algorithm fails to reproduce the normal phase.

However, as can be seen in figure 5.10b, the numerics match the analytic formula perfectly well. This confirms that our numerical approach is working

fine and we can proceed to the analysis of the condensed phase.

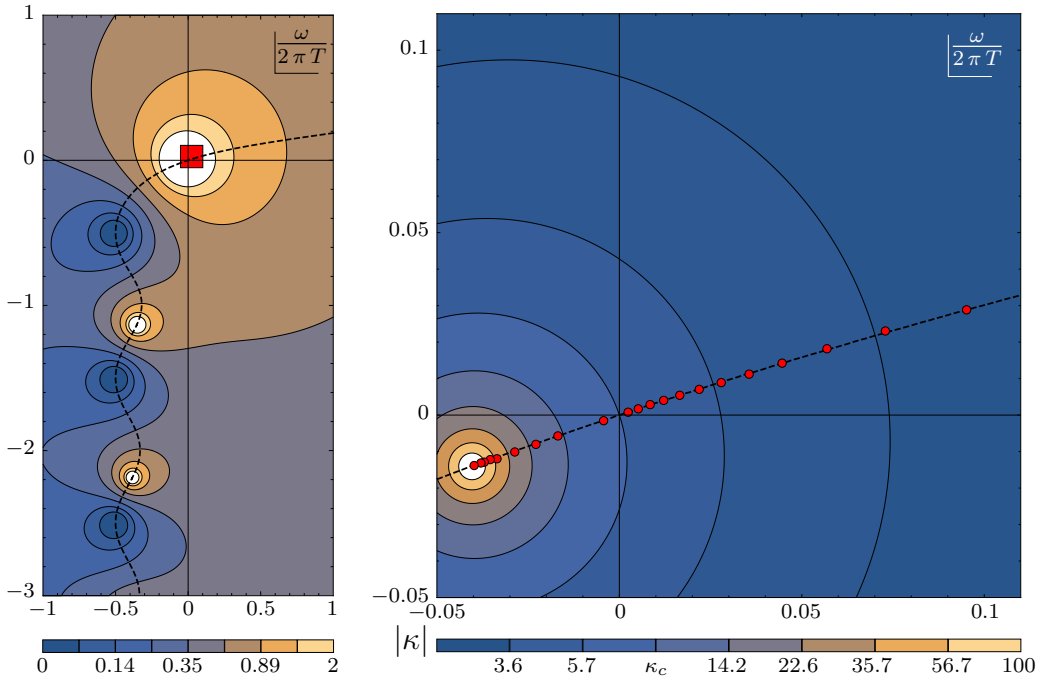

(a) Contour plot of $|\kappa_T|$ in the complex frequency plane. White space denotes cropping for values $|\kappa_T| > 2$.

(b) Blowup of the red square in (a). Red dots indicate QNMs extracted from numerical fitting at different temperatures. White space denotes cropping for values $|\kappa_T| > 100$.

Figure 5.10: Contour plot of $|\kappa_T(\omega)|$ over the complex ω-plane. A blow-up around the origin is shown in (b). Along the dashed curve, $\kappa_T(\omega)$ is real. The contours denote constant values of $|\kappa_T|$, with the colour scale indicating the value. The contour $\kappa_T(\omega) = \kappa_c$ intersects the dashed line at the origin in (b). The red dots are lowest lying QNM found from fitting the time evolution of the scalar operator after the quench to the QNM behaviour defined in eq. (5.22).

5.5.2 Quasinormal modes in the condensed phase

As described in section 5.4, for the analysis of the dynamics in the condensed phase, we can apply either Gaussian or tanh-like quenches which end up at values of κ_T in the condensed phase. For our numerics, we actually chose both approaches in different regimes. This is due to the fact that the numerics used to solve the static behaviour were not accurate enough at very low values

of κ_T, i.e. deep in the condensed phase near $T = 0$. However, equipped with our fully numerical evolution scheme, we could push the system even a bit closer to $T = 0$ by considering quenches starting at higher temperatures, for which we had the static solution needed to initialise the system, and ending up at lower κ_T.

As can be seen in figure 5.8c, unlike in the normal phase, the temporal behaviour of the scalar field does not show real oscillations. Rather, the field get just damped exponentially to its late time equilibrium. This is the case for both of the leading order quasinormal modes. The next to leading order modes display a real frequency, as is shown in figure 5.9 after subtracting both leading order modes from the data.

Because it is an intricate task to find good fits for the higher order modes, this was only performed as a proof of concept for this particular quench. In the following, we will only show the results for the lowest lying quasinormal mode, $\hat{\omega}$. Since they do not feature a real part, we show in figure 5.11 its dependence on the temperature T/T_c rather than in the complex plane as in figure 5.10. We choose to normalise the mode w.r.t. T_c, since normalisation w.r.t. T leads to a divergence as $T \to 0$.

Once more, this divergence is likely related to the fact, that we did not stabilise the potential. In the Kondo model, as $T \to 0$, the Kondo temperature T_K is the only available scale to the system, so we would expect that $\hat{\omega} \sim T_K$ at very low temperatures.

We can compare our results with the literature in two distinct ways. Firstly, just before the results presented in this section were written up in [4], the authors of [68] gave us access to their numerical data. In [68], an elaborate holographic renormalisation procedure is applied to the exact same bottom-up model we consider in this chapter. This allows to extract the quasinormal modes in a different way, by considering perturbation analysis around numerical background solutions. Essentially, the linearised versions of the equations of motion have the form

$$Df(t) = 0\,, \tag{5.24}$$

where f stands for any appearing fields and D is the respective differential operator, which involves second order derivatives in time. Finding the quasinormal modes then reduces to finding the eigenfunctions of D. In the condensed phase, this can be numerically involved because D also depends on the background configuration, so it is only given numerically. Nevertheless, the authors of [68] achieved to find the quasinormal modes. Comparing with their results, shown as diamonds $\diamond$ in figure 5.11, displays excellent agreement with our results obtained by fitting the evolution at late time directly.

At this point, it should be stressed that no holographic renormalisation is needed in our approach.

Secondly, we may compare the behaviour of the lowest lying quasinormal mode with what is expected from the Kondo model in condensed matter theory. According to [68, 116], the large-N Kondo resonance features a distinct behaviour close to the critical temperature, which imprints itself in a quadratic relationship between the imaginary value of the lowest lying quasinormal mode and the vacuum expectation value of the scalar operator, given by

$$|\hat{\omega}_I| \sim \kappa_T^2 \langle \mathcal{O} \rangle^2. \tag{5.25}$$

To find out about this relationship, we can visualise our numerical results on a double logarithmic plot as shown in figure 5.12a. This reveals that the advertised relationship holds true close to $T = T_c$.

In figure 5.11, we see that $\hat{\omega}_I / 2\pi T_c$ also approaches zero as $T \to 0$. In fact, a log-linear plot shown in 5.12b shows that there is a similar relationship at very low temperatures, given by

$$\hat{\omega}_I \sim \log \left(\kappa_T \langle \mathcal{O} \rangle \right) , \tag{5.26}$$

which displays strong deviation from mean-field theory. This is not unexpected, as we discussed earlier: At very low temperatures, the system approaches its ground state. Due to the fact that the scalar potential is not stabilised, the expectation value of the dual operator, $\mathcal{O}$, is diverging. So, the behaviour (5.26) as shown in figure 5.12b is actually an artefact of our model and most likely would change if we stabilise the scalar potential.

5.6 Critical dynamics

So far, we investigated the quasinormal modes of the holographic Kondo model of [60] in both the normal and the condensed phase. We showed, that our results match those obtained in [68] to high accuracy, although the methods applied in [68] have been very different. Especially, the behaviour close to the critical temperature T_c has been interesting and matches with expectations from condensed matter theory, i.e. the scaling of the lowest lying quasinormal mode with the condensate reveals the emergence of the Kondo resonance in the spectrum of the theory.

We can choose the quench profile $\kappa_T(t)$ at will, so we have the opportunity to have a closer look at the critical dynamics. This is done by imposing a Tanh profile for $\kappa_T(t)$ which initially starts in the condensed phase and asymptotes to the critical value of the effective Kondo coupling, $\kappa_T(\infty) = \kappa_c$, which is explicitly given by (3.46).

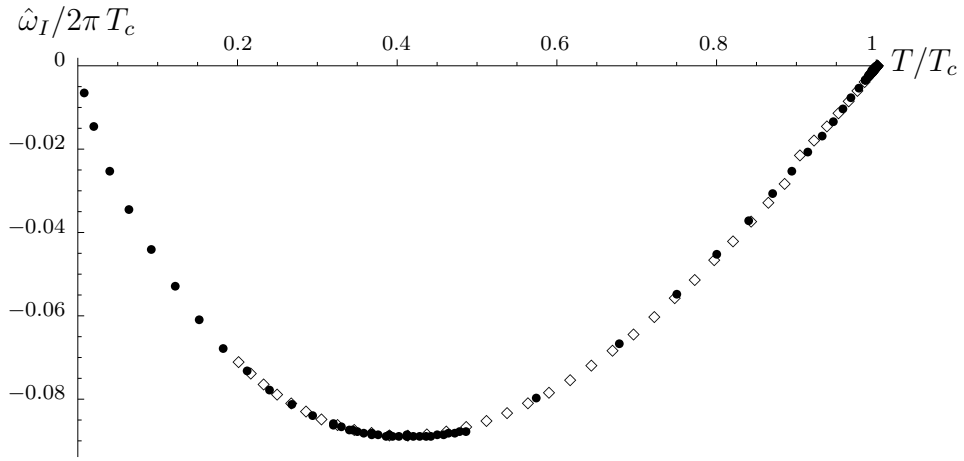

Figure 5.11: Shown is the imaginary part of the lowest-lying quasinormal mode $\hat{\omega}_I$. The bullets • denote our data, while the diamonds ⋄ denote the data of [68], which shows excellent agreement. The real part is vanishing throughout the condensed phase.

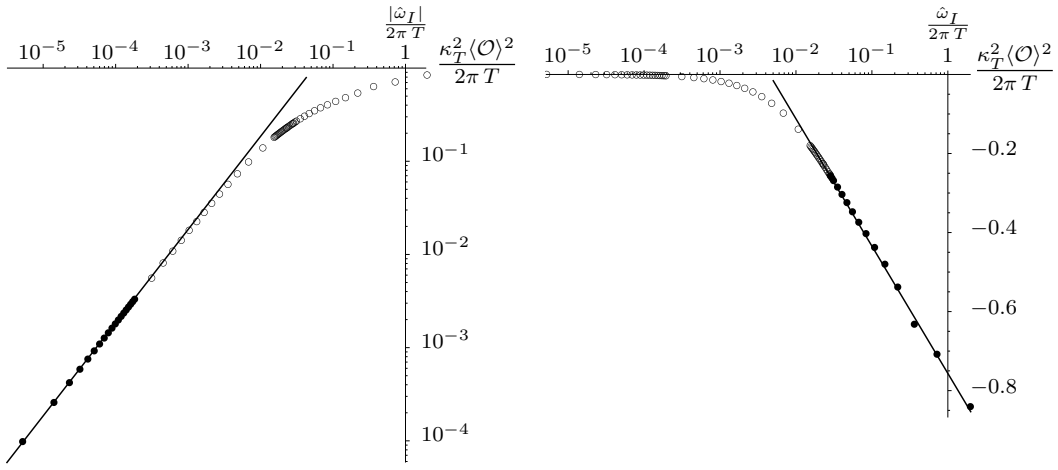

(a) $T \to T_c$ (b) $T \to 0$

Figure 5.12: Behaviour of $\hat{\omega}_I$ vs. $\kappa_T^2 \langle\mathcal{O}\rangle^2$. Close to $T = T_c$ (a), the relationship is linear, $\hat{\omega}_I \sim \kappa_T^2 \langle\mathcal{O}\rangle^2$, while as $T \to 0$ (b), it is logarithmic, $\hat{\omega}_I \sim \log(\kappa_T \langle\mathcal{O}\rangle)$.

In figure 5.11, we saw that in this case $\hat{\omega}_I \to 0$. Due to its definition (5.19), the thermalisation time scale diverges, $\tau_{\text{th}} = 1/\hat{\omega}_I \to \infty$. So, does the system thermalise at all? The answer is *yes*, but without any time scale. This is to be expected as at critical temperatures, field theories are usually well described by conformal field theories, which do not feature any scales.

Indeed, if we let the system evolve long enough, we eventually capture this conformally invariant behaviour by plotting the solution in dependence of logarithmic time. This is shown in figure 5.13. Note, that although the behaviour of $\langle\mathcal{O}\rangle$ mimics a quasinormal mode by $\langle\mathcal{O}\rangle \sim e^{i\omega \log(t)}$, it is *not* a quasinormal mode in the sense of the previous discussion in section 5.5. Upon replacing $t \to \log(t)$, we actually obtain polynomial decay of the form

$$\langle\mathcal{O}\rangle \sim t^{\xi}\,, \quad \xi \equiv i\omega\,, \tag{5.27}$$

where ξ is a *dimensionless* complex number. This clearly distinguishes this 'frequency' in logarithmic time from proper quasinormal modes as seen in section 5.5, which carry units of energy. The time coordinate t obviously should carry units of length and we must find a scale to compare it to in order to render the logarithm $\log t$ meaningful. In the numerics, we used the radius of the event horizon $z_H = (2\pi\, T)^{-1}$ for this purpose, so t is actually normalised w.r.t. the temperature which is $T = T_c$ at the phase transition. The overall polynomial form of the decay is, however, invariant under this rescaling.

It seems quite interesting to find a complex exponent, which might indicate the emergence a discrete scale invariance of the theory [117,118], i.e. the conformal invariance only remains intact for discrete time dilations $t \to \lambda t$, where λ takes discrete values, only. From figures 5.13a and 5.13b, we can fit the complex exponent ξ to be given by

$$\xi = -0.502 + 1.501i \approx -\frac{1}{2} + \frac{3}{2}\,i\,, \tag{5.28}$$

which seems reasonable. We will come back to the real part of this falloff below.

As for the imaginary part, we need to investigate the topic of discrete scale invariance with caution: As we can see in figures 5.13c and 5.13d, the gauge-invariant quantities $|\langle\mathcal{O}\rangle|$ and $\mu \sim \Delta_t$ do *not* feature oscillations in real time. These are the observables of the system, however, and thus it remains unclear, whether the imaginary part in (5.28) really has an implication like discrete scale invariance.

For holographic superconductors, it was found e.g. in [119–121] that $z = 2$ and $\nu = 1/2$, independent of the dimensionality of the theory. This fits to

our analysis, since the holographic Kondo model of [60] essentially mimics a holographic superconductor in the AdS_2 subspace of the defect hypersurface. At this point, we need to be careful with the dimensions: The critical exponent ν is not well-defined in our context, as is describes the spatial decay of correlation functions at criticality, which are obviously not present in the 0+1 dimensions of the dual defect to which the scalar operator $\mathcal{O}$ is constrained. Moreover, phase transitions as such are not possible at finite N in any theory for $d \leq 2$ spatial dimensions due to the Mermin-Wagner-Coleman theorem [95,96]. However, the large-N limit presents a loophole to this theorem as long-range fluctuations are suppressed. Thus, we take the results of [119–121] as strong hints that we can analytically continue $\nu = 1/2$ to lower dimensions in the large-N limit.

The *dynamical critical exponent* of a theory close to criticality is defined via the scaling of its thermalisation time τ_{th} by

$$\frac{1}{\hat{\omega}_I} \overset{(5.19)}{\equiv} \tau_{\text{th}} \sim \xi^z \sim \left(\frac{T_c - T}{T_c}\right)^{-z\,\nu} , \tag{5.29}$$

where ξ denotes the correlation length of the system. So, we can extract the dynamical critical exponent z from the behaviour of the lowest lying quasinormal mode $\hat{\omega}_I$ close to the critical temperature T_c. Its limit from the normal phase and the condensed phase need not be identical a priori.

Approaching T_c from the normal phase, we can extract the behaviour of $\hat{\omega}_I$ analytically if we linearise (3.45) around κ_c. Indeed, as shown in [4], if we linearise $\kappa_T \approx \kappa_c + \kappa_T^{(1)}\omega + O(\omega^2)$ and using $T/T_c = \exp(1/\kappa_c - 1/\kappa_T)$, we find

$$\tau_{\text{th}} \equiv \frac{1}{\hat{\omega}_I} = \frac{\operatorname{Im}\kappa_T^{(1)}}{\kappa_c}\left(\frac{T - T_c}{T_c}\right)^{-1} , \tag{5.30}$$

so we deduce $z\,\nu = 1$ or $z = 2$, as expected from [119–121].

On the other side, in figure 5.11 we see the linear behaviour of $\hat{\omega}_I$ as we get close to the phase transition in the condensed phase. More quantitatively, a double logarithmic plot of $|\hat{\omega}_I|$ vs. $1 - T/T_c$ close to $T = T_c$ reveals a polynomial dependence of the form

$$|\hat{\omega}_I| = a\left(\frac{T - T_c}{T_c}\right)^{b} , \tag{5.31}$$

and we can fit $b \approx 0.992$, which is close enough to $z\,\nu = 1$ so that we conclude $z = 2$ from both sides.

To conclude this discussion about critical dynamics in the holographic model of [60], we come back to figure 5.13 and the fitted decay constants

in equation (5.28). If we take $|\langle\mathcal{O}\rangle|$ as the definite order parameter we can neglect the imaginary part in (5.28). If we can relate its power law falloff at criticality directly to the dynamical critical exponent z, this would yield another powerful test for our numerics.

Indeed, the scaling behaviour of the order parameter can be generalised to the time dependent case and reads

$$|\langle\mathcal{O}(t)\rangle|_T \sim \left(\frac{T-T_c}{T_c}\right)^{\beta} \cdot f(t/\tau_{\text{th}})\,, \tag{5.32}$$

with $\beta = 1/2$ the critical exponent[15] of the order parameter in equilibrium, see figure 3.3 and the corresponding discussion. From this, we can derive the limit for $T \to T_c$, which is given by [122]

$$|\langle\mathcal{O}(t)\rangle|_{T_c} \sim t^{-\beta/z\nu}\,, \tag{5.33}$$

where we used the relation $\tau_{\text{th}} \sim \xi^z$ introduced above. Comparing the exponent, $-\beta/z\nu$, to what we found numerically in (5.28) and using $\beta = 1/2$ from the phenomenology in equilibrium, we once more find $z\nu = 1$, or $z = 2$ if we assume $\nu = 1/2$ in low dimensions.

5.7 Far away from equilibrium

The quasinormal modes analysed in section 5.5 and even the critical dynamics discovered in section 5.6 do not globally depend on the quench shape, i.e. the overall dependence of the Kondo coupling $\kappa_T(t)$ as a function of time. Only its asymptotics, which describe the initial and final temperatures via the relationship (3.44) completely, imprint themselves in the quasinormal modes.[16]

In a setup involving backreaction to the geometry, this would be different: The shape of $\kappa_T(t)$ encodes the amount of energy-stress thrown into the system. If we would quench an operator whose dual is defined throughout the bulk of the gravity dual, this certainly would increase the mass of the black hole and, for Anti de-Sitter asymptotics, the temperature of the black hole and thereby the dual quantum field theory. This is physically expected,

[15] Here, we denote the critical exponent of the order parameter by β, which is common in statistical mechanics. This exponent must not be confused with the expansion parameters of the dual scalar field, β_1 and β_2.

[16] Although not presented in this thesis and expected in any sensible physical theory, this fact was cross checked. The quasinormal modes are shape independent w.r.t. $\kappa_T(t)$ and depend only on its asymptotics.

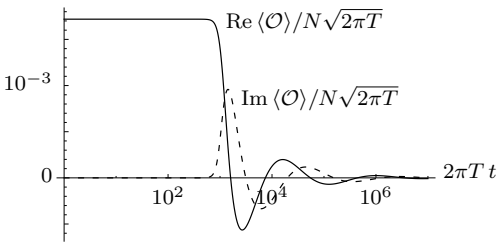

(a) Log-linear plot of $\langle\mathcal{O}\rangle$ vs. time.

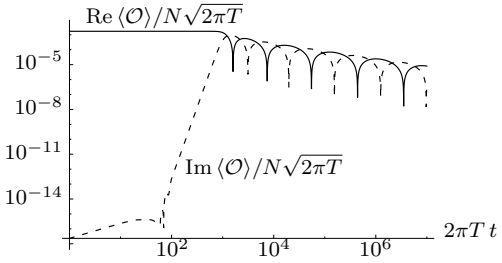

(b) Log-log plot of $\langle\mathcal{O}\rangle$ vs. time.

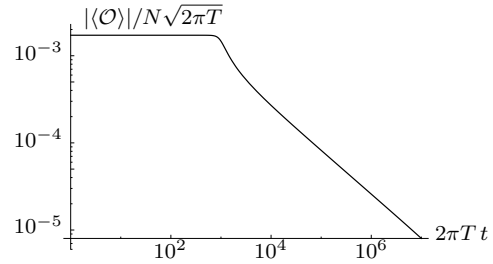

(c) Log-log plot of $|\langle\mathcal{O}\rangle|$ vs. time.

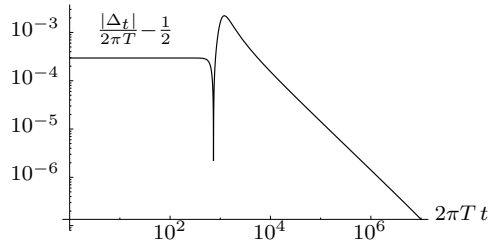

(d) Log-log plot of Δ_t vs. time.

Figure 5.13: A log-linear (a) and log-log (b) plot of $\mathrm{Re}\,\langle\mathcal{O}\rangle$ and $\mathrm{Im}\,\langle\mathcal{O}\rangle$ as functions of time. Below, we see log-log plots of the gauge-invariant quantities $\beta = \langle\mathcal{O}\rangle/N$ and $\Delta_t = \mu - \partial\psi_0$, which are not featuring any real oscillations in (logarithmic) time.

as insertion of energy into an thermal environment results in thermalisation of the system, which potentially changes the overall temperature. An example of such behaviour in the context of holography is considered in [123].

However, in our setup we quench the scalar operator $\mathcal{O} = \psi^\dagger\chi$ which is constrained to the impurity and finds its dual in the scalar operator on the defect hypersurface. Even *if* we considered backreaction to the 2+1 dimensional geometry, it is unclear whether or not the energy-stress inserted on the 1+1 dimensional hypersurface is measurable in the ambient space and can change the temperature.

Here, nevertheless, we search for truly non-linear behaviour of the system far away from equilibrium, which means everything that *cannot* be described by fluctuation analysis around thermal equilibrium. We chose the radial gauge $a_z = 0$ for the gauge field, and fixed the phase of the complex scalar field to vanish initially, $\mathrm{Im}\,\Phi(t_0) = \phi_2(t_0) = 0$. However, this does not constrain the evolution of the phase after quenching the system. As can be seen e.g. in figures 5.5b for a quench from the normal to the condensed phase, asymptotically *both* components ϕ_1 and ϕ_2 are generically non-vanishing. Hence, we are able to compute the phase shift $\Delta\psi$ resulting from this quench.

The asymptotic expansion of the scalar components is given by 5.6. We can relate their expansion coefficients to those of the scalar field's amplitude ϕ and phase ψ, defined by $\Phi = \phi\, e^{i\psi}$. They are given by

$$\phi(t,z) = \sqrt{z}\,(\alpha(t)\log(z) + \beta(t)) + O(z^{3/2})\,, \tag{5.34}$$

$$\psi(t,z) = \psi_0(t) + z\,\psi_1(t) + O(z^2)\,, \tag{5.35}$$

where the relation for α and β was already given in (3.33). The expansion coefficient of the phase can be derived by inserting the expansions of ϕ_1 and ϕ_2 into

$$\psi = \arctan\left(\frac{\phi_2}{\phi_1}\right)\,, \tag{5.36}$$

which is an equivalent definition of the phase. At leading order, the coefficients satisfy the exact same formula, i.e.

$$\psi_0(t) = \arctan\left(\frac{\alpha_2}{\alpha_1}\right) = \arctan\left(\frac{\beta_2}{\beta_1}\right)\,, \tag{5.37}$$

where used the fact that the proportionality between $\alpha_{1/2}$ and $\beta_{1/2}$ is the same due to the Kondo coupling being real as given by equation (5.7).

We then evolved the system after several Gaussian quenches, given by (5.15), with different values of the steepness parameter s. In the meantime, we kept the rest of the parameters fixed. With the numerical results, we

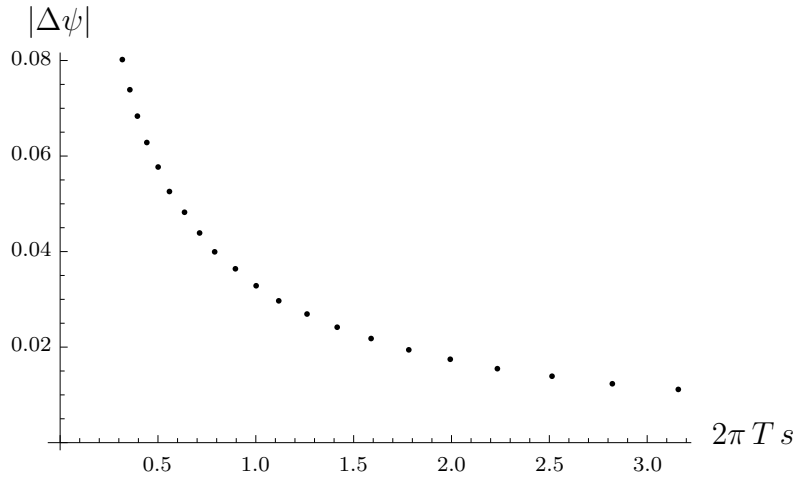

Figure 5.14: Shown is the phase shift $\Delta\psi$ vs. the steepness $2\pi\, T\, s$ of various Gaussian quenches in the condensed phase.

define the phase shift $\Delta\psi$ by

$$\Delta\psi = \psi_0(t_f) - \psi_0(0)\,, \tag{5.38}$$

where t_f denotes the last time slice on the numerical grid and we always started the computations at $t = 0$.

Results for $\Delta\psi$ as a function of the steepness $2\pi\, T\, s$, normalised to the temperature, are shown in figure 5.14. Clearly, the phase shifts seem to follow some smooth behaviour as we change s. Although a proper analysis of this behaviour is left for future research, we state an obvious: The steepness parameter s is a time scale indicating the abruptness of the quench. Taking the limit $s \to 0$ yields an instantaneous quench, while the opposite limit, $s \to \infty$, corresponds to adiabatic changes of the coupling κ_T.

With this in mind, figure 5.14 shows that adiabatic changes of the coupling yields a small phase shift, while steeper quenches increase the phase shift. To conclude this brief section, we should state that these are truly non-linear results, which require knowledge of the full evolution of the system far away from equilibrium and cannot be obtained by perturbation analysis around the equilibrium.

5.8 Beyond the probe limit

So far, we encountered both backreaction at equilibrium and time dependence in the probe limit, i.e. without backreaction. We gained insights in the falloff

of the impurity entropy and the evolution of the system after quenches in both phases and its critical dynamics close to the phase transition. It would be interesting to combine both approaches in order to obtain the spatio-temporal evolution of the Kondo screening cloud after quenches. On the field theory side, this was worked out e.g. in [100] for a free electron gas around the impurity. In our setup, however, the host degrees of freedom are strongly coupled, so we could in principle find something new.

In principle, we derived already everything we need to start actual computations: The equations of motion for all fields, $X_\pm$, a_μ and Φ, on the defect hypersurface are given by

$$\gamma^{\mu\nu} D_\mu D_\nu \Phi = \partial_{\Phi^\dagger} V(\Phi^\dagger \Phi)\,, \tag{5.39}$$

$$\frac{1}{\sqrt{\gamma}} \partial_\mu \sqrt{\gamma}\, f^{\mu\nu} = J^\nu\,, \tag{5.40}$$

$$[K_{\mu\nu} - \gamma_{\mu\nu} \mathrm{Tr} K] = -\kappa_N\, S_{\mu\nu}\,. \tag{5.41}$$

However, this system of equations yields some conceptual problems.

First of all, in both the static backreaction as well as the time dependence in the probe limit, the Chern-Simons field A decoupled from the impurity. It is not clear, whether this will still be the case if we consider time dependent backreaction. Then, in chapter 4 we utilised the constraint equation of the embedding X to reduce the system of equations on the defect hypersurface. In the numerics for the evolution of the system in the probe limit, we relied on a static event horizon. Moreover, the embedding was fixed and we did not change the computational grid dynamically.

All of these methods will likely not work in the computation of time dependent backreaction in our setup. However, we can choose yet another simplification to be able to tackle the problem: We can linearise the backreaction in the gravitational coupling parameter, κ_N. This way, as we will see, we can actually reuse the numerics developed in chapter 5.

At this point, we will once more neglect the Chern-Simons field A for convenience. Furthermore, we assume that a mirror symmetry of the kind $X_-(t,z) = -X_+(t,z)$ is given, so we can reduce our attention to the (+)-side of the entire manifold, as in chapter 4.[17]

We want to compute time dependent backreaction to the geometry in the bulk. In the static case, we chose the bulk geometry to be the BTZ metric, which is the unique finite temperature metric in asymptotic Anti de-Sitter

[17] In chapter 4 this assumption is valid generically as the Chern-Simons field was shown in [2] to decouple. If, however, the Chern-Simons field does not decouple in the case of time dependent backreaction, it will likely break this symmetry due to its chirality. So in this section, symmetry of the embedding functions really is an assumption.

space if we do not compactify the x-direction. Here, we will need to relax the bulk geometry to the general case. Although in 2+1 dimensions, gravity is not a dynamical theory, the metric components could change in dependence of the energy-stress density. Luckily, there exists a closed-form solution to the metric in asymptotic Anti de-Sitter space. In Fefferman-Graham coordinates $\{T, r, X\}$, it reads [124]

$$ds^2_{\text{eFG}} = \frac{1}{r^2}\left(\mathrm{d}r^2 + \tilde{g}_{\mu\nu}\,\mathrm{d}X^\mu \mathrm{d}X^\nu\right)\,, \tag{5.42}$$

where

$$\begin{aligned}\tilde{g}_{TT} =& -\left(1 - \frac{r^2}{L^2}(f_R(X-T) + f_L(X-T))\right)^2 \\ &+ \left(\frac{r^2}{L^2}(f_R(X-T) - f_L(X-T))\right)^2 \qquad (5.43)\\ \tilde{g}_{TX} =& -\frac{2\,r^2}{L^2}(f_R(X-T) - f_L(X-T)) \qquad (5.44)\\ \tilde{g}_{XX} =& \left(1 + \frac{r^2}{L^2}(f_R(X-T) + f_L(X-T))\right)^2 \\ &- \left(\frac{r^2}{L^2}(f_R(X-T) - f_L(X-T))\right)^2 . \qquad (5.45)\end{aligned}$$

Here, f_L and f_R are generic functions and depend only on the lightcone coordinates $X \pm T$ of the asymptotic boundary. They encode the topological nature of 2+1 dimensional gravity: Its degrees of freedom are not local but can be mapped uniquely to boundary conditions.

We can derive the static black brane at a temperature T_H by setting $f_R = f_L = \pi^2\,T_H^2/2$ and obtain

$$ds^2_{\text{FG}} = \frac{1}{r^2}\left(\mathrm{d}r^2 - (1 - r^2\,\pi^2\,T_H^2)^2\,\mathrm{d}T^2 + (1 + r^2\,\pi^2\,T_H^2)^2\,\mathrm{d}X^2\right)\,. \tag{5.46}$$

With AdS-Schwarzschild coordinates $\{t, z, x\}$, the same solution is given by

$$ds^2_{\text{SS}} = \frac{1}{z^2}\left(-f(z)\,\mathrm{d}t^2 + \mathrm{d}z^2/f(z) + \mathrm{d}x^2\right)\,, \tag{5.47}$$

where $f(z) = 1 - z^2/z_H^2$ and $T_H = 1/2\pi z_H$. Comparing with the AdS-Schwarzschild solution, we find the coordinate transformation

$$\phi_1 : SS \hookrightarrow FG,\ \{t, z, x\} \mapsto \{t, \frac{2z}{1 + \sqrt{f(z)}}, x\}\,, \tag{5.48}$$

$$\phi_1^{-1} : FG \hookrightarrow SS,\ \{T, r, X\} \mapsto \{T, \frac{r}{1 + r^2/r_H^2}, X\}\,, \tag{5.49}$$

where $r_H = 2z_H$.

The Chern-Simons field A is topological and does not contribute to the energy-stress tensor away from the defect hypersurface. However, the hypersurface carries the localised surface energy-stress tensor $S_{\mu\nu}$ which does source the geometry in the bulk. In fact, as mentioned earlier, the only way in which $S_{\mu\nu}$ can couple to the gravitational field $g_{\mu\nu}$ in the bulk is by setting boundary conditions on the $f_{L/R}$.

Let $X_+ \equiv X$, a_T and Φ denote all our dynamical fields on the hypersurface after gauge fixing $a_r = 0$. In order to linearise the equations of motion in κ_N, we assume that they can be expanded as

$$\Phi(T,r) = \Phi^{(0)}(T,r) + \kappa_N \, \Phi^{(1)}(T,r) + O(\kappa_N^2)\,, \tag{5.50}$$

$$a_T(T,r) = a_T^{(0)}(T,r) + \kappa_N \, a_T^{(1)}(T,r) + O(\kappa_N^2)\,, \tag{5.51}$$

$$X(T,r) = X^{(0)}(T,r) + \kappa_N \, X^{(1)}(T,r) + O(\kappa_N^2)\,, \tag{5.52}$$

for small κ_N. We want to expand the equations of motion (5.39) - (5.41) order by order in κ_N.

At zeroth order, only the zeroth order components $\Phi^{(0)}$, $a_T^{(0)}$ and $X^{(0)}$ contribute. Due to the occurrence of κ_N on the right hand side of (5.41) the solution of $X^{(0)}$ is given by the trivial background solution $X^{(0)}(T,r) = 0$. The field equations for $\Phi^{(0)}$ and $a_T^{(0)}$ hence yield just the equations of motion (5.3) and (5.4) which we already solved numerically.

At linear order in κ_N, this is not true anymore. The zeroth and first order coefficients of the fields mix in general so we must solve (5.39) and (5.40) on this background. However, the right hand side of (5.41) still carries the factor of κ_N. Hence, only the zeroth order components $\Phi^{(0)}$ and $a_T^{(0)}$ may appear in the energy-stress tensor and we already computed their evolution.

If we restrict our attention to linearised backreaction, this means we have already solved the hard part of this project. By inserting the numerical solutions of $\Phi^{(0)}$ and $a_T^{(0)}$ in the probe limit into the Israel junction conditions (5.41), we can integrate $X^{(1)}(T,r)$ to find the backreaction at linear order in κ_N. This will couple to the boundary conditions $f_{L/R}$ of the exact bulk gravity solution (5.42), which we will thereby receive easily.

Once we found the linearised backreaction of the geometry, we can derive the entanglement entropy or impurity entropy in terms of minimal surfaces in the bulk. In contrast to the case with static backreaction, the covariant formalism to obtain these extremal surfaces is more involved [20]. Therefore, the computations of this linearised approach to gain the spatio-temporal evolution of the Kondo screening cloud is left for future research [5].

5.9 Summary

To summarise, we considered time dependence in the holographic bottom-up model of [60] in the probe limit. The effective Kondo coupling κ_T was promoted to depend on time, which imposes time dependent boundary conditions for the scalar field Φ constrained to the defect hypersurface. The numerics were developed starting from the results of [67]. Especially, we changed the boundary conditions of the gauge field to be able to compare to the results of [68], which considers the same model. The shape of $\kappa_T(t)$ can be chosen almost arbitrary, so we can quench the system from the condensed phase and vice versa. This way, we extracted the lowest lying quasinormal mode $\hat{\omega}_I$ numerically in both phases, with excellent agreement with [68]. Furthermore, the critical dynamics of the model were explored. Close to the critical temperature T_c, we found a relationship $\hat{\omega}_I \sim \kappa_N^2 \langle \mathcal{O} \rangle^2$, which finds its origin in the Kondo resonance. The critical dynamic exponent z was shown to be $z = 2$ in accordance with the literature on dynamical mean-field behaviour both in condensed matter and holographic superconductors. We can compute the evolution of the system far away from equilibrium, which allows to access truly non-linear features like the phase shift of the scalar operator. A road map to develop linearised time dependent backreaction was listed, but working it out is left for future research.

Chapter 6

Conclusion and outlook

"Hold on! You have to slow down, you're losing it. You have to take a breath. Listen to yourself: You're connecting a computer bug I had, with you a computer bug you might have had, and some religious hogwash. You want to find the number 216 in the world? You will be able to find it everywhere: 216 steps from your street corner to your front door, 216 seconds you spend riding on the elevator... When your mind becomes obsessed with anything, you will filter everything else out and find that thing everywhere. [...] But Max! As soon as you discard scientific rigour, you are no longer a mathematician. You're a numerologist!"

Sol – π [6]

Gauge/gravity duality is a powerful tool to study strongly coupled quantum field theories. This thesis dealt with the treatment of backreaction and time dependence in holographic models which include impurities.

After an introduction to the topic in chapter 1, we reviewed the essential basics of superstring theory, especially type IIB superstring theory, in chapter 2. Type IIB string theory was the starting point for the original AdS/CFT correspondence by Juan Maldacena [15], which we explained afterwards. Generalisations of the original conjecture allow us to consider field theories at finite temperature and chemical density. Moreover, a focus was laid on entanglement entropy and the minimal surfaces to which it is related holographically by the Bekenstein-Hawking formula as proposed by Ryu and Takayanagi [19].

We then went on to a special application of the duality in chapter 3, in which we described the Kondo model in condensed matter theory and a holographic model thereof as suggested by [60]. We explained the origin of

this holographic duality as a specific D-brane setup in type IIB string theory. A reduced bottom-up model carries the most important fields to find the results which allow us identify the bottom-up model as a holographic toy model for the Kondo problem. It shows strikingly similar phenomenology as the large-N model in a 1+1-dimensional conformal field theory approach. However, important features cannot be explained by the original model, as it is defined in a static probe limit.

In order to compute holographic entanglement entropy, we need to consider minimal surfaces in the bulk of the gravity dual. Therefore, we generalised the bottom-up model to allow backreaction to the geometry, which was explained in chapter 4. This was achieved by splitting the bulk geometry into two halves, which share a common boundary hypersurface. This hypersurface is holographically dual to the impurity on the field theory side. There are fields constrained to this surface and therefore a localised energy-momentum tensor, too. For gluing both halves back together, we imposed the Israel junction conditions. These force the hypersurface to bend according to its energy-momentum content. We found the impurity entropy by computing specifically engineered proper lengths of geodesics perpendicular to the hypersurface.

In addition to backreaction, we also considered time dependence as a further generalisation to the holographic Kondo model of [60]. By adapting the numerical evolution scheme presented in [67], we found the evolution of the fields in the entire bulk of the dual gravity theory after quenching the effective Kondo coupling. We explained the different quench categories, from the normal to the condensed phase, vice versa, and right onto the critical coupling. We extracted quasinormal modes in both the normal and the condensed phase. In the normal phase, those match precisely the analytic expectations. In the condensed phase, we compared with the results of [68,125] which matched to high precision. It should be kept in mind that the authors of [68, 125] used perturbation theory around numerical backgrounds to extract the quasinormal modes, whereas our approach shows them directly in the temporal behaviour of the fields. In accordance with the literature about generic time dependent holographic, we found that the temporal evolution of the fields is given very quickly by the quasinormal modes, only. There is no intermediate fully non-linear behaviour emerging, which is characteristic for the relaxation of strongly coupled systems. Due to our full evolution scheme, we were moreover able to extract dynamical critical behaviour of the model at the phase transition. Under these circumstances, the fields decay according to a power-law instead of exponentially, as expected. The dynamical critical exponent z was found to be $z = 2$, which matches results from dynamical mean-field theory. Considering that the cross-over transition of the Kondo

model becomes a mean-field phase transition in the large-N limit, this result is physically meaningful.

It is also interesting to consider the spatio-temporal behaviour of the Kondo cloud after quenches of the Kondo coupling in the holographic dual. In order to do so, we need to go beyond the probe limit in the time dependent setup and consider backreaction. The gravitational coupling κ_N can in principle be finite, which, however, renders the evolution equations non-linear. So, we would need compute the evolution of the fields on the hypersurface from scratch, because the geometry also backreacts to the fields due to the appearance of the embedding function X in the field equations of motion. This can be avoided by linearising the system around $\kappa_N = 0$. The Israel junction conditions carry a factor of κ_N in front of the surface energy-stress tensor. This implies that at zeroth order, the junction conditions are trivially satisfied, and the solution to the equations of motion of the fields on the hypersurface is just given by the time evolution without backreaction, as explained in chapter 5. At linear order in κ_N, the evolution of the geometry is then given by integrating it from the zeroth order solution for the energy-stress tensor, directly given by the field content on the brane. We outlined the foundations of this approach in chapter 5.8, the actual calculations are left for future research. Part of the reason for this is that in order to identify the temporal evolution of the entanglement or impurity entropy, we need to apply the covariant proposal suggested in [20] for the holographic computation of entanglement entropy.

Outlook

We end this thesis with an outlook for possible future research apart from time dependent backreaction. First of all, we should keep in mind that the original Kondo model, which involves free electrons instead of strongly coupled ones as in the holographic case, has been solved in quite some detail over the years. Wilson's renormalisation group approach [63] already gave the numerical behaviour of the model throughout the entire renormalisation group flow. The point of the holographic model of [60] and its generalisations considered in this thesis was to consider the case of strongly coupled electrons. Moreover, it serves to prepare a general framework that is adaptable to generalisations of the original Kondo model. These include, among others, considering multiple channels, multiple impurities and the Kondo lattice, especially in strongly coupled hosts. The latter is an unsolved problem of condensed matter physics. It is conceivable that gauge/gravity duality might provide a new approach towards addressing these problems.

Before we turn to further generalisations, we need to recall the cases in

which the model of [60] and the generalisations in this thesis are not reliable any more. This includes most importantly the zero temperature limit $T = 0$, for which we need to stabilise the scalar potential $V(\Phi)$. We always restricted it, as shown in equation (3.20), to include a mass term, only. This mass alters the boundary expansions of the scalar field and defines the scaling dimension of the dual operator $\mathcal{O}$. To match the dimension $\Delta = 1/2$ expected from the conformal field theory approach to the Kondo model [87], we always set the mass such that the Breitenlohner-Freedman bound is saturated. In the probe limit, this means $M = 0$, while for the backreaction we set the mass according to (4.51) to a non-vanishing value. In all cases, the potential of the scalar is unbounded from below, which becomes apparent e.g. in the fact that the scalar expectation value diverges as $T \to 0$. This behaviour is shown in figures 3.3 and 4.4 for the probe limit and with backreaction, respectively. A first approach to stabilise the potential from below is by inserting a Φ^4 term with different sign, implying a Mexican hat potential with a minimum $\partial_\Phi V(\Phi_*) = 0$ at a value Φ_*. Regularity at the horizon involves both the potential as well as its derivative as constraints for the boundary expansions of the fields, as is shown in equations (4.52) - (4.54). From this we see that the fields' behaviour will be special at the minimum of the potential.

Let us conclude this thesis with thoughts about generalisations beyond the single-impurity Kondo model. In the presence of another impurity, generically there is an additional coupling between the impurities themselves, which is called the Ruderman-Kittel-Kasuya-Yosida (RKKY) coupling. An effective Hamiltonian for this system is of the general form [126]

$$H = H_0 + J_K \, \vec{S}_1 \cdot s(\vec{r}_1) + J_K \, \vec{S}_2 \cdot s(\vec{r}_2) + J_{RKKY} \, \vec{S}_1 \cdot \vec{S}_2 \,, \tag{6.1}$$

where H_0 is the kinetic term for the host fermions, $\vec{r}_i$ are the positions of the impurities, $\vec{S}_i$ are the impurities' effective spins, $s(\vec{r})$ is the spin moment of the host metal, J_K denotes the Kondo coupling and J_{RKKY} the RKKY coupling between the impurities. Depending on the relative strengths of the RKKY coupling and the Kondo coupling, another phase emerges and the phase diagram becomes two-dimensional.

In our framework for backreaction, a description of another impurity could be to add an additional defect hypersurface at a finite spatial distance L to the one considered in this thesis, where L should not be confused with the AdS radius. Then, we would have two impurities, one anchored at $x = -L/2$, the other one at $x = +L/2$, and we need to figure out the backreaction of both hypersurfaces to the environment. Applying the Israel junction conditions similar to the case considered in chapter 4, the manifold would need to be split into three parts. However, the RKKY interaction be-

tween the impurities in (6.1) is non-local and it is unclear how to incorporate this in the gravity dual, which is a theory allowing local interactions, only.

There are approaches employing methods from conformal field theory in the case of vanishing separation of the impurities [127, 128], which circumvents the issue of non-locality. In a string theoretic top-down approach, an extension of the brane setup of [60] with two coinciding D5-branes, $N_5 = 2$, seems be a possible way to find a holographic model of this kind. Coinciding D-branes in string theory usually come along with enhanced gauge symmetry in their DBI action.

Indeed, an approach to generalise the holographic model of [60] to the two-impurity problem in this way was suggested in [101]. In that setup, the $U(1)$-gauge field a on the defect hypersurface is enhanced to a $U(2)$-gauge field, which was argued to be the dualisation of adding another impurity to the setup. Apart from elevating the symmetry group of the gauge field a, the action is the same as in the holographic single-impurity Kondo model of [60] as given by (3.15). Hence, our approach to backreaction and time dependence should be applicable to this model, too. Obviously, there is plenty of room to discover dynamical critical behaviour along the phase boundary. Moreover, the behaviour of the holographic entanglement entropy in this setup seems promising.

From these insights, how could an extension to a whole lattice of impurities in the framework of the holographic Kondo model of [60] look like? It does not seem appropriate to take a large-N_5 limit in the models above, because the CFT description is reliable only when the distance between the impurities becomes negligible. With an entire lattice of Kondo impurities, however, we would need to consider more and more impurities as we zoom out to make their separations vanish.

Perhaps, a way to find a dual bottom-up model is to pick up our suggestion from above: Place two defect hypersurfaces at a finite distance and consider *only* the patch of the geometry between those. By virtue of the imposed lattice symmetry, the complement of the geometry must be given by copies of this patch. This setup *could* in principle reveal two phases with an appropriate field content on the hypersurfaces: In one phase, the hypersurfaces go from asymptotic infinity into the event horizon separately, just like in our framework discussed in chapter 4. In the other phase, both hypersurfaces might join in the bulk of the gravity dual, thus cutting off the black hole.

It might be difficult to find an appropriate field content on the brane allowing this kind of behaviour due to energy conditions as was already pointed out in [1]. Nevertheless, this approach may provide a mass gap for the theory which does not depend on the temperature but most likely only on a combi-

nation of the spatial distance L between the impurities and the strength of the Kondo coupling J. Whether or not one has to introduce a RKKY-like coupling between the distinct impurities and how this can be incorporated into the holographic model is, among various other unresolved questions, left for future research.

Acknowledgements

Completing this thesis would not have been possible without the right circumstances.

First of all, I would like to thank Johanna Erdmenger for giving me the opportunity to learn more about the beautiful topic of gauge/gravity duality. I had a very pleasant time in your group at the Max Planck Institute for Physics.

I thank Dieter Lüst for providing such a fruitful environment for research in string theory and related topics at the Max Planck Institute for Physics and LMU, and for being the second referee of this thesis.

Moreover, I am grateful to all of my colleagues for interesting conversations both about physics and off-topic. Working with you was a great experience. Unfortunately, by the time this thesis was finished, most of you already left the Institute. I wish you all the best for your careers, wherever you are and wherever you will go in the future.

I would like to thank my family and friends for continuous support throughout the years. I would not have been able to finish any of this without you. It would not have been fun, either. The world is more interesting with you in it.

Finally, Elisa, I cannot describe in just a few sentences how deeply grateful I am for your pure existence throughout the last couple of years, especially towards the end. I know, that this was not easy for you at times and thank you for bringing me back down to earth once in a while. You convinced me to do the best decision of my life. I am finished now and the times ahead will be more fun, I promise!

Appendix A

Geodesic normal flows

In section 4.3, we motivated the derivation of exact solutions for a static embedding $\mathcal{X}$ of a codimension one hypersurface $\mathcal{D}$ carrying a constant tension from a gauge field a. It was shown that in this case the energy stress tensor yields a constant tension on the hypersurface, i.e.

$$S_{\mu\nu} = \lambda\, \gamma_{\mu\nu}\,. \tag{A.1}$$

So, it is of interest to study constant tension solutions to the Israel junction conditions, given by (4.17), for general dimensions. We will proceed in the same way as we did for the holographic Kondo model: We split the bulk manifold into three parts by $\mathcal{N} = \mathcal{N}_- \cup \mathcal{D} \cup \mathcal{N}_+$, where $\mathcal{N}_\pm$ are the parts to the "left-" and to the "right-hand side" of the hypersurface $\mathcal{D}$, respectively. This can be made explicit by defining a normal vector on $\mathcal{D}$, so that $\mathcal{N}_+$ is the part in which direction the normal vector points. For some coordinate system $(t, \vec{y}, x)$, the embedding is given by

$$\mathcal{X}_\pm : \mathcal{D} \hookrightarrow \mathcal{N}_\pm, (t, \vec{y}) \mapsto (t, \vec{y}, x = X_\pm(t, \vec{x}))\ , \tag{A.2}$$

where t and $\vec{y}$ are coordinates tangential to the hypersurface and the x-position of the embeddings are given by the functions $X_\pm$. We will assume mirror symmetry around the hypersurface, that is

$$X_+(t, \vec{y}) = -X_-(t, \vec{y})\,. \tag{A.3}$$

In this case, the extrinsic curvatures $K_{(\pm)}$ of the embeddings $\mathcal{X}_\pm$ satisfy

$$K_{(-)\mu\nu} = -K_{(+)\mu\nu} \tag{A.4}$$

so that the junction conditions simplify to

$$K_{(+)\mu\nu} = -\frac{\kappa_N \lambda}{2}\left(\frac{1}{d-1}\right)\gamma_{\mu\nu} \equiv c\,\gamma_{\mu\nu}\,. \tag{A.5}$$

We introduced a proportionality constant c_0, which is completely determined by d, κ_N and λ. Since we are only interested in the case with mirror symmetry, we will drop the signs $(\pm)$ on any object from now on and only consider the embedding on the $(+)$-side.

In [60], the case without backreaction to the geometry was considered. This maps to setting $\kappa_N = 0$ and hence $c = 0$ in equation (A.5). The embedding chosen was totally geodesic, $K_{\mu\nu} = 0$, so the junction conditions are trivially satisfied. In the following we will show an explicit construction of solutions to (A.5) for non-vanishing $c \neq 0$ in case we have such a trivial solution with $c = 0$ as a starting point. In brief, the construction is given by following at each point on the hypersurface the geodesic starting perpendicular to the hypersurface for a specific arc length s, which is linearly proportional to c.

We start with a totally geodesic, timelike embedding $\mathcal{X}_0 : \mathcal{D} \hookrightarrow \mathcal{N}$ of a codimension one hypersurface $\mathcal{D}$ into a D-dimensional manifold $\mathcal{N}$. This embedding can be equipped with a normal vector N of unit norm pointing into $\mathcal{N}$. At each point on $\mathcal{D}$, this normal is the starting point for a unique geodesic. By following the entity of geodesics starting on $\mathcal{D}$ for a proper length s, we generate new embeddings denoted by $\mathcal{X}_s$. These embeddings are regular at least up to some finite s due to Gauss' lemma. Moreover, the geodesics are always orthogonal to any such hypersurface defined by $\mathcal{X}_s$, such that this construction does not break down unless we face conjugate points at which the embeddings stop being regular. Hence, we denote the vector field generated by the normal flow also by N, which should not cause confusion in this context.

If the embeddings defined via $\mathcal{X}_s$ still satisfy (A.5), they are solutions of the Israel junction conditions for nonvanishing $c \neq 0$ and we succeeded to find analytic constant tension solutions. In order to show whether this holds, we need to calculate the Lie derivatives of the induced metric and the extrinsic curvature w.r.t. the geodesic normal flow. To make the computation more easy, we define both quantities as tensors in the exterior manifold, which does not enhance the amount of information they carry.

Instead of defining the induced metric as the pullback of the ambient metric g with respect to $\mathcal{X}_s$, it is equivalent to project out its components normal to the embedding by

$$\gamma = g - n \otimes n \,, \tag{A.6}$$

where $n = g(N, \cdot) = N_\alpha \mathrm{d}x^\alpha$ is the normalised dual 1-form to the normal vector field N and index-lowering is due to the ambient metric, $N_\alpha = g_{\alpha\beta} N^\beta$. While following the induced metric along the normal flow generated by N,

its Lie derivative is given by

$$\mathcal{L}_N\gamma = \mathcal{L}_N g - \mathcal{L}_n(n\otimes n) = \mathcal{L}_N g - \mathcal{L}_N(n)\otimes n - n\otimes\mathcal{L}_n(n) = \mathcal{L}_N g\,, \quad \text{(A.7)}$$

where we applied the Leibniz rule for the Lie derivative, and exploited that $\mathcal{L}_N(n) = 0$ if N generates a geodesic flow. The Lie derivative of g is given by

$$(\mathcal{L}_U g)(V,W) = g(\nabla_V U, W) + g(V, \nabla_W U)\,, \quad \text{(A.8)}$$

or, in components,

$$(\mathcal{L}_N\gamma)_{\mu\nu} = (\mathcal{L}_N g)_{\mu\nu} = \nabla_\mu N_\nu + \nabla_\nu N_\mu\,. \quad \text{(A.9)}$$

The extrinsic curvature of the embedding can be defined as a tensor in $\mathcal{N}$ by splitting the covariant derivative in the ambient space into tangential and normal parts

$$\nabla_U V = (\nabla_U V)^{\parallel} + (\nabla_U V)^{\perp} =: \nabla^{\parallel}_U V + K(U,V)N\,. \quad \text{(A.10)}$$

Here, U, V are sections of $T\mathcal{N}$ tangential to $\mathcal{D}$ and $\nabla^{\parallel}$ denotes the induced connection on $\mathcal{D}$ such that $\nabla^{\parallel}_U V \perp N$. Equipped with this splitting, the extrinsic curvature K is defined as

$$K(U,V) := g(N, \nabla_U V) = -g(\nabla_U N, V)\,, \quad \text{(A.11)}$$

or, in components,

$$K_{\mu\nu} = -\nabla_\mu N_\nu = -\nabla_\nu N_\mu = -\nabla_{(\mu} N_{\nu)} = -\frac{1}{2}\left(\nabla_\mu N_\nu + \nabla_\nu N_\mu\right)\,. \quad \text{(A.12)}$$

It satisfies $K(N,V) = 0$ for all $V \in T\mathcal{N}$. Hence we recover a standard result of differential geometry,

$$(\mathcal{L}_N\gamma)_{\mu\nu} = -2K_{\mu\nu}\,. \quad \text{(A.13)}$$

The interesting question is: What happens with the extrinsic curvature of the embedding along the same flow? Acting with the Lie derivative on a general contraction of K

$$\mathcal{L}_N(K(U,V)) = (\mathcal{L}_N K)(U,V) + K(\mathcal{L}_N U, V) + K(U, \mathcal{L}_N V)\,, \quad \text{(A.14)}$$

and solving for $\mathcal{L}_N K$, we obtain

$$\begin{aligned}(\mathcal{L}_N K)(U,V) &= \mathcal{L}_N(K(U,V)) - K(\mathcal{L}_N U, V) - K(U, \mathcal{L}_N V)\\ &= \underbrace{N(K(U,V))}_{(a)} \underbrace{-K([N,U],V)}_{(b)} \underbrace{-K(U,[N,V])}_{(c)}\,. \end{aligned} \quad \text{(A.15)}$$

The individual parts are given by

$$\begin{aligned}
(a) &= N(K(U,V)) \\
&= \nabla_N(g(N,\nabla_U V)) = g(N,\nabla_N\nabla_U V)\,, \\
(b) &= -K([N,U],V) = -g(N,\nabla_{[N,U]}V) \\
&= g(N,R_{NU}V) - g(N,\nabla_N\nabla_U V) + g(N,\nabla_U\nabla_N V)\,, \\
(c) &= -K(U,[N,V]) = -g(N,\nabla_U[N,V]) \\
&= -g(N,\nabla_U\nabla_N V) + g(N,\nabla_U\nabla_V N)\,.
\end{aligned} \tag{A.16}$$

For the computation of (b) we used

$$R_{XY}Z := \nabla_X(\nabla_Y Z) - \nabla_Y(\nabla_X)Z - \nabla_{[X,Y]}Z\,, \tag{A.17}$$

and for that of (c) that the Levi-Civita connection has vanishing torsion, i.e. $[X,Y] = \nabla_X Y - \nabla_Y X$. In summary, we obtain

$$\begin{aligned}
(\mathcal{L}_N K)(U,V) &= (a) + (b) + (c) \\
&= g(N,\nabla_N\nabla_U V) + g(N,R_{NU}V) - g(N,\nabla_N\nabla_U V) \\
&\quad + g(N,\nabla_U\nabla_N V) - g(N,\nabla_U\nabla_N V) + g(N,\nabla_U\nabla_V N) \\
&= g(N,R_{NU}V) + g(N,\nabla_U\nabla_V N) \\
&= \underbrace{g(N,R_{NU}V)}_{(d)} - \underbrace{g(\nabla_U N,\nabla_V N)}_{(e)}\,.
\end{aligned} \tag{A.18}$$

Although not obvious, $\mathcal{L}_N K$ is symmetric in its arguments and vanishes if either of those is proportional to N.

We would like to have the above expression more explicitly in terms of the Ricci scalar and Ricci tensor, so we apply the Ricci decomposition

$$R = A + B + C\,. \tag{A.19}$$

Here, A is the trace part and B the pseudo-trace part of the Riemann tensor, both of which are functions of the Ricci curvature and metric only. The Weyl tensor C vanishes in three dimensions. In components, the decomposition reads

$$\begin{aligned}
R_{abcd} = &\frac{-R}{(D-1)(D-2)}\,(g_{ac}\,g_{bd} - g_{ad}\,g_{bc}) + C_{abcd} \\
&+ \frac{1}{D-2}\,(R_{ac}\,g_{bd} + R_{bd}\,g_{ac} - R_{ad}\,g_{bc} - R_{bc}\,g_{ad})
\end{aligned} \tag{A.20}$$

with the definitions for the Ricci and scalar curvature

$$R_{ab} := R^c_{\ acb} \qquad R := g^{ab}\,R_{ab}\,. \tag{A.21}$$

Staying in components, we find

$$\begin{aligned}(d)_{\mu\nu} =& N^\alpha N^\beta R_{\alpha\mu\beta\nu} = -\frac{R}{(D-1)(D-2)}\gamma_{\mu\nu} \\ &+ \frac{1}{D-2}\left(N^\alpha N^\beta R_{\alpha\beta} g_{\mu\nu} + R_{\mu\nu} - N^\alpha R_{\alpha\nu} N_\mu - N^\beta R_{\beta\mu} N_\nu\right) + N^\alpha N^\beta C_{\alpha\mu\beta\nu}\end{aligned}$$

$$\begin{aligned}(e)_{\mu\nu} =& - g(\nabla_\mu N, \nabla_\nu N) \\ =& - g_{\alpha\beta}(\nabla_\mu N^\alpha)(\nabla_\nu N^\beta) = -g^{\alpha\beta}(\nabla_\mu N_\alpha)(\nabla_\nu N_\beta) \overset{(A.12)}{=} -g^{\alpha\beta} K_{\alpha\mu} K_{\beta\nu}\,.\end{aligned} \tag{A.22}$$

Summing up, the Lie derivative of the extrinsic curvature along the geodesic normal flow is in coordinates given by

$$\begin{aligned}(\mathcal{L}_N K)_{\mu\nu} =& -\frac{R}{(D-2)(D-1)}\gamma_{\mu\nu} + N^\alpha N^\beta C_{\alpha\mu\beta\nu} - g^{\alpha\beta} K_{\alpha\mu} K_{\beta\nu} \\ &+ \frac{1}{D-2}\left(N^\alpha N^\beta R_{\alpha\beta} g_{\mu\nu} + R_{\mu\nu} - N^\alpha R_{\alpha\nu} N_\mu - N^\beta R_{\beta\mu} N_\nu\right).\end{aligned} \tag{A.23}$$

We will now further specify the ambient manifold $\mathcal{N}$, and restrict ourselves to Einstein manifolds for which

$$R_{\mu\nu} = \frac{R}{D}\, g_{\mu\nu}\,. \tag{A.24}$$

Furthermore, we assume vanishing Weyl curvature, $C = 0$, which is always true in three dimensions and for conformally flat manifolds in higher dimensions. In this case, (A.23) reduces to

$$(\mathcal{L}_N K)_{\mu\nu} = \frac{R}{D(D-1)}\gamma_{\mu\nu} - g^{\alpha\beta} K_{\alpha\mu} K_{\beta\nu}\,. \tag{A.25}$$

If the normal geodesic flow starts with an embedding $\mathcal{X}_0 : \mathcal{D} \hookrightarrow \mathcal{N}$ such that the extrinsic curvature initially satisfies

$$K_{\mu\nu}\Big|_{s=0} = c\,\gamma_{\mu\nu}\Big|_{s=0}\,, \tag{A.26}$$

the Lie derivative (A.25) simplifies to

$$(\mathcal{L}_N K)_{\mu\nu}\Big|_{s=0} = \left(\frac{R}{D(D-1)} - c^2\right)\gamma_{\mu\nu}\Big|_{s=0} \tag{A.27}$$

at the initial surface. Intuitively, there is no reason why the proportionality between induced metric and extrinsic curvature could be destroyed. The Lie derivatives only involve terms allowed by the proportionality.

To make this statement manifest, we utilise a coordinate system in which the normal vector is always given by $N^\alpha = \{1, 0, \ldots\}$. The equations now read

$$\partial_s \gamma_{\mu\nu} = -2K_{\mu\nu}\,, \tag{A.28}$$

$$\partial_s K_{\mu\nu} = \tilde{R}\,\gamma_{\mu\nu} - g^{\alpha\beta}K_{\alpha\mu}K_{\beta\nu}\,, \tag{A.29}$$

where we defined $\tilde{R} = R/D(D-1)$. This is a coupled system of first order ODEs in s, admitting a unique solution depending only on the initial conditions $\gamma(0)$ and $K(0)$. We can make an ansatz for this solution by

$$K_{\mu\nu}(s) = c(s)\,\gamma_{\mu\nu}(s) \tag{A.30}$$

which is supposed to be satisfied at some $s = s_0$ initially. Differentiating (A.30) with respect to s and applying (A.29), we find

$$\tilde{R}\,\gamma_{\mu\nu} - \underbrace{g^{\alpha\beta}K_{\alpha\mu}K_{\beta\nu}}_{=c^2(s)\,\gamma_{\mu\nu}} \overset{\text{(A.29)}}{=} \partial_s K_{\mu\nu} \overset{\text{(A.30)}}{=} c'(s)\,\gamma_{\mu\nu} + c(s)\,\underbrace{\partial_s\gamma_{\mu\nu}}_{=-2K_{\mu\nu}}\,. \tag{A.31}$$

After reshuffling, this yields

$$\Big(c'(s) - (\tilde{R} + c^2(s))\Big)\,\gamma_{\mu\nu} = 0\,, \tag{A.32}$$

which is an ODE for $c(s)$ since $\gamma_{\mu\nu}$ cannot vanish. If the scalar curvature, $\tilde{R} = R/D(D-1)$, is constant in $\mathcal{N}$, it can be solved by separation of variables with its solution given by

$$c(s) = \begin{cases} -\sqrt{|\tilde{R}|}\,\tanh\left(\sqrt{|\tilde{R}|}\,(s-s_0) - \operatorname{artanh}\left(c_0/\sqrt{|\tilde{R}|}\right)\right) & \text{if } \tilde{R} < 0 \\ c_0/\left(1 - c_0(s-s_0)\right) & \text{if } \tilde{R} = 0 \\ \sqrt{\tilde{R}}\,\tan\left(\sqrt{\tilde{R}}\,(s-s_0) + \arctan\left(c_0/\sqrt{\tilde{R}}\right)\right) & \text{if } \tilde{R} > 0 \end{cases}, \tag{A.33}$$

where we defined $c(s_0) \equiv c_0$. Before elaborating the distinct cases, it might be a good idea to review our assumptions: We have a codimension one hypersurface $\mathcal{D}$ embedded in $\mathcal{N}$, which

- satisfies the proportionality given in (A.5) initially,
- whose ambient manifold $(\mathcal{N}, g)$ has vanishing Weyl curvature, and

- has constant scalar curvature everywhere.

If these assumptions are satisfied, we showed that the proportionality (A.5) continues to hold as we change the constant tension on the hypersurface. We conclude this appendix with a discussion of the three cases of negative, positive, and vanishing scalar curvature:

Negative scalar curvature, $\tilde{R} < 0$, is the most important case for applications of the geodesic normal flow to backreaction in the holographic Kondo model as described in chapter 4. Here, all assumptions are satisfied as the ambient spacetime is given by a BTZ black brane, which due to its construction has a constant scalar curvature. If the constant tension is positive, which possibly is the only reasonable case anyways, we find that the arc length of the geodesics, s, needs to be positive due to (A.33). The amplitude of the artanh function is bound by one, which implies a nontrivial bound for the proportionality constant,

$$|c(s)| < \sqrt{\tilde{R}}\,. \tag{A.34}$$

Upon comparing to (A.5), this yields exactly the bound (4.47) found for the backreaction of the field content in the holographic Kondo model discussed in section 4.3.

Vanishing scalar curvature, $\tilde{R} = 0$, is given by a flat ambient spacetime and is probably the most intuitive case. The construction works if and only if $c(s_0) \neq 0$ since otherwise, the function $c(s)$ cannot be driven away from zero due to (A.33). However, the construction works with negative feedback for nonvanishing initial values. For $c_0 > 0$, this describes can for example describe a static sphere in Minkowski space. As we follow the geodesic normal flow of outwards directed geodesics, the radius of the sphere increases and its extrinsic curvature decreases.

Positive scalar curvature, $\tilde{R} > 0$, is given by asymptotically de Sitter spaces. As we increase the constant tension of the hypersurface, we find from (A.33) that the arc length parameter s decreases. Thus, the volume of the spacetime shrinks as we follow the flow. An extreme case similar to the bound found for negative scalar curvature is that the proportionality constant diverges at $|s| = \pi/(2\tilde{R})$. Hence, is is not the amount of energy-stress on the hypersurface which is bounded, but the movement of the hypersurface due to backreaction.

Appendix B

Numerical approach to backreaction

In this appendix, we give some details on how we solved the static backreaction for the holographic Kondo model of [60], as published in [2]. As mentioned in section 4.4, one trick which was applied was to solve the constraint equation of the static Israel junction conditions w.r.t. the radial derivative of the embedding. For convenience, we define

$$\mathcal{X}^2(z) = 1 + h(z)X'^2(z)\,, \tag{B.1}$$

along with its positive square root

$$\mathcal{X} = \sqrt{\mathcal{X}^2}\,. \tag{B.2}$$

With this, the zz-component of the Israel junction conditions (4.30) is given by

$$\begin{aligned} 0 = \frac{1}{4\,L^2\,z^2\,h^2}\Big(&\kappa_N z^4\,h\,a_t'^2 - 2\,\kappa_N\,L^2\,z^2\,\left(a_t^2\,\Phi^2\,\mathcal{X}^2 + h^2\,\Phi'^2\right) \\ &+ 2\,L^3\,z\,h\,h'\,X'\,\mathcal{X} + 2\,\kappa_N\,L^4\,M^2\,h\,\Phi^2\,\mathcal{X}^2 - 4\,L^3\,h^2\,X'\,\mathcal{X}\Big)\,, \end{aligned} \tag{B.3}$$

where we omitted the arguments of the functions. Despite its complexity, (B.3) is actually solvable for X'. There are four solutions: Two of them have non-vanishing imaginary parts and can be neglected, as X and its derivative are supposed to be real-valued. One of the remaining solutions can also be rejected, as the asymptotic expansion near $z = 0$ yields $X'(0) > 0$. However, due to our analysis of the analytic background solution (4.41), we know that $X'(0) < 0$. The unique solution, which cannot be sorted out by considerations like that is given by

$$X'(z) = -\sqrt{\frac{B}{2\,A}} \tag{B.4}$$

where we defined

$$A = h^2 L^2 \left(4 h^3 L^2 - C^2 \kappa_N^2 \Phi^4 + h L^2 z h' (z h' - 4 h)\right) , \tag{B.5}$$

$$\begin{aligned} B = {} & h^2 \kappa_N^2 \Phi^2 z^4 a'^2 C \\ & + L \left[h^2 L z \left(2 h \kappa_N^2 \Phi^2 z \Phi'^2 \left(a^2 z^2 - h L^2 M^2\right) + L^2 h' (4 h - z h')\right)\right. \\ & \left. + 2 h \kappa_N^2 L \Phi^4 C^2 + \sqrt{D} - 4 h^4 L^3\right] , \end{aligned} \tag{B.6}$$

$$\begin{aligned} D = {} & h^4 (z h' - 2 h)^2 \left[L^4 \left(4 h \kappa_N^2 \Phi^2 z^2 \Phi'^2 \left(a^2 z^2 - h L^2 M^2\right)\right.\right. \\ & \left.\left. + 4 h^3 \kappa_N^2 z^4 \Phi'^4 + L^2 (z h' - 2 h)^2\right) + h \kappa_N^2 z^8 a'^4\right. \\ & \left. + \kappa_N^2 L^2 z^4 a'^2 \left(\Phi^2 C - 2 h^2 z^2 \Phi'^2\right)\right] , \end{aligned} \tag{B.7}$$

$$C = h L^2 M^2 - a^2 z^2 . \tag{B.8}$$

This is an ordinary differential equation for X in the radial coordinate z depending only on the field configurations of Φ and a_t. In the field equations of Φ and a_t, the embedding appears only via the induced metric on the hypersurface, which is given by

$$\mathrm{d}s^2 = \frac{1}{z^2} \left(-h(z) \mathrm{d}t^2 + \frac{1 + h(z) X'(z)^2}{h(z)} + \mathrm{d}x^2\right) , \tag{B.9}$$

which tells us why the factor $\mathcal{X}^2$ defined in (B.1) appears all over the place. However, it also shows that the field equations of motion really just depend on $X'(z)$. Since we solved for it in (B.4), we can insert this solution into the equations of motion for Φ and a_t and obtain two ordinary differential equations which only depend on those fields and functions we know. They become quite involved, which is why we do not write them here.

The computation of the field configurations of Φ and a_t is then performed by a three-fold approach: Close to the boundary, we apply the boundary expansions of the fields Φ and a_t, and insert them into (B.4). We compute them up to fourth order by defining

$$\Phi \mapsto \sqrt{z} \left(\alpha \log z + \beta + \sum_{i=1}^{3} z^i \left(\sum_{j=0}^{1+3i} b_{ij}^{\Phi} \log^j(z)\right)\right) , \tag{B.10}$$

$$a_t \mapsto Q/z + \mu + \sum_{i=1}^{3} c_i \log^i(z) + \sum_{i=1}^{3} z^i \sum_{j=0}^{2+3i} b_{ij}^{a_t} \log^j(z) , \tag{B.11}$$

where Q is already determined by (4.50), α and β are supposed to satisfy (3.30), and the rest of the coefficients c_{ij}^f can be solved for Q, μ, α, and β.

Note that the number of logarithmic terms we need to include at every power of z is linearly increasing in the power of z. The upper bound of the number of logarithmic terms is an empiric formula, although one could probably derive such a bound by a more sophisticated analysis of the equations.[18]

In principle, the expansion coefficients can be solved in full dependence of arbitrary values of Q, L, z_H and κ. It is, however, *much* more efficient to fix their numerical values before computing the expansions. For the computations, we chose $\kappa = 1$, $L = 1$, $z_H = 1$, $C = 1/2$ and thus $Q = -8/\sqrt{255}$ by virtue of (4.50). The coefficients c_i are then analytically given by

$$c_1 = -\frac{16972802\alpha^2 - 16712702\alpha\beta + 8486401\beta^2}{520200\sqrt{255}}\,, \tag{B.12}$$

$$c_2 = \frac{\alpha(8356351\alpha - 8486401\beta)}{520200\sqrt{255}}\,, \tag{B.13}$$

$$c_3 = -\frac{8486401\alpha^2}{1560600\sqrt{255}}\,, \tag{B.14}$$

and the higher order coefficients are also analytically solved for, but would require several more pages to write them down.

Applying the boundary expansions yields the values of Φ and a_t close to the asymptotic boundary at $z = 0$. We use this approximation until the asymptotic cutoff $\epsilon_{bnd} = 10^{-3}$ by inserting the values of α, β and μ which we solved for numerically by integrating the equations of motion of Φ and a_t.

Between the asymptotic cutoff ϵ_{bnd} and the horizon cutoff ϵ_{hor}, we integrate (B.4) numerically by the shooting method for which we use MATHEMATICA's ParametricNDSolve function. Beyond the horizon cutoff ϵ_{hor}, we use the horizon expansion in the same way as for the values close to the asymptotic boundary. The horizon expansions are given by

$$\Phi \mapsto \sum_{i=0}^{N} h_i^{\Phi}\,(1-z)^i\,, \tag{B.15}$$

$$a_t \mapsto \sum_{i=0}^{N} h_i^{a_t}\,(1-z)^i\,, \tag{B.16}$$

which luckily do not contain logarithmic terms at any order due to regularity at the event horizon. There are two parameters, equivalent to $\Phi'(z_H)$ and $a_t(z_H)$, which cannot be chosen or solved for, but which need to satisfy the

[18] The real issue is that taking derivatives of a logarithmic term of the form $z^a \log^b(z)$ lowers the order in z by one, but mixes the orders in $\log^b(z)$. With complicated equations of motion, tracking the appearances of the logarithmic terms is thus involved.

regularity conditions given in (4.52) and (4.53). The rest of the expansion coefficients can be solved in terms of $\Phi(z_H)$ and $a_t'(z_H)$. This can easily be performed analytically up to high orders. We choose to expand the fields up to tenth order at the horizon which allows us to choose the horizon cutoff as $\epsilon_{hor} = z_H \cdot 9/10$.

At this point, we found the field configurations of Φ and a_t throughout the hypersurface. In order to compute entanglement and impurity entropies of symmetric patches around the defect, we need the embeddings and their derivatives at excellent precision on a predefined set of points in the radial direction. Hence, we chose to interpolate the embeddings by computing their values $X(z)$ on a Chebyshev-Gauss-Lobatto grid, $z \in CGL(0, 1, 101)$, after setting $z_H = 1$ by a coordinate transformation $z \mapsto z/z_H$. The grid is defined by

$$CGL(x_0, L, n) := \left\{ x_0 + \frac{L}{2}\left(1 - \cos\left(\frac{\pi k}{n-1}\right)\right) \middle| k \in 0 \dots n-1 \right\} , \quad \text{(B.17)}$$

and spans a set of n points between (and including) x_0 and $x_0 + L$. The interpolation is then given by summing up the Chebyshev-Gauss-Lobatto polynomials up to order n with appropriate weights. In MATHEMATICA, this is done automatically if we interpolate the field values on the grid by using the built-in function `Interpolate` and setting the option `InterpolationOrder` to `All`. The derivatives at the nodes are given directly by (B.4). The field values and derivatives should converge exponentially with the number of grid points, which we choose to be $n = 101$.

Starting on these grid points, we can find the normal vectors from the derivatives just by requiring

$$g_{MN} T^N N^M = 0 , \quad \text{(B.18)}$$

where T is a tangential to the embedding, and normalising N. With the embedding values and those normal vectors determined on the Chebyshev grid, the geodesics starting normal to the embedding are determined completely and can be given analytically but subject to the numerical error from the computation of the embeddings.

The expressions can be found in the appendix of [109]. Here, we summarise the important ones we need in our case for a static embedding. Let $(z_b, X(z_b))$ be the position on which a single geodesic starts normal to the defect hypersurface. Due to $X'(z_b) < 0$, it propagates further into the bulk $\gamma^z > z_b$ and eventually turns around at some point (z_*, X_*). After that, it propagates towards the asymptotic boundary, $\gamma^z < z_*$ and asymptotes to $z = 0$ at some finite value $\gamma^x(z = 0) =: \ell$.

The value of the turning position is found to read

$$z_*(z_b, X'(z_b)) = z_b\sqrt{1 + X'(z_b)^2\, h(z_b)}\,. \tag{B.19}$$

A geodesic propagating in a BTZ background on an equal time slice from some z_1 to some different z_2 covers a distance in its x-coordinate given by

$$\Delta X(z_1, z_2, z_*, z_H) = -z_H \log\left(\frac{\sqrt{z_H^2 - z_1^2} - \sqrt{z_*^2 - z_1^2}}{\sqrt{z_H^2 - z_2^2} - \sqrt{z_*^2 - z_2^2}}\right)\,. \tag{B.20}$$

Combining these results, we find ℓ as a function of z_b, $X(z_b)$, $X'(z_b)$ and z_H to read

$$\ell(z_b, X, X', z_H) = \underbrace{X + \Delta X(z_*, z_b, z_*, z_H)}_{X_*} + \Delta X(z_*, 0, z_*, z_H)\,, \tag{B.21}$$

where we omitted function arguments, i.e. z_* is a function of z_b and X' due to (B.19) and ℓ is always positive, $\ell > 0$, in our setup. The renormalised proper length of this geodesic is given by[19]

$$\mathcal{L}_{ren}(z_b, X, X', z_H) = \log\left(\frac{z_b}{\sqrt{1 - z_b^2/z_H^2} - \sqrt{1 - z_b^2/z_*^2}}\right)\,, \tag{B.22}$$

where, again, z_* is a function of z_b and X' due to (B.19).

With all these definitions, we can map each set of $(z_b, X(z_b), X'(z_b))$ for each value of z_b in the Chebyshev-Gauss-Lobatto grid (B.17) to a table of values $(\ell, \mathcal{L}_{ren})$. We do this for all embeddings at each temperature $0 < T < T_c$ we evaluated, which makes a set of 132 different embeddings, each mapping to a set of 101 pairs $(\ell, \mathcal{L}_{ren}(\ell))$. The first and last of these pairs are always trivially given by $(0, 0)$, for the geodesic starting at asymptotic infinity $z_b = 0$, and (∞, ∞), for the geodesic starting – and staying forever – at the event horizon. The last remark readily follows from the facts, that static event horizons are totally geodesic surfaces, that geodesics starting tangential to such surfaces stay tangential, and that the normal vector to the embedding at the event horizon is always tangential to the event horizon.

According to the Ryu-Takayanagi formula (2.91), the entanglement entropy of a region A symmetrically around the defect, whose boundary ∂A

[19] In these computations, we chose to renormalise the geodesics with and without the defect separately by subtracting the asymptotic divergence, although we advertised that this is not needed for the defect entropy. In this way, we do not run into numerical issues as we have to compute them both in order to build the difference. It makes no difference for the result.

has a distance ℓ to the impurity, is given by twice the proper length $\mathcal{L}_{ren}(\ell)$ of those geodesics. To find the impurity entropy, $S_D(\ell) = S(\ell) - S_0(\ell)$, we need to subtract the entanglement entropy of the same patch but without the impurity. This is done by removing twice the geodesic length $\mathcal{L}_0(\ell)$ of the geodesic which starts at $x = \ell$ and ends up perpendicular to the trivial embedding $X = 0$, which corresponds via (2.91) to the entanglement entropy if there is no impurity. The resulting quantity, $\Delta\mathcal{L}(\ell) = \mathcal{L}(\ell) - \mathcal{L}_0(\ell)$, needs to be normalised by the factor $1/4G_N$ appearing in (2.91) and then corresponds to the holographic dual of the impurity entropy as defined in (4.32).

Appendix C

Numerical time evolution scheme

In chapter 5, we analysed the holographic Kondo model of [60] in the presence of a time dependent Kondo coupling. Here, we will explain some details of the numerical implementation. First of all, we need to notice that most of the implementation of the numerical algorithm has been performed by Strydom in [67]. For this thesis, we adapted this algorithm: Firstly, we changed the gauge fixing, which actually caused a change in the behaviour of the quasinormal modes. Moreover, the evolution algorithm was optimised by using a small trick, which increased its performance by an order of magnitude. Various other changes of the numerical code were performed, too, which however were not as important, so we will focus on those in the following.

Gauge fixing

In [67], the author took the radial gauge, which was already chosen in [60] and is a natural choice for holographic models. This fixes the gauge freedom up to a function of time, $\lambda(t)$, since the transformation of the radial component of the gauge field

$$a_z \to a_z + \partial_z \Lambda(t,z)\,, \tag{C.1}$$

is invariant under $\Lambda(t,z) \to \Lambda(t,z) + \lambda(t)$. On top of the radial gauge, this residual gauge freedom has been utilised in [67] to fix the phase of the scalar field by demanding $\psi(t, z \to 0) = 0$, which is possible by choosing $\lambda(t)$ such that the complex scalar field transforms as

$$\Phi(t,z) \equiv e^{i\psi(t,z)}\phi(t,z) \to e^{i\lambda_*(t)}\Phi(t,z) = e^{i(\psi(t,z)+\lambda_*(t))}\phi(t,z)\,, \tag{C.2}$$

where we must choose $\lambda_*(t) = -\psi(t,0)$ to obtain a vanish phase asymptotically.

It might seem, that this should not have any effect on the physics. However, the gauge transformation we need to carry out in order to achieve the demanded behaviour of the phase is a *large* gauge transformation in two senses: Firstly, it doesn't vanish at the asymptotic boundary and secondly, it diverges. This was already noticed in [67]. The first fact implies that there are issues in general, since gauge choices need to be taken carefully if boundaries are involved. The second fact is specific to the AdS_2-subspace to which the gauge field in constrained.

This hints towards the fact, that a fixing the gauge in AdS_2 subspaces without being careful can alter the physics. Actually, this could be seen in the behaviour of the quasinormal modes. If we kept the phase fixed asymptotically, $\alpha_2 = 0 = \beta_2$ as derived in [67]. The lowest lying quasinormal of $\langle|\mathcal{O}|\rangle$, determined by the temporal behaviour of β_2, obtains a real part in its frequency at low temperatures. Since $\beta_2 = 0$, it follows that $\beta_1 = \beta$ and we really describe the quasinormal mode of the modulus of the scalar operator. Comparing with figure 5.11, in which the lowest lying quasinormal mode is purely imaginary at all temperatures, this clearly displays a different behaviour to our numerics, in which we released the constraint to the phase. Due to this, we choose not to constrain the phase. In the algorithm developed in [67], we therefore need to reintroduce α_2 and β_2 as dynamical boundary coefficients, which is straightforward. They are solved for in the time evolution scheme, and various plots are shown in chapter 5.

The time evolution scheme

We optimised the time evolution scheme of [67] by introducing analytic derivatives for the computation of the Jacobian matrix. In order to understand what this means, we first need to introduce the basics of the numerical code itself, which is done in the following. Before we begin explaining the evolution scheme, we need to mention that it does not operate on the coordinates (t, z, x) as in the metric given in (5.2), but rather on Eddington-Finkelstein coordinates (v, y, x). The coordinate map between those frames reads

$$\begin{aligned} y &= \sqrt{z}\,, \\ v &= t - z_H^2 \,\mathrm{artanh}\,(z/z_H) \\ x &= x\,, \end{aligned} \tag{C.3}$$

such that the new metric is given by

$$\mathrm{d}s^2_{EF} = \frac{1}{y^4}\left(\tilde{f}(y)\mathrm{d}v^2 - 2\,\mathrm{d}v\,\mathrm{d}y + \mathrm{d}x^2\right)\,, \tag{C.4}$$

where $\tilde{f}(y) = 1 - y^4/y_H^4$ and we defined $y_H = \sqrt{z_H}$. There are some advantages in the adapted Eddington-Finkelstein frame: Firstly, the temporal coordinate v is constant on characteristic slices, which means that perturbations outside of the event horizon can approach it in finite Eddington-Finkelstein time. In Schwarzschild time t, perturbations approach the horizon only asymptotically. Since the computation domain is necessarily finite, changing to a characteristic coordinate frame is a must in black hole physics if we want to observe thermalisation. Moreover, the factors of $\sqrt{z}$ appearing in the boundary expansions of the scalar field (5.6) change to y, which makes boundary expansions easier to read and increases convergence close to the asymptotic boundary. Finally, as $y \to 0$, we can can identify $t = v$, which means that the time dependence of the asymptotic boundary coefficients remains the same. Hence, we can directly read off the temporal evolution of them once we solve the equations in the gravity bulk.

In the algorithm used to compute the numerical evolution of a_t and $\Phi = \phi_1 + i\phi_2$, the gravity bulk is discretised on a numerical grid. The nodes, on which the fields are discretised, are distributed on a Chebyshev-Gauss-Lobatto grid, given by (B.17), in the radial direction. The outermost node is lying on the boundary cutoff $\epsilon_{\text{bnd}} = 10^{-3}$, while the innermost point is chosen to be located *inside* the event horizon at $\epsilon_{\text{hor}} = 1 + 10^{-3}$.[20] This has the advantage, that we need not to worry about regularity conditions being satisfied at the event horizon anymore: If we choose the initial values at $t = 0$ to satisfy the regularity conditions, they keep being regular due to the fact that the Chebyshev polynomials are regular. Discretising field on a Chebyshev-Gauss-Lobatto grid is the same as expanding them in Chebyshev polynomials, so the irregular modes vanish automatically.

At the asymptotic boundary, $y = 0$, we need to compute time dependent boundary expansions of all the fields involved. This is necessary, as $y = 0$ is a singular point in the partial differential equations and hence we run into numerical problems if we cannot get away form it. The algorithm which carries out the expansions can be found in [67]. The only difference in this thesis is that we need to reintroduce $\beta_2(t)$ and $\alpha_2(t)$ as advertised above. This changes the boundary expansions, but the algorithm fortunately continues to work just fine. Next, we impose the boundary condition $\alpha_i(t) = \kappa_T(t)\beta_i(t)$ directly on the boundary expansions. The boundary expansions of the fields are used to map their asymptotic boundary coefficients $(\kappa_T(t), \beta_1(t), \beta_2(t), \mu(t))$ to the respective field values at the boundary cutoff ϵ_{bnd}.

For the temporal direction, a regular grid was chosen. To evolve the sys-

[20] Here, we normalised the lengths to z_H, the position of the event horizon, so that $z_H \mapsto 1$, which is equivalent to $z \mapsto z/z_H$, $t \mapsto t/z_H$.

tem numerically, we need to define initial values and derivatives. The initial values are found by solving the static problem[21] at $t = 0$ for some value of $\kappa_T(t = 0)$ and the derivatives are always set to vanish initially. Equivalently, the field values at several initial time slices are chosen to coincide, where the number of initial time slices depends on the order of the evolution algorithm. This approach is fine as long as we make sure that the time derivative of the quench profile $\kappa_T(t)$ initially vanishes, too. We are using Tanh- and Gauss-like quenches, which are exponentially approaching their asymptotic limits apart from their midpoint t_0 as defined in (5.15) and (5.16). Hence, this is approximately the case, if we take the midpoint t_0 of the quenches to be away far enough from $t = 0$, for example by setting $t_0 = 5/s$, where s is the steepness parameter as defined in (5.15) and (5.16). Note that for quenches onto the critical value κ_c, we rather use $t_0 = 5/\log(s)$ due to (5.17).

Given a set of partial differential equations which are n^{th} order in time, we typically define $g^{(k)} \equiv \partial_t^k g$ for $1 \leq k \leq n-1$ and g any dynamical field we want to solve for. We replace any occurrence of higher order derivatives in the equations of motions, so the differential equations become first order in time and are closed upon adding the definitions in the previous sentence. The number of fields has increased due to the ones we just defined. If we label all the fields by f^a, where $a \in \{1 \ldots\}$ indexes the different fields, the equations of motion are now given by

$$F^a(\{f^m\}, \{\partial_t f^m\}) = 0\,. \tag{C.5}$$

For the m^{th} field in this set, let us label its discretised field values at the radial note i and temporal node j by $f^a_{i,j}$. Given those field values on all spatial nodes of all time slices indexed by $\{\ldots, j-2, j-1, j\}$, our task is to find the field values on the next temporal node, $j+1$, and iterate the process until we gained enough information about the evolution and decide to stop.

We can utilise several methods to do so, where two main categories are distinguished: *Explicit* and *implicit* methods. The algorithm developed in [67] uses an implicit method similar to the Crank-Nicolson scheme. In principle, any evolution scheme is an approximation for any derivatives in (C.5) for each field f^a in terms of the field values on the numerical grid. The discretised equations of motion then read

$$F^a_{i,j}(\{f^b_{k,l}\}) = 0\,. \tag{C.6}$$

The Crank-Nicolson scheme discretises the equations of motion is such a way that we cannot directly solve (C.6) for the field values $f^a_{i,j+1}$ on the next time

[21] Reducing the equations of motion in dependence of the Eddington-Finkelstein coordinate (v, y) to the static case by setting any derivatives $\partial_v(\cdot) = 0$, we obtain the exact same static problem as was already solved in [60].

slice. Rather, we need to iteratively solve a set of algebraic equations which are nonlinear in $f^a_{i,j}$ and $f^a_{i,j+1}$. This is basically done by the Newton-Raphson algorithm, which is a root-finding algorithm for the discretised equations. To find a root, we first evaluate the equations on some initial guess for the values of the fields at time slice $j+1$. Taking the ones on the previous time slice, j, is always a good start. The equations will, in general, be non-vanishing in this first step, so we need to adapt the guessed field values on the next time slice. Doing this randomly is not a good idea, so to find the optimal direction of the next guess, we compute the gradient of the equations of motion with respect to each variable, i.e. the $f^a_{i,j+1}$. We define the *Jacobian matrix* by

$$J^a_{i,j}(f^b_{k,l}) = \frac{\partial F^a_{i,j}}{\partial f^b_{k,l}}\,, \tag{C.7}$$

which obviously is a fairly complicated object. Having found this gradient, however, we can go into the opposite direction, which generically takes us closer to the root. Iterating this process guarantees convergence to the solution of the algebraic equation at time step $j+1$.

Computing the Jacobian matrix

The computation of the gradient can be done numerically by evaluating the equations on infinitesimally perturbed values, which needs a lot of evaluations of the equations in each time step. A more efficient approach is to compute this gradient once and for all at the beginning of the evolution. This is done by differentiating the discretised equations of motion (C.6) analytically with respect to each field value. We obtain an analytic gradient and can reuse it in each iteration, which speeds up the evolution scheme by approximately an order of magnitude.

Bibliography

[1] Johanna Erdmenger, Mario Flory, and Max-Niklas Newrzella. Bending branes for DCFT in two dimensions. *JHEP*, 01:058, 2015.

[2] Johanna Erdmenger, Mario Flory, Carlos Hoyos, Max-Niklas Newrzella, and Jackson M. S. Wu. Entanglement Entropy in a Holographic Kondo Model. *Fortsch. Phys.*, 64:109–130, 2016.

[3] J. Erdmenger, M. Flory, C. Hoyos, M-N. Newrzella, A. O'Bannon, and J. Wu. Holographic impurities and Kondo effect. *Fortsch. Phys.*, 64:322–329, 2016.

[4] Johanna Erdmenger, Mario Flory, Max-Niklas Newrzella, Migael Strydom, and Jackson M. S. Wu. Quantum Quenches in a Holographic Kondo Model. *JHEP*, 04:045, 2017.

[5] J. Erdmenger, M. Flory, Max-Niklas Newrzella, M. Rozali, and Jackson M. S. Wu. Spatio-temporal evolution of the Kondo cloud in a holographic Kondo model. *To be published.*

[6] Darren Aronofsky. π – *faith in chaos.* Protozoa Pictures, USA, 1998.

[7] R. Schodel et al. A Star in a 15.2 year orbit around the supermassive black hole at the center of the Milky Way. *Nature*, 2002. [Nature419,694(2002)].

[8] B. P. Abbott et al. Observation of Gravitational Waves from a Binary Black Hole Merger. *Phys. Rev. Lett.*, 116(6):061102, 2016.

[9] B. P. Abbott et al. GW151226: Observation of Gravitational Waves from a 22-Solar-Mass Binary Black Hole Coalescence. *Phys. Rev. Lett.*, 116(24):241103, 2016.

[10] S. W. Hawking. Particle Creation by Black Holes. *Commun. Math. Phys.*, 43:199–220, 1975. [,167(1975)].

[11] J. D. Bekenstein. Black holes and the second law. *Lett. Nuovo Cim.*, 4:737–740, 1972.

[12] Andrew Strominger and Cumrun Vafa. Microscopic origin of the Bekenstein-Hawking entropy. *Phys. Lett.*, B379:99–104, 1996.

[13] Gerard 't Hooft. Dimensional reduction in quantum gravity. In *Salamfest 1993:0284-296*, pages 0284–296, 1993.

[14] Leonard Susskind. The World as a hologram. *J. Math. Phys.*, 36:6377–6396, 1995.

[15] Juan Martin Maldacena. The Large N limit of superconformal field theories and supergravity. *Int. J. Theor. Phys.*, 38:1113–1133, 1999. [Adv. Theor. Math. Phys.2,231(1998)].

[16] Edward Witten. Anti-de Sitter space and holography. *Adv. Theor. Math. Phys.*, 2:253–291, 1998.

[17] G. W. Gibbons and S. W. Hawking. Cosmological Event Horizons, Thermodynamics, and Particle Creation. *Phys. Rev.*, D15:2738–2751, 1977.

[18] Shinsei Ryu and Tadashi Takayanagi. Aspects of Holographic Entanglement Entropy. *JHEP*, 08:045, 2006.

[19] Shinsei Ryu and Tadashi Takayanagi. Holographic derivation of entanglement entropy from AdS/CFT. *Phys. Rev. Lett.*, 96:181602, 2006.

[20] Veronika E. Hubeny, Mukund Rangamani, and Tadashi Takayanagi. A Covariant holographic entanglement entropy proposal. *JHEP*, 07:062, 2007.

[21] Aitor Lewkowycz and Juan Maldacena. Generalized gravitational entropy. *JHEP*, 08:090, 2013.

[22] Thomas Faulkner, Aitor Lewkowycz, and Juan Maldacena. Quantum corrections to holographic entanglement entropy. *JHEP*, 11:074, 2013.

[23] A. Connes. Geometry and the Quantum. *ArXiv e-prints*, March 2017.

[24] Ali H. Chamseddine, Alain Connes, and Viatcheslav Mukhanov. Geometry and the Quantum: Basics. *JHEP*, 12:098, 2014.

[25] Ali H. Chamseddine and Alain Connes. The Spectral action principle. *Commun. Math. Phys.*, 186:731–750, 1997.

[26] Sebastian de Haro, Sergey N. Solodukhin, and Kostas Skenderis. Holographic reconstruction of space-time and renormalization in the AdS / CFT correspondence. *Commun. Math. Phys.*, 217:595–622, 2001.

[27] Kostas Skenderis. Lecture notes on holographic renormalization. *Class. Quant. Grav.*, 19:5849–5876, 2002.

[28] Mark Van Raamsdonk. Building up spacetime with quantum entanglement. *Gen. Rel. Grav.*, 42:2323–2329, 2010. [Int. J. Mod. Phys.D19,2429(2010)].

[29] Mark Van Raamsdonk. Lectures on Gravity and Entanglement. In *Proceedings, Theoretical Advanced Study Institute in Elementary Particle Physics: New Frontiers in Fields and Strings (TASI 2015): Boulder, CO, USA, June 1-26, 2015*, pages 297–351, 2017.

[30] Ted Jacobson. Thermodynamics of space-time: The Einstein equation of state. *Phys. Rev. Lett.*, 75:1260–1263, 1995.

[31] T. Padmanabhan. Thermodynamical Aspects of Gravity: New insights. *Rept. Prog. Phys.*, 73:046901, 2010.

[32] Erik P. Verlinde. Emergent Gravity and the Dark Universe. *SciPost Phys.*, 2(3):016, 2017.

[33] Mark Srednicki. Entropy and area. *Phys. Rev. Lett.*, 71:666–669, 1993.

[34] J. Eisert, M. Cramer, and M. B. Plenio. Area laws for the entanglement entropy - a review. *Rev. Mod. Phys.*, 82:277–306, 2010.

[35] Roman Orus. A Practical Introduction to Tensor Networks: Matrix Product States and Projected Entangled Pair States. *Annals Phys.*, 349:117–158, 2014.

[36] G. Vidal. Entanglement Renormalization. *Phys. Rev. Lett.*, 99(22):220405, 2007.

[37] Brian Swingle. Entanglement Renormalization and Holography. *Phys. Rev.*, D86:065007, 2012.

[38] Daniel Harlow and Patrick Hayden. Quantum Computation vs. Firewalls. *JHEP*, 06:085, 2013.

[39] Fernando Pastawski, Beni Yoshida, Daniel Harlow, and John Preskill. Holographic quantum error-correcting codes: Toy models for the bulk/boundary correspondence. *JHEP*, 06:149, 2015.

[40] Eric Mintun, Joseph Polchinski, and Vladimir Rosenhaus. Bulk-Boundary Duality, Gauge Invariance, and Quantum Error Corrections. *Phys. Rev. Lett.*, 115(15):151601, 2015.

[41] Daniel Harlow. The Ryu–Takayanagi Formula from Quantum Error Correction. *Commun. Math. Phys.*, 354(3):865–912, 2017.

[42] Yann LeCun, Yoshua Bengio, and Geoffrey Hinton. Deep learning. *Nature*, 521(7553):436–444, 2015.

[43] P. Mehta and D. J. Schwab. An exact mapping between the Variational Renormalization Group and Deep Learning. *ArXiv e-prints*, October 2014.

[44] Wen-Cong Gan and Fu-Wen Shu. Holography as deep learning. 2017.

[45] Jae-Weon Lee. Quantum fields as deep learning. 2017.

[46] P. Kovtun, Dan T. Son, and Andrei O. Starinets. Viscosity in strongly interacting quantum field theories from black hole physics. *Phys. Rev. Lett.*, 94:111601, 2005.

[47] Ulrich Heinz, Chun Shen, and Huichao Song. The viscosity of quark-gluon plasma at RHIC and the LHC. *AIP Conf. Proc.*, 1441:766–770, 2012.

[48] Johanna Erdmenger, Nick Evans, Ingo Kirsch, and Ed Threlfall. Mesons in Gauge/Gravity Duals - A Review. *Eur. Phys. J.*, A35:81–133, 2008.

[49] Mohammed Mia, Keshav Dasgupta, Charles Gale, and Sangyong Jeon. Toward Large N Thermal QCD from Dual Gravity: The Heavy Quarkonium Potential. *Phys. Rev.*, D82:026004, 2010.

[50] D. T. Son. Gauge-gravity duality and heavy-ion collisions. *AIP Conf. Proc.*, 957:134–141, 2007.

[51] Jorge Casalderrey-Solana, Hong Liu, David Mateos, Krishna Rajagopal, and Urs Achim Wiedemann. Gauge/String Duality, Hot QCD and Heavy Ion Collisions. 2011.

[52] Romuald A. Janik and Robert B. Peschanski. Gauge/gravity duality and thermalization of a boost-invariant perfect fluid. *Phys. Rev.*, D74:046007, 2006.

[53] Allan Bayntun, C. P. Burgess, Brian P. Dolan, and Sung-Sik Lee. AdS/QHE: Towards a Holographic Description of Quantum Hall Experiments. *New J. Phys.*, 13:035012, 2011.

[54] Mitsutoshi Fujita, Matthias Kaminski, and Andreas Karch. SL(2,Z) Action on AdS/BCFT and Hall Conductivities. *JHEP*, 07:150, 2012.

[55] Matthew Lippert, René Meyer, and Anastasios Taliotis. A holographic model for the fractional quantum Hall effect. *JHEP*, 01:023, 2015.

[56] Sean A. Hartnoll, Christopher P. Herzog, and Gary T. Horowitz. Building a Holographic Superconductor. *Phys. Rev. Lett.*, 101:031601, 2008.

[57] Sean A. Hartnoll, Christopher P. Herzog, and Gary T. Horowitz. Holographic Superconductors. *JHEP*, 12:015, 2008.

[58] Sarah Harrison, Shamit Kachru, and Gonzalo Torroba. A maximally supersymmetric Kondo model. *Class. Quant. Grav.*, 29:194005, 2012.

[59] Paolo Benincasa and Alfonso V. Ramallo. Holographic Kondo Model in Various Dimensions. *JHEP*, 06:133, 2012.

[60] Johanna Erdmenger, Carlos Hoyos, Andy O'Bannon, and Jackson Wu. A Holographic Model of the Kondo Effect. *JHEP*, 12:086, 2013.

[61] J. Kondo. Resistance Minimum in Dilute Magnetic Alloys. *Prog. Theor. Phys.*, 32(1):37–49, 1964.

[62] M. P. Sarachik, E. Corenzwit, and L. D. Longinotti. Resistivity of mo-nb and mo-re alloys containing 1 *Phys. Rev.*, 135:A1041–A1045, Aug 1964.

[63] Kenneth G. Wilson. The Renormalization Group: Critical Phenomena and the Kondo Problem. *Rev. Mod. Phys.*, 47:773, 1975.

[64] Mitsutoshi Fujita, Tadashi Takayanagi, and Erik Tonni. Aspects of AdS/BCFT. *JHEP*, 11:043, 2011.

[65] Tadashi Takayanagi. Holographic Dual of BCFT. *Phys. Rev. Lett.*, 107:101602, 2011.

[66] Mario Flory. *Entanglement and defect entropies in gauge/gravity duality.* PhD thesis, LMU Munich (main), 2016.

[67] Migael Strydom. *Magnetic vortices in gauge/gravity duality.* PhD thesis, Munich U., 2014.

[68] Johanna Erdmenger, Carlos Hoyos, Andy O'Bannon, Ioannis Papadimitriou, Jonas Probst, and Jackson M. S. Wu. Two-point Functions in a Holographic Kondo Model. *JHEP*, 03:039, 2017.

[69] Martin Ammon and Johanna Erdmenger. *Gauge/gravity duality.* Cambridge Univ. Pr., Cambridge, UK, 2015.

[70] Jan Zaanen, Ya-Wen Sun, Yan Liu, and Koenraad Schalm. *Holographic Duality in Condensed Matter Physics.* Cambridge Univ. Press, 2015.

[71] J. Polchinski. *String theory. Vol. 1: An introduction to the bosonic string.* Cambridge University Press, 2007.

[72] J. Polchinski. *String theory. Vol. 2: Superstring theory and beyond.* Cambridge University Press, 2007.

[73] Ralph Blumenhagen, Dieter Lüst, and Stefan Theisen. *Basic concepts of string theory.* Theoretical and Mathematical Physics. Springer, Heidelberg, Germany, 2013.

[74] K. Becker, M. Becker, and J. H. Schwarz. *String theory and M-theory: A modern introduction.* Cambridge University Press, 2006.

[75] F. Gliozzi, Joel Scherk, and David I. Olive. Supersymmetry, Supergravity Theories and the Dual Spinor Model. *Nucl. Phys.*, B122:253–290, 1977.

[76] Joseph Polchinski. Dirichlet Branes and Ramond-Ramond charges. *Phys. Rev. Lett.*, 75:4724–4727, 1995.

[77] Ofer Aharony, Oren Bergman, Daniel Louis Jafferis, and Juan Maldacena. N=6 superconformal Chern-Simons-matter theories, M2-branes and their gravity duals. *JHEP*, 10:091, 2008.

[78] Gerard 't Hooft. A Planar Diagram Theory for Strong Interactions. *Nucl. Phys.*, B72:461, 1974.

[79] Peter Breitenlohner and Daniel Z. Freedman. Stability in Gauged Extended Supergravity. *Annals Phys.*, 144:249, 1982.

[80] S. S. Gubser, Igor R. Klebanov, and Alexander M. Polyakov. Gauge theory correlators from noncritical string theory. *Phys. Lett.*, B428:105–114, 1998.

[81] Joseph I. Kapusta. *Finite Temperature Field Theory*, volume 360 of *Cambridge Monographs on Mathematical Physics*. Cambridge University Press, Cambridge, 1989.

[82] Michel Le Bellac. *Thermal Field Theory*. Cambridge University Press, 2011.

[83] J. I. Kapusta and Charles Gale. *Finite-temperature field theory: Principles and applications*. Cambridge University Press, 2011.

[84] Edward Witten. Anti-de Sitter space, thermal phase transition, and confinement in gauge theories. *Adv. Theor. Math. Phys.*, 2:505–532, 1998.

[85] J. S. Bell. On the Einstein-Podolsky-Rosen paradox. *Physics*, 1:195–200, 1964.

[86] Juan Maldacena and Leonard Susskind. Cool horizons for entangled black holes. *Fortsch. Phys.*, 61:781–811, 2013.

[87] Ian Affleck and Andreas W. W. Ludwig. The Kondo effect, conformal field theory and fusion rules. *Nucl. Phys.*, B352:849–862, 1991.

[88] Ian Affleck. A Current Algebra Approach to the Kondo Effect. *Nucl. Phys.*, B336:517–532, 1990.

[89] N. E. Bickers. Review of techniques in the large-N expansion for dilute magnetic alloys. *Rev. Mod. Phys.*, 59:845–939, 1987.

[90] Alexander Cyril Hewson. *The Kondo Problem to Heavy Fermions*. Cambridge Studies in Magnetism. Cambridge University Press, 1993.

[91] P Coleman and N Andrei. Diagonalisation of the generalised anderson model. *Journal of Physics C: Solid State Physics*, 19(17):3211, 1986.

[92] Piers Coleman. Mixed valence as an almost broken symmetry. *Phys. Rev. B*, 35:5072–5116, Apr 1987.

[93] T. Senthil, S. Sachdev, and M. Vojta. Fractionalized Fermi Liquids. *Physical Review Letters*, 90(21):216403, May 2003.

[94] T. Senthil, M. Vojta, and S. Sachdev. Weak magnetism and non-Fermi liquids near heavy-fermion critical points. *Physical Review B*, 69(3):035111, January 2004.

[95] N. D. Mermin and H. Wagner. Absence of ferromagnetism or antiferromagnetism in one- or two-dimensional isotropic heisenberg models. *Phys. Rev. Lett.*, 17:1133–1136, Nov 1966.

[96] Sidney Coleman. There are no goldstone bosons in two dimensions. *Comm. Math. Phys.*, 31(4):259–264, 1973.

[97] Edward Witten. Multitrace operators, boundary conditions, and AdS / CFT correspondence. 2001.

[98] Maximo Banados, Claudio Teitelboim, and Jorge Zanelli. The Black hole in three-dimensional space-time. *Phys. Rev. Lett.*, 69:1849–1851, 1992.

[99] Christian Latta, Florian Haupt, Markus Hanl, Andreas Weichselbaum, Martin Claassen, Wolf Wuester, Parisa Fallahi, Stefan Faelt, Leonid Glazman, Jan von Delft, et al. Quantum quench of kondo correlations in optical absorption. *arXiv preprint arXiv:1102.3982*, 2011.

[100] M. Nuss, M. Ganahl, E. Arrigoni, W. von der Linden, and H. G. Evertz. Nonequilibrium, spatio-temporal formation of the Kondo screening-cloud on a lattice. *ArXiv e-prints*, September 2014.

[101] Andy O'Bannon, Ioannis Papadimitriou, and Jonas Probst. A Holographic Two-Impurity Kondo Model. *JHEP*, 01:103, 2016.

[102] W. Israel. Singular hypersurfaces and thin shells in general relativity. *Nuovo Cim.*, B44S10:1, 1966. [Nuovo Cim.B44,1(1966)].

[103] C. Kaeonikhom. Israel Junction Conditions on Hypersurface from Variational Principle Approach. In *Proceedings of the First National Symposium on Physics Graduate Research*, 2006. see www.if.nu.ac.th/sites/default/files/publications/ChakkritNSPG1.pdf.

[104] Ofer Aharony, Oliver DeWolfe, Daniel Z. Freedman, and Andreas Karch. Defect conformal field theory and locally localized gravity. *JHEP*, 07:030, 2003.

[105] Dongsu Bak, Michael Gutperle, and Shinji Hirano. A Dilatonic deformation of AdS(5) and its field theory dual. *JHEP*, 05:072, 2003.

[106] Eric D'Hoker, John Estes, and Michael Gutperle. Exact half-BPS Type IIB interface solutions. I. Local solution and supersymmetric Janus. *JHEP*, 06:021, 2007.

[107] Roberto Giambò and Fabio Giannoni. Minimal geodesics on manifolds with discontinuous metrics. *J. London Math. Soc.*, 67:527–544, 2003.

[108] Max-Niklas Newrzella. Calculation of time-dependent phenomena in AdS/CFT correspondence, 2014.

[109] V. Balasubramanian, A. Bernamonti, N. Copland, B. Craps, and F. Galli. Thermalization of mutual and tripartite information in strongly coupled two dimensional conformal field theories. *Phys. Rev.*, D84:105017, 2011.

[110] P.W. Phillips. *Advanced Solid State Physics*. Advanced Book Program. Avalon Publishing, 2003.

[111] Mario Flory. A complexity/fidelity susceptibility g-theorem for $AdS_3/BCFT_2$. *JHEP*, 06:131, 2017.

[112] Daniel Friedan and Anatoly Konechny. On the boundary entropy of one-dimensional quantum systems at low temperature. *Phys. Rev. Lett.*, 93:030402, 2004.

[113] Douglas Stanford and Leonard Susskind. Complexity and Shock Wave Geometries. *Phys. Rev.*, D90(12):126007, 2014.

[114] Leonard Susskind. Computational Complexity and Black Hole Horizons. *Fortsch. Phys.*, 64:44–48, 2016. [Fortsch. Phys.64,24(2016)].

[115] Adam R. Brown, Daniel A. Roberts, Leonard Susskind, Brian Swingle, and Ying Zhao. Holographic Complexity Equals Bulk Action? *Phys. Rev. Lett.*, 116(19):191301, 2016.

[116] P. Coleman. *Introduction to Many-Body Physics*. Cambridge University Press, 2015.

[117] Didier Sornette. Discrete scale invariance and complex dimensions. *Phys. Rept.*, 297:239–270, 1998.

[118] Gianluca Calcagni. Complex dimensions and their observability. *Phys. Rev.*, D96(4):046001, 2017.

[119] Kengo Maeda, Makoto Natsuume, and Takashi Okamura. Universality class of holographic superconductors. *Phys. Rev.*, D79:126004, 2009.

[120] Makoto Natsuume. Critical phenomena in the AdS/CFT duality. *Prog. Theor. Phys. Suppl.*, 186:491–497, 2010.

[121] Julian Sonner, Adolfo del Campo, and Wojciech H. Zurek. Universal far-from-equilibrium Dynamics of a Holographic Superconductor. 2014. [Nature Commun.6,7406(2015)].

[122] U.C. Täuber. *Critical Dynamics: A Field Theory Approach to Equilibrium and Non-Equilibrium Scaling Behavior*. Cambridge University Press, 2014.

[123] M. J. Bhaseen, Jerome P. Gauntlett, B. D. Simons, Julian Sonner, and Toby Wiseman. Holographic Superfluids and the Dynamics of Symmetry Breaking. *Phys. Rev. Lett.*, 110(1):015301, 2013.

[124] M. J. Bhaseen, Benjamin Doyon, Andrew Lucas, and Koenraad Schalm. Far from equilibrium energy flow in quantum critical systems. 2013. [Nature Phys.11,5(2015)].

[125] Johanna Erdmenger, Carlos Hoyos, Andy O'Bannon, Ioannis Papadimitriou, Jonas Probst, and Jackson M. S. Wu. Holographic Kondo and Fano Resonances. *Phys. Rev.*, D96(2):021901, 2017.

[126] C. Jayaprakash, H. R. Krishna-Murthy, and J. W. Wilkins. Two-Impurity Kondo Problem. *Physical Review Letters*, 47:737–740, September 1981.

[127] Ian Affleck and Andreas W. W. Ludwig. Exact critical theory of the two impurity Kondo model. *Phys. Rev. Lett.*, 68:1046–1049, 1992.

[128] I. Affleck, A. W. W. Ludwig, and B. A. Jones. Conformal-field-theory approach to the two-impurity Kondo problem: Comparison with numerical renormalization-group results. *Physical Review B*, 52:9528–9546, October 1995.